

Copyright

by

Bryan John Lochman

2010

**The Thesis Committee for Bryan John Lochman
Certifies that this is the approved version of the following thesis:**

**Technique for Imaging Ablation-Products Transported in High-Speed
Boundary Layers by using Naphthalene Planar Laser-Induced
Fluorescence**

**APPROVED BY
SUPERVISING COMMITTEE:**

Supervisor:

Noel T. Clemens

Venkatramanan Raman

**Technique for Imaging Ablation-Products Transported in High-Speed
Boundary Layers by using Naphthalene Planar Laser-Induced
Fluorescence**

by

Bryan John Lochman, B.S.

Thesis

Presented to the Faculty of the Graduate School of

The University of Texas at Austin

in Partial Fulfillment

of the Requirements

for the Degree of

Master of Science in Engineering

The University of Texas at Austin

August, 2010

Dedication

For my loving wife and amazing parents who have always shown me the support and encouragement that have pushed me to complete all the goals I have set before myself.

Acknowledgements

First and foremost I would like to thank my advisor Dr. Noel T. Clemens for giving me the opportunity to work on this project. His advice and guidance has greatly shaped this project's success. I would also like to thank all others who have worked directly on this project. Thank you to Dr. Zach Murphree who has helped tremendously on the setup and data collection of the naphthalene fluorescence study. Thanks are also due to Dr. Venkat Narayanaswamy for his diligent help on understanding naphthalene spectroscopy. Thank you to Dr. Jeremy Jagodzinski for his initial work on this project. I have also received invaluable support from Eddie Zihlman for his help in solving all compressor related issues and Donna Soward for dealing with all last minute orders. I would also like to thank staff members Timothy Valdez, Ricardo Palacios, and Travis Crooks for all the generous help I have received. I also am very grateful for the help from visiting professor Dr. Bulent Yuceil and fellow graduate students Kevin Marr, Ross Burns, and Sumeet Trehan.

Finally, I would like to gratefully acknowledge the financial support offered by NASA under cooperative agreement number NNX08AD03A.

August 2010

Abstract

Technique for Imaging Ablation-Products Transported in High-Speed Boundary Layers by using Naphthalene Planar Laser-Induced Fluorescence

Bryan John Lochman, M.S.E.

The University of Texas at Austin, 2010

Supervisor: Noel T. Clemens

A new technique is developed that uses planar laser-induced fluorescence (PLIF) imaging of sublimated naphthalene to image the transport of ablation products in a hypersonic boundary layer. The primary motivation for this work is to understand scalar transport in hypersonic boundary layers and to develop a database for validation of computational models. The naphthalene is molded into a rectangular insert that is mounted flush with the floor of a Mach 5 wind tunnel. The distribution of naphthalene in the boundary layer is imaged by using PLIF, where the laser excitation is at 266 nm and the fluorescence is collected in the range of 320 to 380 nm. To investigate the use of naphthalene PLIF as a quantitative diagnostic technique, a series of experiments is conducted to determine the linearity of the fluorescence signal with laser fluence, as well

as the temperature and pressure dependencies of the signal. The naphthalene fluorescence at 297 K is determined to be linear for laser fluence that is less than about 200 J/m^2 . The temperature dependence of the naphthalene fluorescence signal is found at atmospheric pressure over the temperature range of 297K to 525K. A monotonic increase in the fluorescence is observed with increasing temperature. Naphthalene fluorescence lifetime measurements were also made in pure-air and nitrogen environments at 300 K over the range 1 kPa to 40 kPa. The results in air show the expected Stern-Volmer behavior with decreasing lifetimes at increasing pressure, whereas nitrogen exhibits the opposite trend. Preliminary PLIF images of the sublimated naphthalene are acquired in a Mach 5 turbulent boundary layer. Relatively low signal-to-noise-ratio images were obtained at a stagnation temperature of 345 K, but much higher quality images were obtained at a stagnation temperature of 380 K. The initial results indicate that PLIF of sublimating naphthalene may be an effective tool for studying scalar transport in hypersonic flows.

Table of Contents

List of Tables	x
List of Figures	xi
Nomenclature	xv
Chapter 1: Introduction	1
Chapter 2: Literature Review	4
2.1 Ablation.....	4
2.1.1 High Temperature Ablation	4
2.1.2 Low Temperature Ablation.....	7
2.2 Naphthalene as an Ablator and Tracer.....	9
2.3 Spectroscopic Measurements of Hydrocarbon Tracer-Molecules.....	12
2.4 Naphthalene Spectroscopy.....	14
Chapter 3: Experimental Program	22
3.1 Facilities.....	22
3.1.1 Mach 5 Wind Tunnel Facility	22
3.1.2 Temperature Controlled Jet of Naphthalene Facility.....	24
3.2 Naphthalene Mach 5 Wind Tunnel Floor Model.....	25
3.2.1 First Campaign Floor Model.....	25
3.2.2 Second Campaign Floor Model	28
3.3 Naphthalene LIF complimentary Investigations.....	33
3.3.1 Fluorescence Linearity Measurement System	33
3.3.2 Temperature Dependence Measurement System.....	34
3.3.3 Pressure Dependence Measurement System.....	35
3.4 Mach 5 Wind Tunnel PLIF System	37
3.4.1 Planar Laser Induced Fluorescence (PLIF).....	37
3.4.2 PLIF System Setup	38
3.4.3 Image Processing	41
Chapter 4: Results	42

4.1 Mach 5 Naphthalene Ablation Results: First Campaign	45
4.2 Mass/Heat Transfer Analysis	46
4.3 Complementary Investigations of Naphthalene LIF	50
4.3.1 Naphthalene LIF Linearity	50
4.3.2 Naphthalene LIF Temperature Dependence	54
4.3.3 Naphthalene LIF Pressure Dependence	57
4.3.3.1 Preliminary Fluorescence Study	57
4.3.3.2 Fluorescence Lifetime Pressure Dependence	59
4.4 Mach 5 Naphthalene Ablation Results: Second Campaign	66
4.4.1 Improvement of Naphthalene PLIF Images	66
4.4.2 Thermocouple Measurements	72
4.4.3 Average of Instantaneous PLIF Images	74
4.4.4 Obtaining Quantitative Measurements	76
Chapter 5: Conclusions and Future Work	80
5.1 Conclusions	80
5.2 Future Work	81
Bibliography	83
Vita	88

List of Tables

Table 2.1: Physical Properties of Naphthalene	10
---	----

List of Figures

Figure 1.1: Re-entry schematic.....	1
Figure 2.1: Diagram of heat transfer effects in high temperature ablation	5
Figure 2.2: Absorption of naphthalene.....	9
Figure 2.3: Emission of naphthalene	10
Figure 2.4: Vibrational-electronic energy level diagram of gas-phase naphthalen. There are two electronic systems, singlet and triplet, where each electronic state is associated with a manifold of closely-spaced vibrational levels	15
Figure 3.1: Schematic of the Mach 5 blowdown facility located at the Pickle Research Campus of the University of Texas at Austin	23
Figure 3.2: Schematic of the first campaign naphthalene floor plug	26
Figure 3.3: Naphthalene crystals melting on a hot plate	26
Figure 3.4: Naphthalene floor plug after molding plate is removed	27
Figure 3.5: Naphthalene floor plug installed into test section.....	27
Figure 3.6: Second campaign naphthalene floor plug installed in the Mach 5 wind tunnel.....	28
Figure 3.7: Dimensions of the naphthalene plug and thermocouple/heat flux sensor locations in the second campaign naphthalene floor plug	30
Figure 3.8: Dimensions of the downstream fused silica window in the second campaign naphthalene floor plug.....	31
Figure 3.9: Second campaign naphthalene floor plug installed in the Mach 5 wind tunnel test section.....	32

Figure 3.10: Naphthalene LIF linearity measurement and temperature dependence setup	34
Figure 3.11: Naphthalene LIF pressure dependence measurement cell	36
Figure 3.12: Naphthalene LIF pressure dependence measurement setup	36
Figure 3.13: Schematic diagram of the naphthalene PLIF setup in the Mach 5 wind tunnel. (a) Overall assembly and (b) inside the test section	39
Figure 3.14: Back-illuminated CCD camera focusing on a field of view downstream of the naphthalene plug in the Mach 5 test section	40
Figure 3.15: Compact RIO System with thermocouples	40
Figure 4.1: Example naphthalene instantaneous PLIF images from the first campaign in the Mach 5 wind tunnel	43
Figure 4.2: Composite of two instantaneous naphthalene PLIF images taken from two adjacent locations at different times. Uncorrelated velocity field image is displayed behind the images to show the boundary layer thickness	44
Figure 4.3: Calculated temperature of the wall of the naphthalene plug as a function of the stagnation temperature	48
Figure 4.4: Calculated heat flux through the naphthalene plug as a function of the stagnation temperature	49
Figure 4.5: Calculated naphthalene plug depth removal rate as function of temperature	49
Figure 4.6: Beam profiles of naphthalene and air jet with varying input energy from the laser	51

Figure 4.7: Dependence of naphthalene LIF signal on laser fluence at 297 K and 1 atm. The naphthalene is carried in air and the laser wavelength is 266nm	53
Figure 4.8: Temperature dependence of the naphthalene LIF signal at atmospheric pressure ($T_0=300\text{K}$).....	55
Figure 4.9: Temperature dependence of the naphthalene absorption cross-section at atmospheric pressure ($T_0=300\text{K}$).....	56
Figure 4.10: Naphthalene jet exhausting into air with (a) nitrogen driving the flow, (b) air driving the flow and (c) same image as in (b) except with a rescaled color map that highlights the low signal range	58
Figure 4.11: Pressure dependence of the naphthalene (a) fluorescence lifetime and (b) the natural logarithm of the fluorescence lifetime	60
Figure 4.12: Stern-Volmer plot of naphthalene vapor in a pure-air environment. Note that the plot is linear at high pressure ($>2\text{ kPa}$), and deviation from linearity can be seen close to 1 kPa.	62
Figure 4.13: Fluorescence lifetime measurements for naphthalene diluted in nitrogen and air.....	64
Figure 4.14: Fluorescence lifetime measurements for naphthalene diluted in nitrogen (current work) and argon (Beddard et al., 1973)	64
Figure 4.15: Stagnation temperature during a typical run	67
Figure 4.16: Instantaneous naphthalene PLIF images during (a) the first campaign and (b) the second campaign.....	69
Figure 4.17: Instantaneous naphthalene PLIF images in a Mach 5 turbulent boundary layer.....	70

Figure 4.18: Composite of two instantaneous naphthalene PLIF images taken at two adjacent locations at different times	71
Figure 4.19: Naphthalene plug with thermocouples imbedded at varying depths	72
Figure 4.20: Thermocouple measurements at different depths during a typical Mach 5 wind tunnel run	73
Figure 4.21: Average of 18 instantaneous naphthalene PLIF images	74
Figure 4.22: Normalized average fluorescence signal through the Mach 5 boundary layer with standard deviation	75
Figure 4.23: Normalized average fluorescence signal profiles through the Mach 5 boundary layer. Uncorrected signal and signal corrected for temperature effects	79

Nomenclature

Symbols

c	=	speed of light
C_f	=	skin friction coefficient
C_p	=	specific heat capacity
D	=	mass diffusivity
E_l	=	laser energy (J)
h	=	Plank's constant
h_h	=	heat transfer coefficient
h_m	=	mass transfer coefficient
h_{sg}	=	latent heat of vaporization
k_f	=	rate of spontaneous emission
k_{int}	=	rate of energy transfer from S1 not due to collisions
k_Q	=	collisional quenching rate
\dot{m}''	=	mass flux
n	=	total number density
n_i	=	number density of colliding species i
M	=	Mach number
P	=	total pressure (Pa)
P_i	=	partial pressure of species i (Pa)
Pr	=	Prandtl number
r	=	recovery factor
Re_∞	=	free-stream Reynolds number
S_0	=	Singlet ground state

S_1	=	Singlet 1st electronic excited state
S_2	=	Singlet 2nd electronic excited state
S_f	=	fluorescence signal
Sc	=	Schmidt number
T	=	temperature (K)
T_r	=	recovery temperature (K)
T_s	=	surface temperature (K)
T_∞	=	free-stream temperature (K)
U_∞	=	free-stream velocity
ΔV	=	probe volume

Greek

α	=	thermal diffusivity
γ	=	specific heat ratio
δ_{99}	=	99% velocity boundary layer thickness (m)
η_{opt}	=	collection optics collection efficiency
λ	=	wavelength (nm)
ν	=	kinematic diffusivity
$\bar{\nu}$	=	wavenumber (cm^{-1})
$\langle v \rangle_{i-Na}$	=	mean relative speed between species i and naphthalene
ρ_{vs}	=	surface vapor density
ρ_∞	=	free-stream vapor density
σ_a	=	absorption cross-section
σ_i	=	quenching cross section of species i
τ_f	=	time-decay constant
ϕ	=	fluorescence yield

χ_i = mole fraction of species i

Subscripts

i = designates species i

r = recovery value

ref = reference value (300 K)

0 = stagnation value

∞ = free-stream value

Chapter 1: Introduction

Ablation modeling has received renewed interest owing to NASA's interest in planetary-atmosphere entry (Greathouse et al., 2007), as well as the US Air Force's interest in developing hypersonic long-range aircraft and missiles. Figure 1.1 displays a schematic of the highly complex coupled processes that occur on these thermal protection systems. These processes include high-temperature non-equilibrium chemistry, radiation, turbulence, mass/heat transfer, radiation, gas-solid reactions and mechanical erosion (Smits et al., 2009).

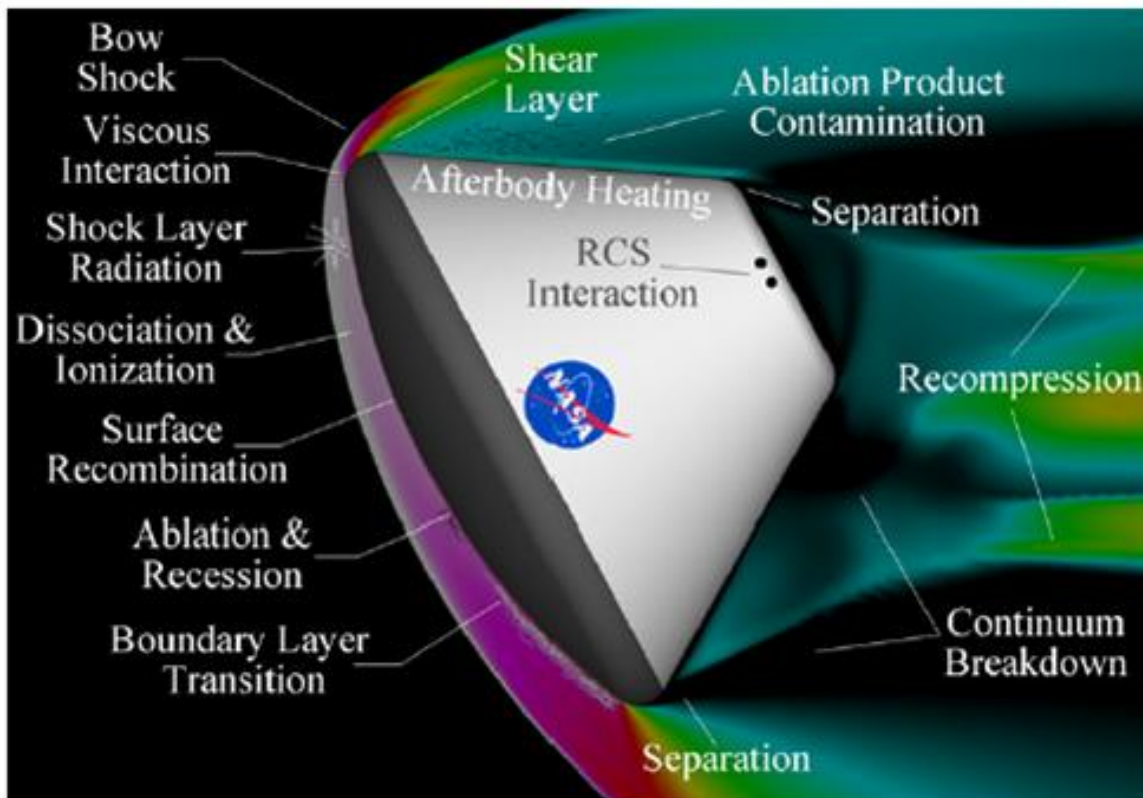


Figure 1.1 Re-entry schematic (courtesy of NASA)

The coupled nature of these thermophysical processes makes developing computational models of ablation particularly challenging (Gnoffo et al., 1999). In particular, modeling efforts are limited by the lack of suitable validation data acquired under realistic conditions. For this reason, this study is aimed at considering a limited-physics problem, where a low-temperature sublimating ablator is used to capture the surface-gas transpiration and resulting transport of the ablation products in the turbulent boundary layer. The sublimating ablator used is naphthalene, which has the particularly useful property that it can be imaged using planar laser-induced fluorescence (PLIF).

A major goal of this work is the simultaneous acquisition of naphthalene PLIF and particle image velocimetry (PIV) to enable the computation of the scalar/velocity correlations that are used in Large Eddy Simulation (LES) and Reynolds Averaged Navier-Stokes (RANS) model development. Large Eddy Simulations explicitly resolve the large scale motion of the flow, while approximating the small scale structures of the flow with an appropriate sub-grid scale model (Gatski et al., 1996).

The current investigation is focused on the development of the naphthalene sublimation technique for investigating scalar transport of ablation products in low-enthalpy hypersonic flows. The overall objective of the work is to develop a quantitative diagnostic technique, so the photophysical properties of naphthalene were also studied. This investigation has the following goals:

1. Make detailed measurements of naphthalene scalar fields in a Mach 5 turbulent boundary layer using planar laser-induced fluorescence (PLIF)
2. Develop a method to measure temperature and heat flux through a naphthalene floor plug while in the Mach 5 flow
3. Study the linearity of the naphthalene laser induced fluorescence signal (LIF) with laser fluence in order to allow for sheet corrections to be made

4. Study the temperature dependence of the naphthalene LIF signal at varying pressures
5. Study the pressure dependences of the naphthalene LIF signal

Chapter 2: Literature Review

2.1 ABLATION

2.1.1 High Temperature Ablation

The complex process of high temperature ablation that occurs on the thermal protection systems of re-entry vehicles is characterized by several physical processes including high-temperature non-equilibrium chemistry, radiation, turbulence, mass/heat transfer, radiation, gas-solid reactions and mechanical erosion (Smits et al., 2009). Figure 2.1 displays the detailed heat transfer process that occurs during high temperature ablation. The thermochemical ablation involves the formation of a multilayer surface that consists of a char layer, reaction layer and virgin material layer. The thermal degradation of the material results in the formation of the char layer from the loss of solid material in decomposition and the formation of carbonaceous char residue. The production of decomposition gases occurs through this process and this gas escapes through the porous char layer that forms. Through continuous heating, the char layer will eventually be removed resulting in a recession-rate of the char layer. The temperature at the surface will be maintained after the char layer begins being removed, thus this is the point of the failure temperature of the material (Ho et al., 2007).

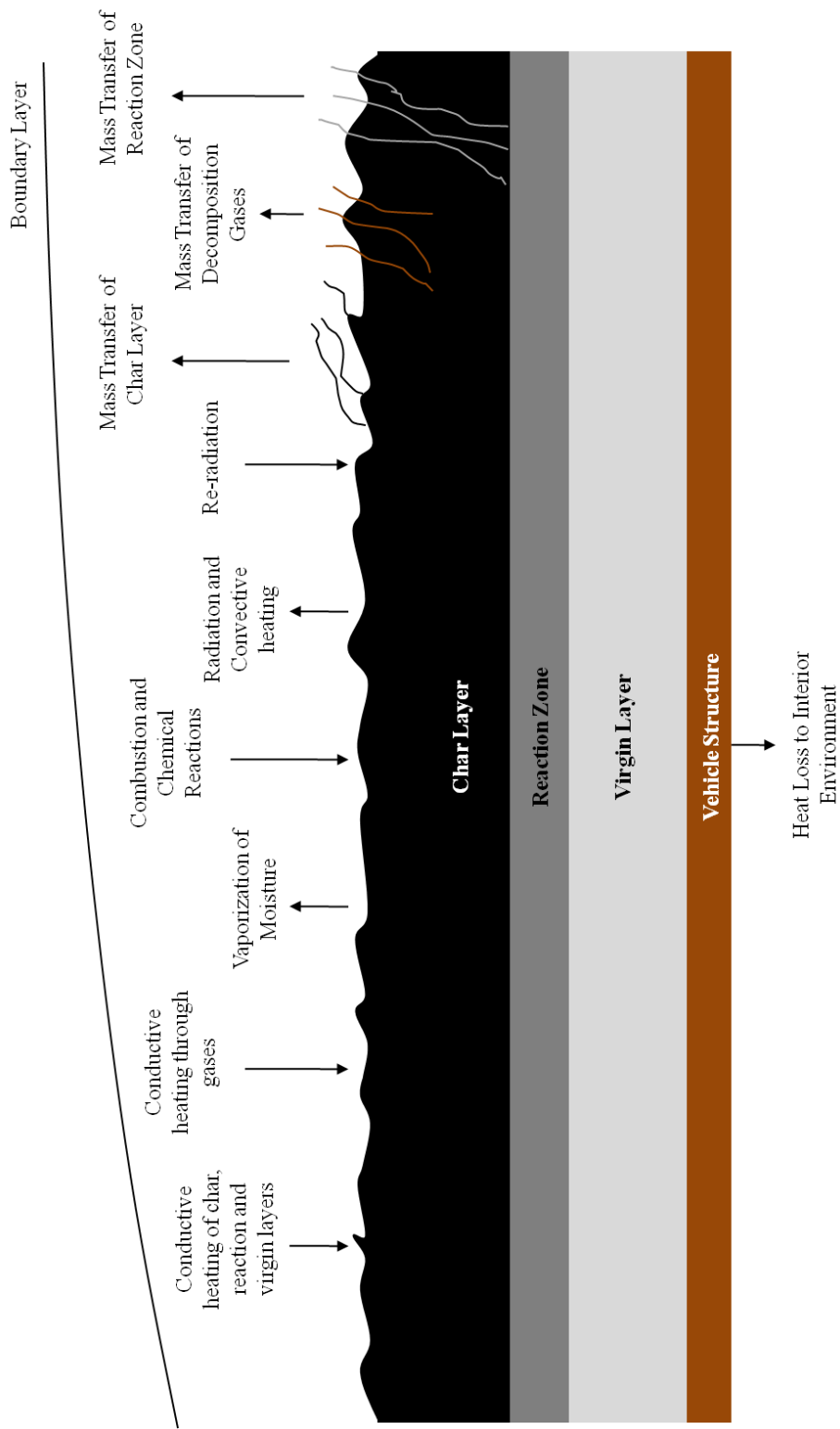


Figure 2.1 Diagram of mass/heat transfer effects in high temperature ablation

A large portion of testing high temperature ablators has gone into testing the thermal properties of these materials in re-entry situations. A detailed survey of experimental testing of high temperature ablation is given by Ho et al. (2007). An early study by Vojvodich and Winkler (1963) studied the insulation efficiency of several thermal protection materials in a high-energy arc-jet Mach 5.5 wind tunnel. Both low and high conductive heating rates were tested by varying the model geometry. The materials tested were typical insulating charring materials and were tested in both air and nitrogen environments. The materials were found to provide better insulation efficiency when exposed for short duration run times with high heating rates rather than for long duration run times with low heating rates. Recently, Milos and Chen (2009) investigated the thermal properties of a Phenolic Impregnated Carbon Ablator that is a candidate for use on the Orion Crew Module. Arc jet tests were conducted over a range of stagnation heat flux and pressure conditions in order to validate a thermal response property model.

In addition to the study of material thermal properties, past investigations have focused on the char-recession rate. The char-recession rate and thermal response of five phenolic-nylon-based materials were investigated by McLain et al. (1968). The investigation was carried out in a Mach 5 arc-heated tunnel. Arc-heated tunnels are heated through a magnetically rotated electric arc. Measured char-recession rates were obtained through the analysis of motion-picture film and through testing the ablative material for successively longer exposures. In addition, Covington et al. (2008) evaluated surface recession rates of the Stardust spacecraft forebody heat shield in order to obtain a measure for the ablative performance of the material. These tests were carried out in a high-energy arc jet facility with conditions appropriate for the Stardust re-entry. The data on the thermal performance of the PICA material forming the heat shield were

done through varying the model size and arc jet operating condition. The data were used to correct computer models that predict the response of the re-entry vehicle.

2.1.2 Low Temperature Ablation

Since the 1950s low temperature ablation studies have been conducted so as to create a limited physics problem that is more economical and easier to maintain in a test environment. Materials used as low temperature ablators have included camphor, CO₂ (dry-ice), water ice, naphthalene, ammonium chloride, and wax (Kohlman and Richardson, 1969).

Similarly to high temperature ablation studies, recession rates have been a focus of past investigations. Camphor and dry-ice have seen the most use in these studies. Charwat (1968) used two low-temperature sublimating ablators, camphor and naphthalene, to determine nose-tip recession rates of supersonic projectiles. Tests were performed on cones with flat and hemispherical noses in a Mach 3 flow. The general evolution of their profiles were traced using film records, which allowed for the sublimation history of the tips and the occurrence of grooves, striations, and surface markings to be extracted. Kohlman and Richardson (1969) investigated the viability of using CO₂ (dry-ice) models for studying ablation. They developed a fabrication method for CO₂ models and noted several advantages over other low temperature ablators: the ablation products are safe, the sublimation rate is low in the sublimation temperature range (-78° C to -130° C), and the low temperature vapor pressure is the same order of magnitude as higher temperature ablators. Photographs were acquired a second apart to measure the recession rate and imbedded thermocouples in the model were used to infer the heat transfer. The use of camphor and dry ice models were used by Lipfert and Genovese (1971) to simulating re-entry ablation. The models were steel-tipped 15° half-angle cones mounted in a Mach 6 flow. Direct surface recession measurements were

made during each run. In addition, gas sampling probes as well as a boundary-layer survey apparatus were used to make measurements of boundary layer parameters. Camphor 5° half-angle cone models were also used by Griffith et al. (1977) to study the ablation effects in laminar flow conditions.

Callaway et al. (2008) and Callaway et al. (2010) used dry-ice as a low temperature ablating model material in a Mach 3 flow. Images were taken at 500 frames per second to determine the ablation rate in the preliminary study and high speed schlieren (1000 Hz) was used for visualization in the second study. Callaway et al. (2010) developed a method to capture the surface topology during a run. Photogrammetry was used to measure the 3D recessing surface. A dot projection technique using a low power laser system and three to four laser grids measured the recessing ablative surface. Two to three of the grids were focused on the model surface and another grid was focused on the tunnel floor to provide anchor points and the scale of the wind tunnel. The images were uploaded into PhotoModeler to extract measurements and the shape change could be quantified with sub-millimeter accuracy.

In addition, water ice has been utilized in the past to study ablation onset times. Sifton and Goldstein (2000) investigated the effects of a forward-facing cavity on severe heating and ablation onset times. Water ice was chosen as the low temperature ablative material due to it being inexpensive, well characterized, nontoxic, neither flammable nor corrosive, and having a low sublimation rate at low temperatures. A high speed video camera operating at 30 Hz was used to characterize the ablation onset time.

Patterns created during ablation, such as streamwise striations and crosshatching have also been studied using low-temperature ablators (Stock and Ginoux, 1971). Stock and Ginoux (1971) used wax cones with pointed steel tips to investigate crosshatching that occurs during re-entry. Stock (1975) investigated the cross-hatching phenomenon by

using camphor and wax models, and concluded that the viscosity of the ablation material influences the streamwise spacing of the pattern that develops.

2.2 NAPHTHALENE AS AN ABLATOR AND TRACER

Naphthalene ($C_{10}H_8$) is a polycyclic aromatic hydrocarbon that sublimates at low temperature. The naphthalene vapor absorbs light over a band extending from 220 nm to 310 nm (Figure 1.1) and it emits fluorescence over the range 300 nm to 400 nm (Figure 1.2), depending on the pump wavelength (Du, 1998). These absorption and emission properties allow naphthalene to be imaged using planar laser-induced fluorescence (PLIF). The naphthalene sublimation technique shares some characteristics with techniques that transpire a non-reacting fluorescent gas such as nitric oxide into the heat-shield boundary layer (Inman et al., 2008), but it adds the complexity that the ablation products result from a true, albeit simplified, ablation process.

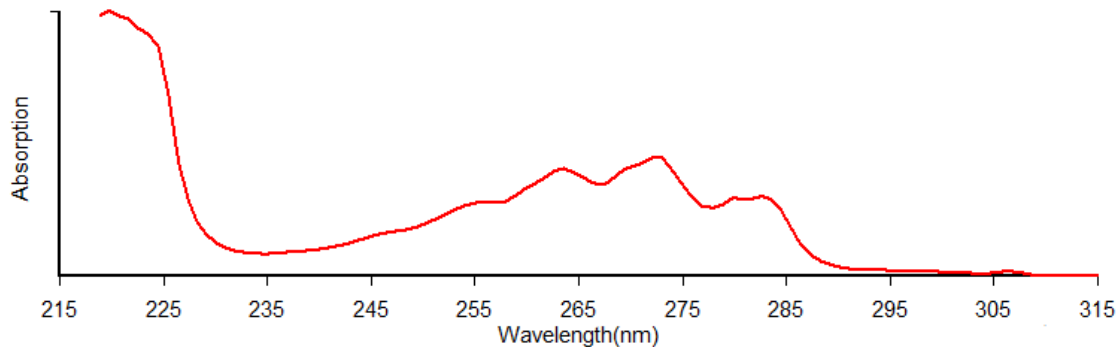


Figure 2.2 Absorption of naphthalene (Figure reproduced from Du (1998))

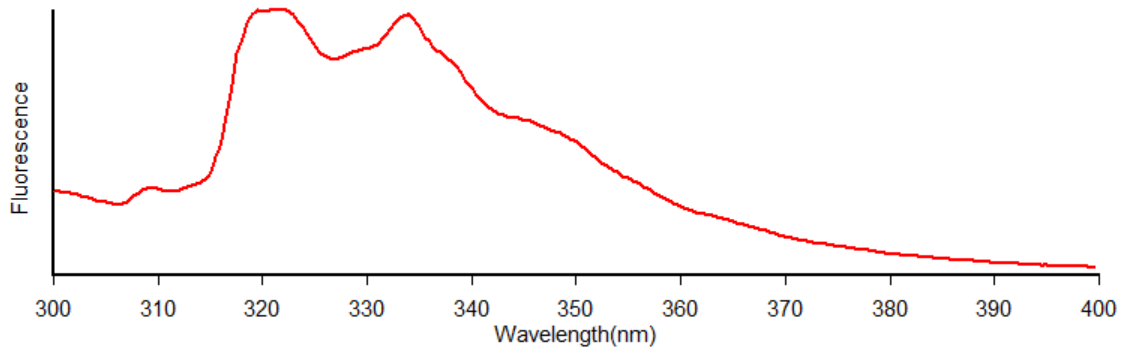


Figure 2.3 Emission of naphthalene (Figure reproduced from Du (1998))

Naphthalene is a solid in crystalline form at room temperature and has a melting temperature of 353 K. Relevant physical properties of naphthalene are given in Table 1. At temperatures lower than its melting point mass is removed by sublimation. Although the vapor pressure of naphthalene is very low at 300 K, the vapor pressure is strongly dependent on temperature and will increase by three times every 10 K increase in temperature (De Kruif et al., 1981). This strong temperature dependence allows for greatly increased sublimation rates at higher temperatures. The low melting point of naphthalene (353 K) makes naphthalene ideal for casting objects of complex geometry that also can be imbedded with measurement devices. Naphthalene can also be readily formed into virtually any simple shape by either machining it from preformed blocks with a mill, coating surfaces by dipping/spraying, and by sintering. Sintering is a

Table 2.1 Physical Properties of Naphthalene	
Molecular Formula	C ₁₀ H ₈
Molar Mass (kg/kg-mole)	128
Melting Temperature (K)	353 K
Vapor Pressure at 300 K (Pa) [14]	13.4 Pa
Vapor Pressure at 350 K (Pa) [14]	668.5 Pa

necessary solution for objects that require greater structural strength due to the more crystalline structure that is formed. In fact sintering can provides shear strength three times that of a cast model as well as providing a more homogenous structure (Charwat, 1968).

In the past, sublimating ablators, such as naphthalene, have been extensively used in low-speed flow applications to measure the convective heat transfer rate from surfaces. The heat transfer rate is inferred from the ablation rate by using the heat-mass transfer analogy. Essentially, the heat transfer rate is inferred from a measurement of the mass loss, either by weighing the ablated material or by measuring the recession depth (Goldstein et al., 1995). Furthermore, low-temperature sublimating ablators, such as camphor and naphthalene, have been used to determine nose-tip recession rates of supersonic projectiles (Charwat, 1968). Camphor has a higher melting temperature and so is often preferred for shape-change studies in some higher-enthalpy supersonic wind tunnels. Chartwat (1968) describes a method for sintering naphthalene by compressing it to 4000 psi to improve the shear stress from 55 psi (when casted) to 160 psi. Additionally, a procedure for measuring the local temperature of the surface of naphthalene was developed. A fluorescent powder was added to the naphthalene before sintering and was irradiated using an ultra-violet mercury lamp, which caused the surface to fluoresce with varying intensity for different temperatures.

To date, naphthalene PLIF has not been used in supersonic flows, but it has seen some use as a fuel marker in low-speed reacting flow experiments conducted by Kaiser et al. (2003). Kaiser et al. (2003) added 5% of 1-methylnaphthalene to a fuel stream and used PLIF to image the unburned fuel. The naphthalene fluorescence was excited using the 4th harmonic of an Nd:YAG laser, and the fluorescence was imaged using an image-intensified CCD camera (ICCD camera). In addition a two-color PLIF technique was

developed to measure temperature from a suitable ratio of different parts of the fluorescence spectrum with a single excitation wavelength (Kaiser et al., 2005). This technique was made viable by the measurements of Ossler et al. (2001), who showed that the absorption coefficient of naphthalene at 266nm was insensitive to temperature.

In Kaiser et al. (2005) the quenching of naphthalene fluorescence was seen to be dominated by oxygen at 500 K. In Ni and Melton (1996) the dependence of the naphthalene PLIF signal on temperature was used to image the temperature of the unreacted fuel in a jet flame. The fluorescence lifetime of naphthalene was found to decrease from 180 ns at 25 °C to 35 ns at 450 °C, which was used to calculate the temperature in oxygen-free environments. Lifetime-based thermometry techniques have the advantage that the concentration (absolute or relative) of the excited species is not required. Furthermore, a few studies have measured the rates of collisional quenching of naphthalene fluorescence. For example, quenching rates for naphthalene in N₂, O₂, and H₂O were measured by Martinez et al. (2004). The effect of temperature on the lifetime of naphthalene fluorescence was also studied in oxygen free environments by Ni and Melton (1996). A more detailed discussion of the spectroscopy of naphthalene is given in the section 2.4.

2.3 SPECTROSCOPIC MEASUREMENTS OF HYDROCARBON TRACER-MOLECULES

A great deal of insight into needed measurements can be obtained by consulting studies that investigated the spectroscopy of other complex hydrocarbons, such as acetone and 3-pentanone.

Ghandhi et al. (1996) and Grossmann et al. (1996) studied the pressure and temperature dependence of LIF of two keytones, acetone and 3-pentanone. Ghandi et al. (1996) studied the LIF signal in a temperature controlled jet and a motored engine. A quadrupled Nd:YAG laser (266 nm) beam was focused onto the jet output using a 1 m

focal length lens while a thermocouple monitored the output temperature of the jet. The fluorescence signal decreased with increasing temperature for both compounds, which was argued to occur due to shifts in the absorption spectrum. However, the fluorescence was found to be insensitive to pressure. Grossmann et al. (1996) studied the pressure and temperature dependence of the keytones using a heated, high-pressure cell, which had operating conditions of 383 to 650 K and 0 to 5000 kPa, and an excitation wavelength of 248, 277, and 312 nm. The pressure dependence for both molecules in synthetic air show the fluorescence intensity rises initially and then decreases after the initially increase. The authors argue that the initially increase is due to vibrational relaxation to levels with higher fluorescence quantum yields and the later decrease is due to quenching of the S_1 state with O_2 . The determined temperature dependence of the absorption strength was used to measure the temperature using the ratio of the fluorescence intensity of two different wavelengths

Acetone fluorescence temperature dependence has been thoroughly studied at six excitation wavelengths by Thurber et al. (1998). The temperature dependence of the absorption coefficient and fluorescence yield were extracted from measurements made of the fluorescence signal by normalizing the signal for the acetone number density and laser fluence. The temperature of the acetone seeded nitrogen jet was varied from 295 K to 1000 K by using a furnace with an optically accessible flow cell mounted inside it. Similar to Grossmann et al. (1996), Thurber et al. (1998) developed a technique to measure temperature by using the ratio of fluorescence signals when pumped with different excitation wavelengths. Specifically, five different excitation-wavelength combinations were used to obtain different temperature dependencies of the ratio of fluorescence signals.

Bryant et al. (2000) also investigated low temperature and low pressure effects of acetone laser induced fluorescence. They used a static gas chamber which could be cooled to 230 K and had a pressure range from .02 to 1 atm. The optically accessible cell was cooled by liquid nitrogen which flowed through copper tubing coiled around the exterior. Non-uniform cooling and icing and condensation of acetone vapor on the fused quartz windows provided challenging problems in this investigation. The flow rate of the liquid nitrogen had to be controlled around separate sections to reduce non-uniform cooling, while dry air was utilized to prevent icing. A jet of room temperature air across the windows was used to eliminate condensation on the windows.

2.4 NAPHTHALENE SPECTROSCOPY

The energy-level structure of the naphthalene molecule is complex because of the presence of a large-number of vibronic states that are entangled with one another.

Figure 1 shows a simplified illustration of the energy levels that are close to the photon energy of the fourth harmonic of the Nd:YAG laser ($\lambda=266$ nm or $\nu=37,600$ cm^{-1}), since this is the excitation frequency that is used in the current investigation.

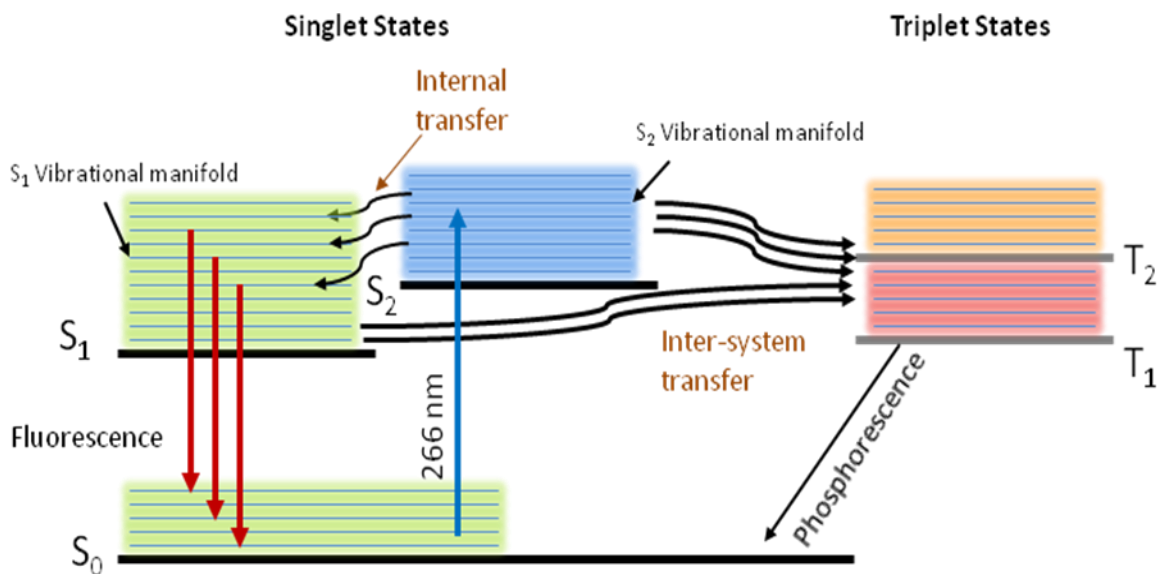


Figure 2.4 Vibrational-electronic energy level diagram of gas-phase naphthalene. *There are two electronic systems, singlet and triplet, where each electronic state is associated with a manifold of closely-spaced vibrational levels.*

The first and second excited singlet electronic states, denoted as S_1 and S_2 respectively, are located at an energy level of 32027 and 35815 cm^{-1} above the ground electronic state (S_0). Each electronic state is associated with a manifold of closely-spaced vibrational energy levels. These vibrational levels are classified as either a “totally symmetric” (TS) or “non-totally-symmetric” (NTS), depending on the symmetry of the vibration. In general, the vibrational levels in the TS group have a shorter lifetime compared to the NTS group (Behlen et al., 1981). In addition, since the energy level difference between the S_1 and the S_2 states are quite small, the vibrational manifolds of the two states overlap and form a larger entangled manifold.

There also exist excited triplet vibronic states T_1 and T_2 , whose energy level structure is very similar to the singlet levels S_1 and S_2 . In Figure 2.1, the excitation by a

266 nm photon is illustrated, which excites the naphthalene molecule from the ground state to the second excited state, S_2 . Almost all of the excited molecules undergo an “internal conversion” to the vibrational levels of S_1 (Laor and Ludwig, 1971). This conversion from the higher singlet state to the lowest excited singlet state is a radiationless process and is a purely intramolecular process (Watts and Strickler, 1966). The internal conversion process takes place much faster than the fluorescence lifetime of the $S_2 \rightarrow S_0$ transition (Stockburger et al., 1975b). Most of the fluorescence, therefore, results from $S_1 \rightarrow S_0$ vibronic transitions even though the S_2 state is pumped. Excitation to the third excited state, S_3 , takes place at 42000 cm^{-1} . The radiative lifetimes observed when exciting the S_3 state is much different than when exciting the S_1 and S_2 state due to vastly different processes regarding quantum yields, intersystem crossing, and emission spectra (Laor and Ludwig, 1971).

A fraction of the molecules in the S_1 and S_2 states makes an “inter-system transfer” to triplet vibronic states T_1 and T_2 . The inter-system crossing from the S_1 state can best be described as a crossing from the S_1 to T_2 or other higher triplet state which is then followed by an internal conversion from the T_2 or higher state to the T_1 state (Ashpole et al., 1971). The rate of inter-system transfer increases with increasing pressure. For example, the inter-system transfer is considerable for pressure over 150 torr (Beddard et al., 1973). Soep et al. (1973) found that as the pressure of the gas decreases the triplet yield of naphthalene decreases almost to zero and that the inter-system crossing process in naphthalene appears to be practically irreversible. The molecules in the triplet states T_1 and T_2 undergo both collisional de-excitation and radiative transition. The radiative transitions from the triplet to the ground (singlet) state represent long-lived phosphorescence with a lifetime of order milliseconds. The inter-system transfer, however, is small for 266 nm excitation, and so the dominant emission is $S_1 \rightarrow S_0$.

Several studies have also investigated different aspects of naphthalene fluorescence. The fluorescence signal with units of photons, under the assumption of broadband detection and weak excitation, is given by:

$$S_f(P, T) = \frac{E_L}{hc/\lambda} \eta_{opt} \Delta V \chi_{naph} n(P, T) \sigma(\lambda, T) \phi(\lambda, T, P, \chi_i) \quad (2.1)$$

where E_L is the laser fluence (J/m^2), h is Planck's constant, c is the speed of light, λ is the wavelength of the laser, η_{opt} is the collection optics collection efficiency, ΔV is the probe volume, χ_{naph} is the naphthalene mole fraction, n is the total number density, σ is the absorption cross-section, ϕ is the fluorescence yield, P is pressure and T is temperature. If we assume that the fluorescence results from the S_1 state, and that the spontaneous emission rate and electronic quenching rates are the same for each state, then we can write the fluorescence yield as,

$$\phi(\lambda, T, P, \chi_i) = \frac{k_f}{k_f + k_{int} + k_Q} \quad (2.2)$$

where k_f is the rate of spontaneous emission, k_{int} is the rate of de-excitation of S_1 not due to collisions, and k_Q is the collisional quenching rate. Here we model the quenching rate as,

$$k_Q = \sum_i n_i \sigma_i \langle v \rangle_{i-Na} \quad (2.3)$$

where n_i is the number density of colliding species i , σ_i is the quenching cross section of species i , and $\langle v \rangle_{i-Na}$ is the mean relative speed between species i and naphthalene.

When naphthalene is seeded in air, oxygen is the dominant quencher, as reported by Martinez et al. (2004), and Kaiser and Long (2005). Thus we have:

$$k_Q = n_{O_2} \sigma_{O_2} \langle v \rangle_{O_2-Na} \quad (2.4)$$

When the species is excited by a short-pulse laser, the fluorescence decay typically follows an exponential form with time-decay constant. There are two electronic systems, singlet and triplet, where each electronic state is associated with a manifold of closely-spaced vibrational levels.

$$\tau_f = (k_f + k_{int} + k_Q)^{-1} \quad (2.5)$$

The equations above are for an extended two-level model with broadband detection, and they are reasonable approximations under some conditions, but take caution that they can be highly inaccurate in others (e.g., low pressure).

A study by Sockburger et al. (1975a) has focused on understanding the single vibrational level fluorescence at low pressure and at near absolute zero temperature. A vibronic coupling theory is used to interpretate the vibrational structure. Gattermann and Stockburger (1975) have investigated the intersystem transfer to the triplet states and the corresponding phosphorescence. A triplet lifetime from the 0_0^0 band of 4.2 μ s was derived.

The fluorescence lifetimes and quantum yields of the first and higher excited states have been studied by several groups. A detailed review of the studies on fluorescence and non-radiative lifetimes and the quantum yields for different vibronic states is given by Avouris et al. (1977). The fluorescence lifetimes and quantum yields have been found to decrease with increasing excitation energy (Beddard et al., 1974). A

work by the same group, Beddard et al. (1973), observed naphthalene fluorescence decay time as a function of pressure in argon gas. For short excitation wavelength (< 305 nm), the lifetimes and yields were found to increase with increasing pressure, while they decrease with increasing pressure for longer excitation wavelengths (> 305 nm). They proposed that the increase in lifetimes and yields with increasing pressure for short excitation wavelengths could be attributed to collisionally induced intramolecular vibrational redistribution. The higher energy vibrational modes have a shorter fluorescence lifetime, thus as the pressure increases the Boltzmann distribution of the S_1 state forms and the lifetimes increase and become independent of pressure and wavelength. The fluorescence decay waveform was reported to be bi-exponential by Reyle and Brechignac (2000) and Behlen and Rice (1981). The bi-exponential trace is because of the simultaneous decay of two types of vibronic states. The timescale of the longer lifetime transitions was about $1 \mu\text{s}$ and the shorter lifetime ranged between 85 to 400 ns (Reyle and Brechignac, 2000).

The shorter duration decay corresponds to the fluorescence of the vibronic states of S_1 level. The range of lifetimes within the S_1 vibronic states is because of the differences in the lifetime of different groups of vibrational levels, which differ in their symmetry. For the present investigation, the fluorescence decay corresponds to the vibronic states of S_1 level only. Most of the above fluorescence decay measurements were performed in a vibrationally frozen condition (very low temperature) and at extremely low pressures. At these conditions, the effect of collisional de-excitation is not present. Suto et al. (1992) and Schlag et al. (1971a) performed fluorescence decay measurements at a temperature of about 300 K. They reported a much smaller quantum yield and fluorescence lifetime compared to the single vibrational level measurements. Hsieh et al. (1974) and Lim and Huang (1973) observed the fluorescence lifetimes of

naphthalene in a collision-free conditions from which they extracted the nonradiative decay rate. They reported a break in the nonradiative decay rates versus excitation energy at photon energy corresponding to the S_2 state. The authors suggested that the S_2 to S_1 internal conversion causes a change in the vibrational distribution. This distribution is maintained through the time scale of the S_1 radiationless decay, which leads to the conclusion that the intramolecular vibrational energy redistribution is not a fast process and collisions are necessary to affect the vibrational distribution.

Only a few studies have focused on measuring electronic quenching rates of gas-phase naphthalene. For example, quenching measurements of oxygen, nitrogen, methane, noble gases and nitric oxide have been reported but only at a limited range of conditions by Behlan and Rice (1981), Kaiser and Long (2005) and Martinez et al. (2004). Oxygen is reported to be one of the major quenching agents of naphthalene and its quenching effect was studied by Kaiser and Long (2005) and Martinez et al. (2004). Kaiser and Long (2005) measured the quenching of naphthalene by oxygen and nitrogen at room temperature and above. They reported that oxygen dominates the quenching process. Similar conclusions were drawn by Martinez et al. (2004) who measured O_2 and N_2 quenching rates with an excitation at 308 nm at low pressure. They found that the O_2 quenching cross-section is about an order of magnitude larger than that of N_2 . A study by Ossler et al. (2001) observed the temperature dependence of the quenching cross-section of naphthalene. The decay rate of naphthalene fluorescence was examined in the temperature range of 400 to 1000 K and the quenching cross-section was extracted. In addition, at temperatures below 540 K a Stern-Volmer behavior shows the decay rate of naphthalene fluorescence was found to increase with an increase in the partial pressure of oxygen, which was similarly observed by Kaiser et al. (2005) at 500 K. At higher

temperatures this Stern-Volmer behavior was seen to break down and a second order dependence on the oxygen concentration appeared.

Chapter 3: Experimental Program

The following chapter details the experimental facilities, design and operation of experiments, and the experimental techniques used to acquire all data in this investigation.

3.1 FACILITIES

The wind tunnel experiments were conducted at the High-Speed Wind Tunnel Laboratory located at the Pickle Research Campus of the University of Texas at Austin. Complementary investigations of fluorescence linearity, and temperature/pressure dependence were conducted in a temperature-controlled jet of naphthalene exhausting into atmospheric conditions or a pressure-controlled cell.

3.1.1 Mach 5 Wind Tunnel Facility

The naphthalene ablation experiments were conducted in the blowdown Mach 5 wind tunnel facility as shown in Figure 3.1. The Mach 5 tunnel is driven by a 2550 psia pressure tank that is charged either by a Worthington HB4 four-stage compressor or a Norwalk four-stage compressor. The air was stored in eight high pressure tanks with total volume of 4 m³ (140 ft³). During each run the stagnation pressure was kept at 2.52 MPa (360 psi) by a 1.5 in. Dahl valve operated by a Moore 352 controller and exhausts to the atmosphere. The air is heated before the test section by two banks of 420 kW nichrome wire resistive heaters controlled by a Love Controls 1543 controller to give a variable stagnation temperature from 345 K to 380 K. The stagnation pressure was monitored by a Setra 204 pressure transducer and the stagnation temperature was monitored by a J-type thermocouple.

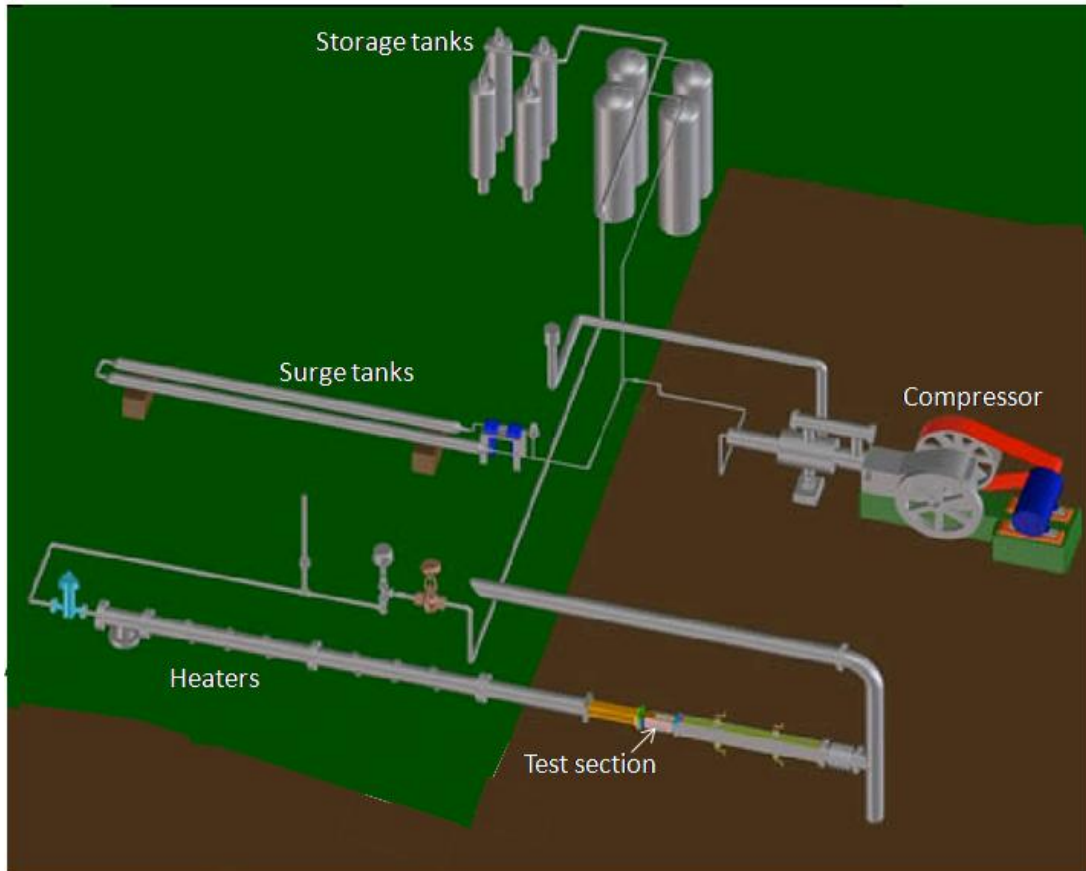


Figure 3.1 Schematic of the Mach 5 blowdown facility located at the Pickle Research Campus of the University of Texas at Austin

The Mach 5 test section for the wind tunnel was 152 mm (6 in.) wide by 178 mm (7 in.) tall by 762 mm (27 in.) long. The freestream Mach number was $M_\infty = 4.95$, Reynolds number was $Re_\infty = 49.5 \times 10^6 \text{ m}^{-1}$ ($15.1 \times 10^6 \text{ ft}^{-1}$), and velocity was $U_\infty = 750 \text{ m/s}$. The freestream turbulence intensity is less than 0.3%. Optical access to the flow was provided by a fused silica window mounted on the sidewall measuring 381 mm (15 in.) long, 51 mm (2 in.) tall, and 19 mm (.75 in.) thick

3.1.2 Temperature Controlled Jet of Naphthalene Facility

The investigations of naphthalene fluorescence linearity, and temperature/pressure dependence were conducted in a temperature-controlled jet of naphthalene exhausting into atmospheric conditions or a pressure-controlled cell. The naphthalene jet was driven by a 90 psia pressure tank charged by the house air compressor or a compressed air bottle of nitrogen, industrial air, breathing air, or ultra zero air. During each run the mass flow rate was monitored using an Omega FMA-1610-NIST mass flow meter and controlled using a needle valve. The pressure cell was made of a Kurt J. Lesker Company CF flanged 6-way cross with tube outer diameter of 2 $\frac{3}{4}$ in. (Part No. C6-0275). The pressure cell was drawn to a vacuum using a large vacuum reservoir drawn down by a two stage Roots Connorsville Rotary Positive Vacuum Pump. The pressure in the pressure cell was monitored by a MKS Baratron Capacitance Manometer (Type 626) and could be set between 1 kPa to 40 kPa. The temperature of the jet was controlled using a Omegalux AHPF-102 In-Line Air Heater. The in-line heater was capable of heating the jet from 297 K to 550 K by using a Staco Energy Products Variable Autotransformer (Type 3PN1010) to control the voltage to the heater. The temperature of the jet was monitored using a type-J thermocouple when exhausted to atmospheric conditions and type-T thermocouple when exhausted to the pressure controlled cell.

The jet diameter was 12.7 mm (.5 in.) when exhausting into atmospheric conditions and 19.1 mm (.75 in.) when exhausting into the pressure controlled cell. Optical access to the flow was provided by a fused silica window measuring 38.1 mm (1.5 in.) in diameter and 6.34 mm (.25 in.) thick.

3.2 NAPHTHALENE MACH 5 WIND TUNNEL FLOOR MODEL

The Mach 5 wind tunnel experimental models were flush mounted floor models. There were two versions of the floor model created, one for a first campaign that was very preliminary to show feasibility and the second for the second campaign that had been optimized for improved diagnostics.

3.2.1 First-Campaign Floor Model

The original model contained a naphthalene plug that was 50.8 mm (2 in.) wide by 25.4 mm (1 in) long. This model was developed in two stages. The first stage consisted of a creating a model with a cavity that had no method to secure the naphthalene plug in place after it had been poured. Testing this model in the wind tunnel resulted in the naphthalene plug being sucked out of the cavity and into the flow. Therefore, the design was modified by consisted of adding a 6.35 mm (.25 in.) lip around the naphthalene to secure it in the plug. This model is shown in Figure 3.2. The model was designed so the naphthalene would be cast inside it after a plate is installed over the top. There were two fill holes that opened into the cavity, one of which allowed the molten naphthalene to be poured into and the other allowed for air to escape.

The naphthalene pouring procedure was developed with the first floor model. The naphthalene crystals were melted using a hot plate as seen in Figure 3.3. The naphthalene was then poured into the floor model with the molding plate installed over the open cavity, so as to seal the cavity. Once the naphthalene solidified the cover was

removed, and the resulting surface was relatively flat and smooth. The naphthalene was allowed to solidify for approximately 12 hours before use. The molding plate was then removed and any excess naphthalene that was not flush with the floor plug was sanded down using fine grit sandpaper (800 grit or better). Once the naphthalene was sanded the resulting surface was relatively flat and smooth, as shown in Figure 3.4. The model was then ready to be installed into the wind tunnel as shown in Figure 3.5.

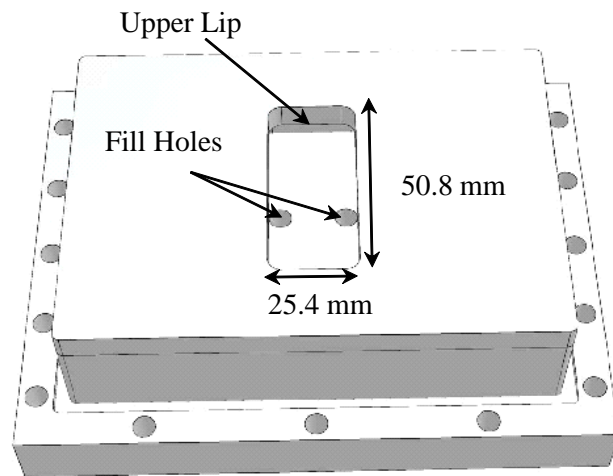


Figure 3.2 Schematic of the first campaign naphthalene floor plug



Figure 3.3 Naphthalene crystals melting on a hot plate

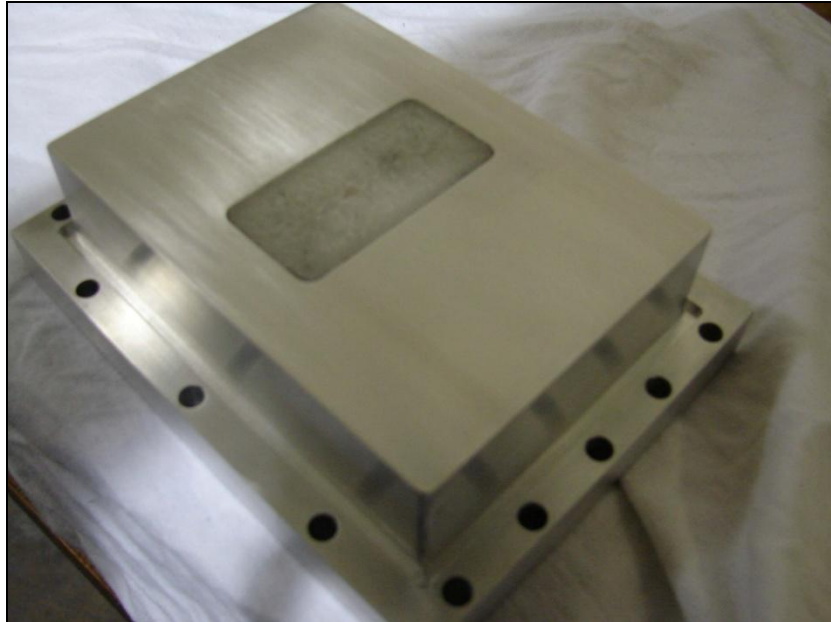


Figure 3.4 Naphthalene floor plug after molding plate is removed

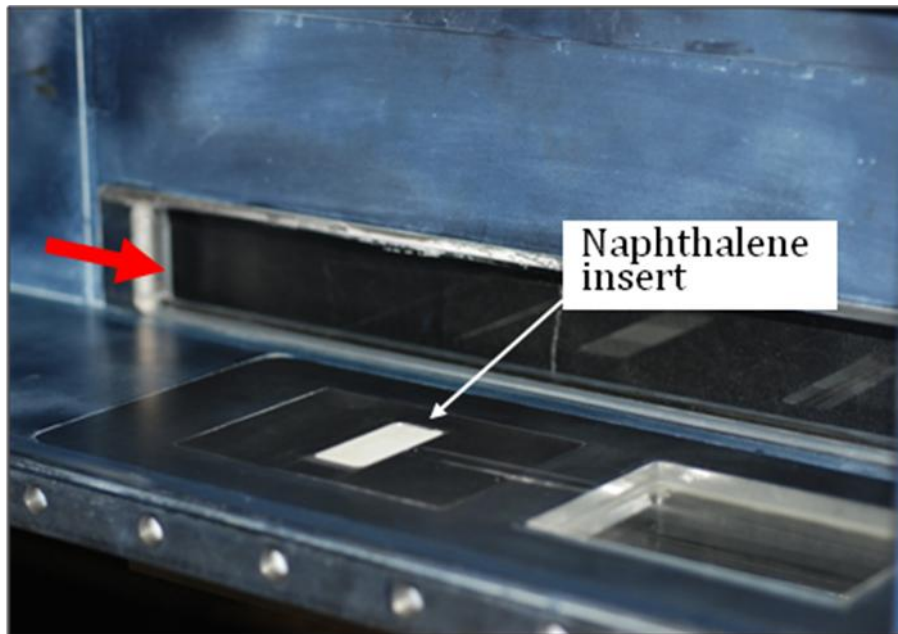


Figure 3.5 Naphthalene floor plug installed into test section

3.2.2 Second-Campaign Floor Model

The second model design increased the size of the naphthalene plug to be 101.6 mm (4 in.) long by 57.2 mm (2.25 in.) wide. This design is shown schematically in Figure 3.6. This model had a 6.35 mm (.25 in.) lip around the naphthalene so as to secure it in the plug and prevent the plug from being sucked into the wind tunnel.

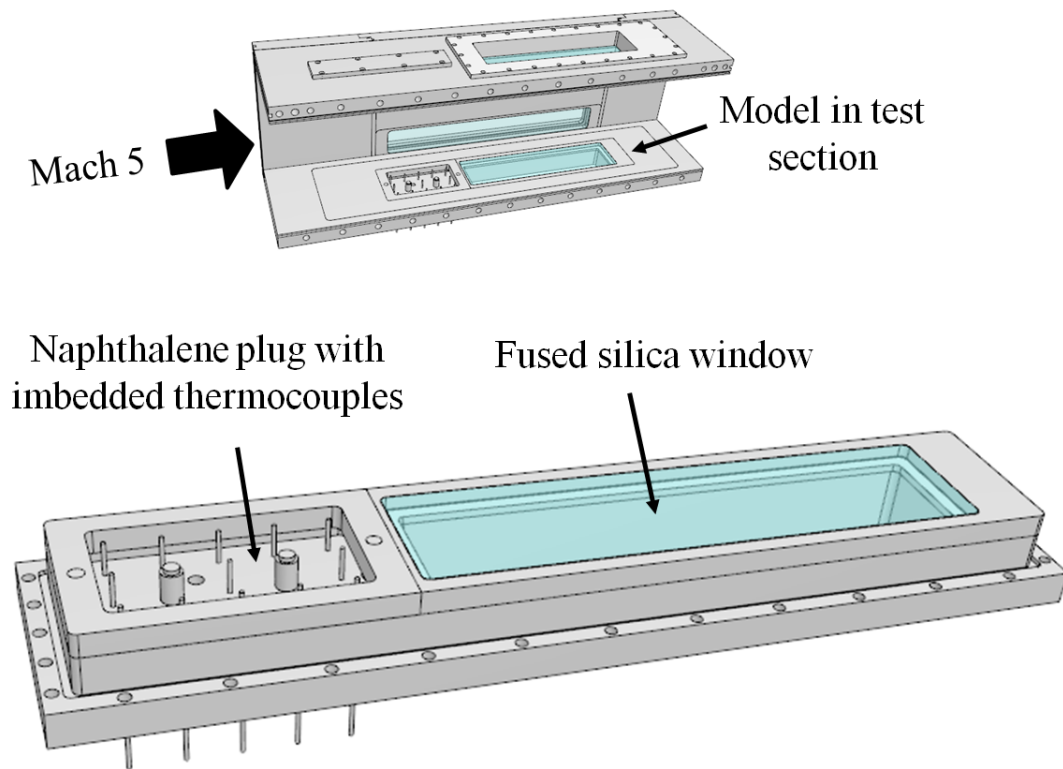


Figure 3.6 Second-campaign naphthalene floor plug installed in the Mach 5 wind tunnel

The naphthalene plug could be imbedded with up to 15 thermocouple equally spaced in a 5 by 3 array 22.2 mm (.875 in) apart, with 5 installed length wise at three span wise positions as seen in Figure 3.7. The closest the thermocouples could be to the edge of the naphthalene plug was 6.35 mm (.25 in). This space prevented any non-homogenous effects in the solidified naphthalene plug that could occur during pouring. The thermocouples could be imbedded at the any depth within the naphthalene or at the surface of the naphthalene plug at each position. In the design heat flux sensors could replace two of the center line thermocouples and could be imbedded in the naphthalene. In addition, a heat flux sensor or thermocouple could be installed 6.35 mm (.25 in.) upstream and downstream of the naphthalene plug.

A fused silica window was added downstream of the naphthalene plug to allow for the laser sheet to pass through the floor, thus reducing reflections. The optical access enabled a field of view that ranged from 23.5 mm (.925 in.) to 264.8 mm (10.425 in) downstream of the downstream edge of the naphthalene plug, as seen in Figure 3.8. Moreover, the fused silica optical access from all sides of the test section enabled plan-view imaging. The plan-view imaging can range from from 23.5 mm (.925 in.) to 264.8 mm (10.425 in) downstream of the downstream edge of the naphthalene plug, which is identical to the side-view measurements.

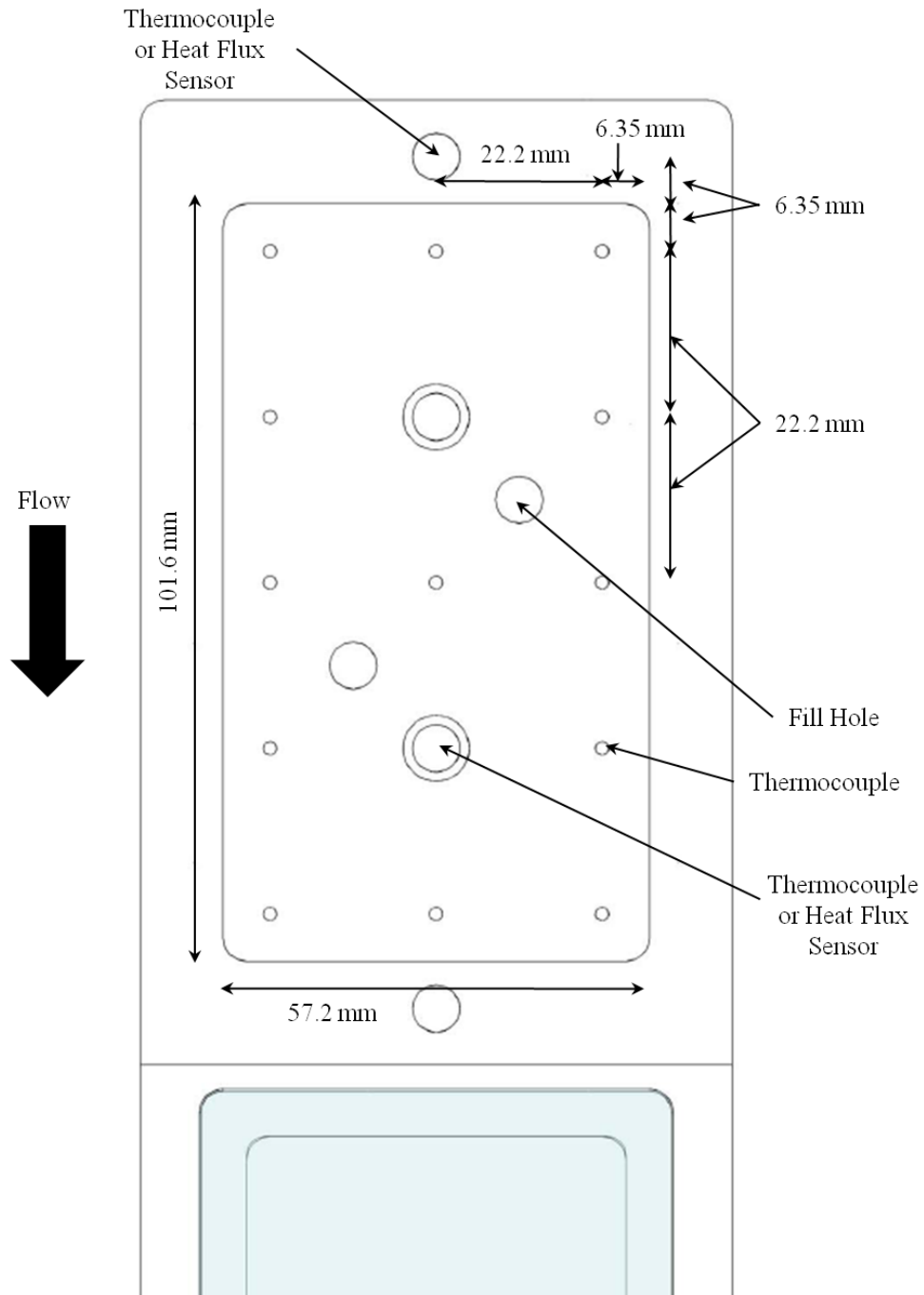


Figure 3.7 Dimensions of the naphthalene plug and thermocouple/heat flux sensor locations in the second campaign naphthalene floor plug

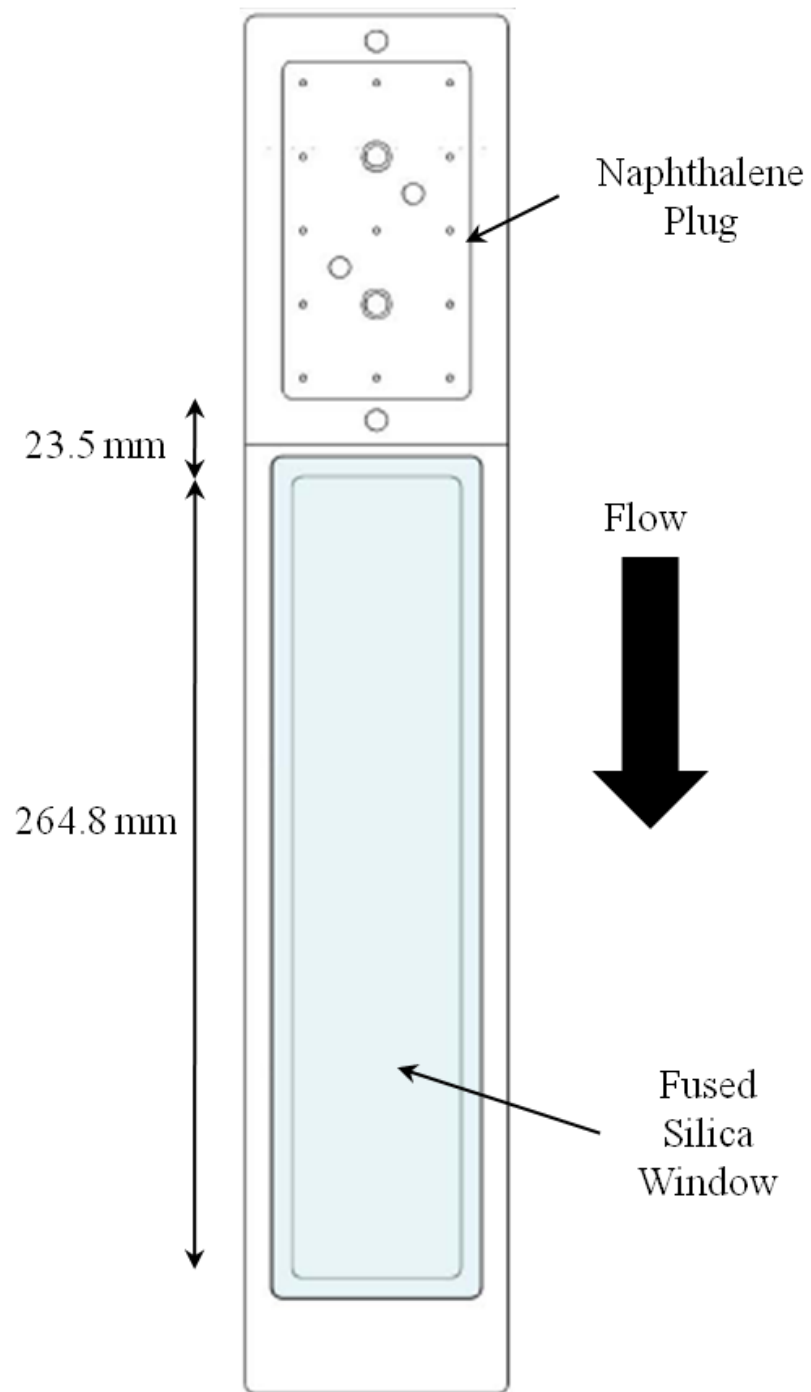


Figure 3.8 Dimensions of the downstream fused silica window in the second campaign naphthalene floor plug

The naphthalene plug was formed using a similar molding procedure as in the first campaign model. This procedure entailed heating solid naphthalene past its melting point, then pouring it into the naphthalene plug. The fused silica window was removed during the pouring procedure, so it would not become damaged, and the molding plate was installed over the cavity. The thermocouples were installed before the molding procedure and were positioned such that they were imbedded within the naphthalene after it has solidified. After the naphthalene solidified, the molding plate was removed and the plug was installed into the test section floor (Figure 3.9).

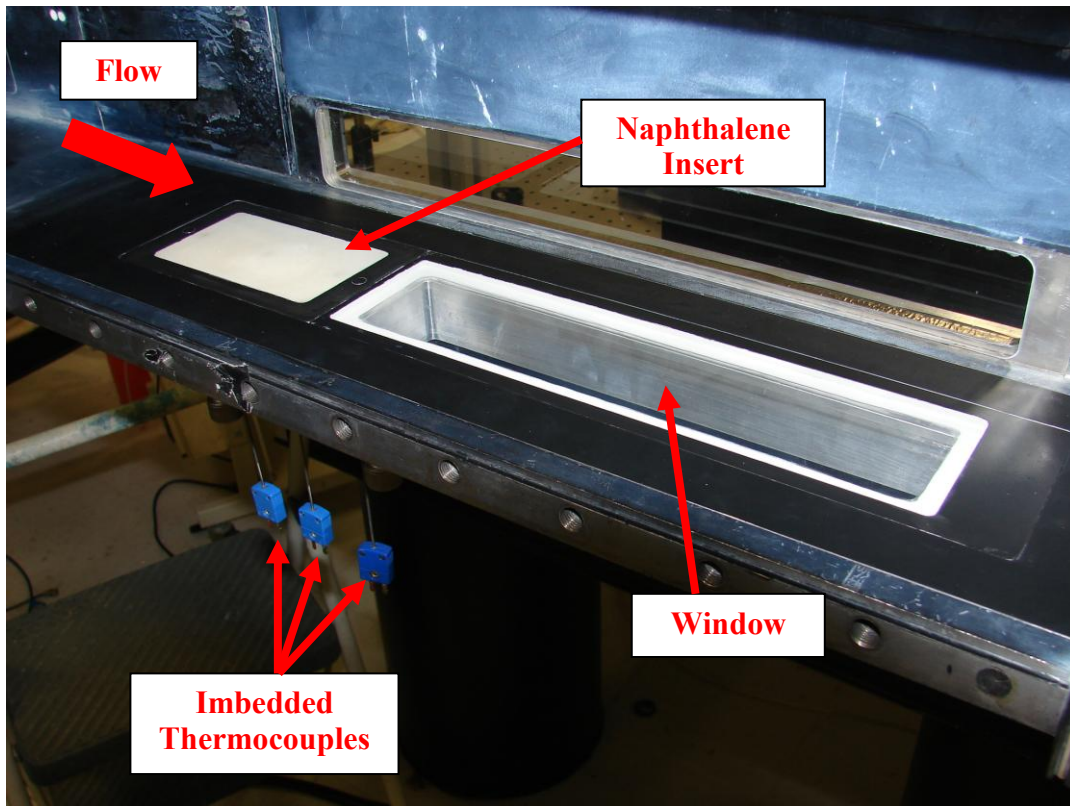


Figure 3.9 Second campaign naphthalene floor plug installed in the Mach 5 wind tunnel test section

3.3 NAPHTHALENE LIF COMPLEMENTARY INVESTIGATIONS

3.3.1 Fluorescence Linearity Measurement System

A jet of naphthalene-laden air exhausting into atmospheric conditions was used to study the saturation effects of the naphthalene fluorescence. The schematic of the setup is shown in Figure 3.10. Air from the house air compressor was passed through a cell filled with naphthalene crystals. The naphthalene concentration was saturated at a constant room temperature of 298 K. The flow rate was monitored and kept at 10 SLPM using a needle valve. This vapor-laden flow was then passed through the in-line heater (Omegalux AHPF-102), which was turned off during this investigation. A jet was formed as the flow exits from a 12.7 mm (.5 in.) tube. To avoid condensation of the naphthalene on the walls of a test cell, these measurements were made in a free jet. The fluorescence was excited with a quadrupled Nd:YAG laser (Spectra- Physics Model PIV 400) operating at 266 nm. The beam was passed through a varying number of fused silica flats, which are used to change the energy of the beam. A total of sixteen fused silica flats were used. To obtain the lowest fluences, a 90 percent beam splitter was used along with the fused silica flats. A 1m spherical lens was used to focus the beam in order to reduce the beam diameter to significantly less than the outlet diameter of 12.7 mm. The 1 m spherical lens was placed 292 mm away from the center of the jet. The beam propagation direction was perpendicular to the axis of the jet. A PixelVision SpectraVideo Model SV512V1 back-illuminated CCD camera (512 x 512 pixels) was used to image the naphthalene fluorescence in the potential core of the jet. The camera was shuttered to 99 ms so as to only capture one laser pulse per frame. The linearity of the LIF signal was studied by changing the energy of the beam while keeping the temperature constant.

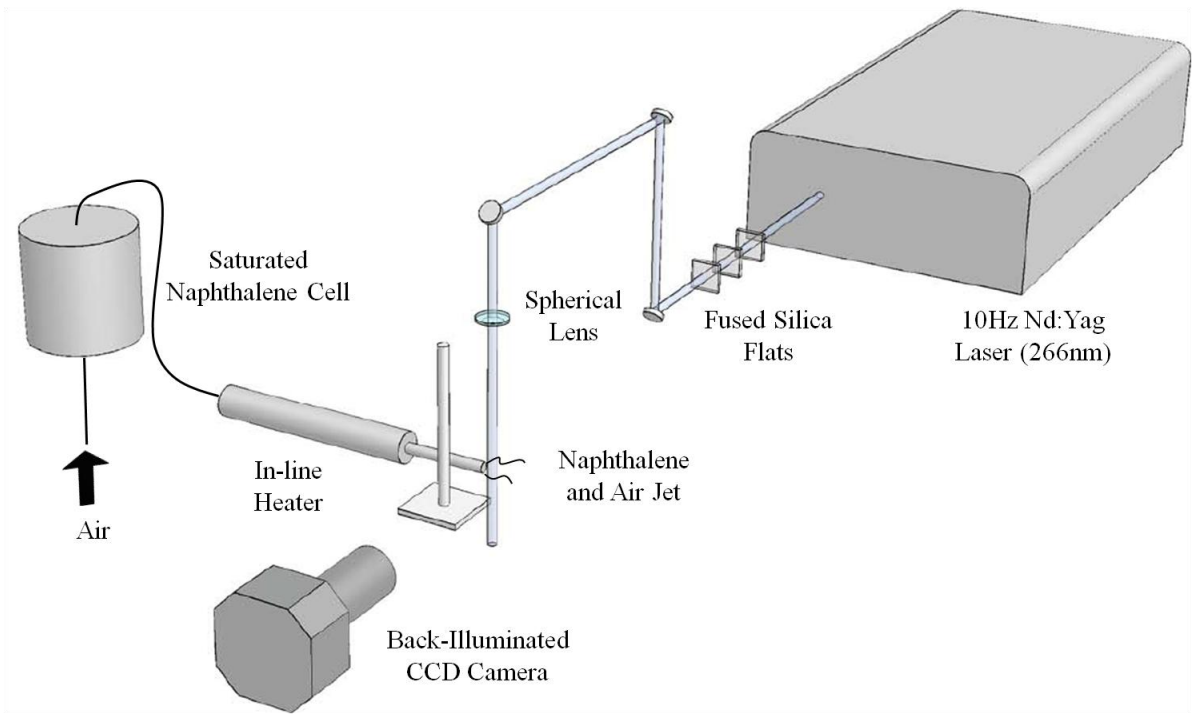


Figure 3.10 Naphthalene LIF linearity measurement and temperature dependence setup

3.3.2 Temperature Dependence Measurement System

In a related experiment the temperature dependence of the naphthalene fluorescence from 297 K to 525 K was investigated by varying the temperature of the jet while keeping the energy constant. The energy was kept low enough to be within the linear regime using a fixed number of fused silica flats. The experimental setup is displayed in Figure 3.13. The vapor-laden flow exiting the saturated naphthalene cell was passed through the in-line heater (Omegalux AHPF-102) capable of heating the air to 525 K. A type-J thermocouple was used in conjunction with an Omega Type-J Thermocouple Thermometer (Model 650) to monitor the outlet temperature of the jet.

The jet issued into atmospheric pressure and the flow rate was maintained at 30 SLPM. The inlet air temperature to the saturated naphthalene cell was monitored using the flow meter, so the naphthalene concentration in air could be corrected for changing vapor pressure.

3.3.3 Pressure Dependence Measurement System

The experiments to investigate the pressure dependence of the LIF signal were conducted in a temperature controlled jet of naphthalene-vapor laden air exhausted into a pressure controlled cell. The experimental setup is the same as in Figure 3.9 except instead of exhausting into atmospheric conditions the jet is exhausted into a vacuum cell (Kurt J. Lesker Company CF flanged 6-way cross with tube outer diameter of 2 $\frac{3}{4}$ in., Part No. C6-0275), as shown in Figure 3.11. The cell had fused silica windows on three sides to allow for the 266nm laser beam to pass through and for imaging the fluorescence. The cell was kept at a constant pressure (vacuum) by flowing the gas through a metering valve and then into a large vacuum chamber kept at a vacuum using a two stage Roots Connersville Rotary Positive Vacuum Pump. To determine the pressure dependence of the naphthalene fluorescence decay, the pressure in the test cell was varied from 1 kPa to 40 kPa, while keeping the mass flow rate at 30 SPLM. The jet was kept at a constant temperature of 297 K and was monitored by a type-T thermocouple. If not cleaned after every run, the naphthalene would condense on the windows and would be burned by the absorption of the laser light. The fluorescence decay signal was measured using a 1P28 photomultiplier tube (PMT) with a 60 mm fused silica focusing lens. Three Schott WG-295 filters and two Schott UG-5 filter were used to transmit the fluorescence (in the range 295nm to 400nm), while rejecting most of the elastically scattered light. The laser energy was set at few tens of micro joules to avoid non-linear effects in the PMT.

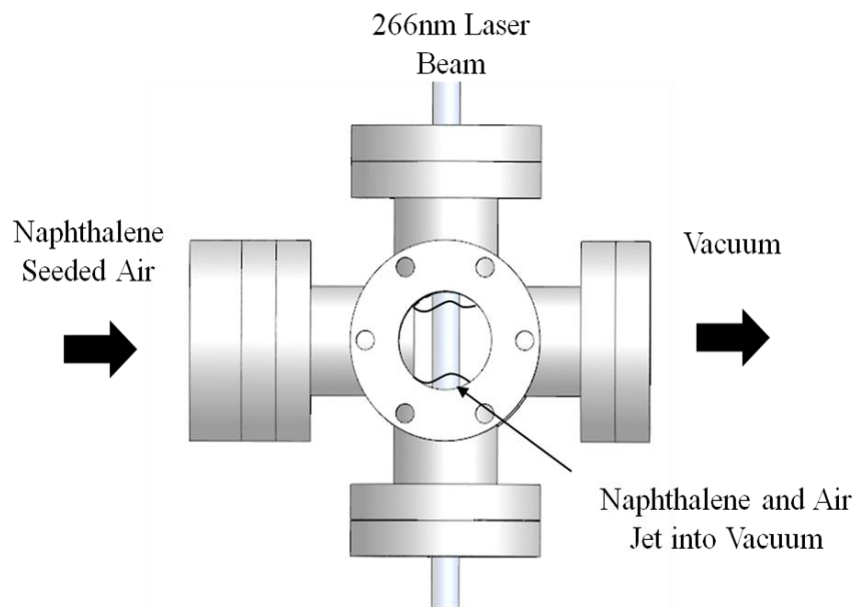


Figure 3.11 Naphthalene LIF pressure dependence measurement cell

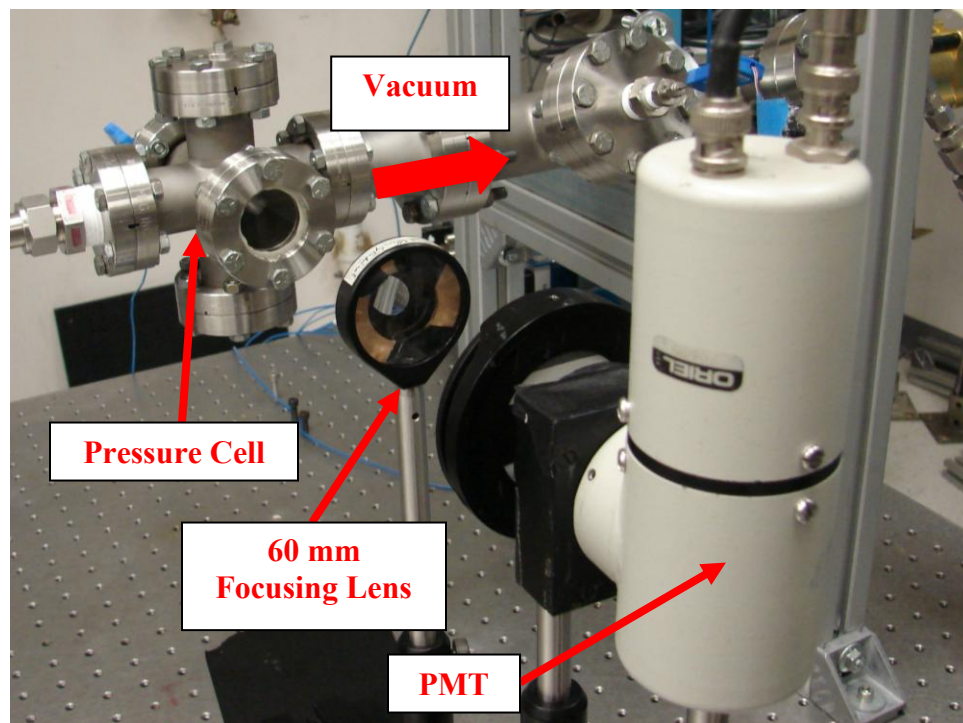


Figure 3.12 Naphthalene LIF pressure dependence measurement setup

3.4 MACH 5 WIND TUNNEL PLIF SYSTEM

Planar laser induced fluorescence (PLIF) was used to visualize the naphthalene scalar field in the Mach 5 wind tunnel. A concise description of this method, the PLIF system setup, and the image processing procedure, are discussed below.

3.4.1 Planar Laser Induced Fluorescence (PLIF)

Eckbreth (1988) has an in depth description of the PLIF technique that will be truncated below. The planar laser-induced fluorescence (PLIF) technique typically involves the excitation of atomic/molecular electronic transitions, which in this case occurs at UV wavelengths for naphthalene as discussed in Chapter 1. The PLIF technique utilizes a laser sheet which can be used to obtain quantitative information of two-dimensional slice of the flowfield.

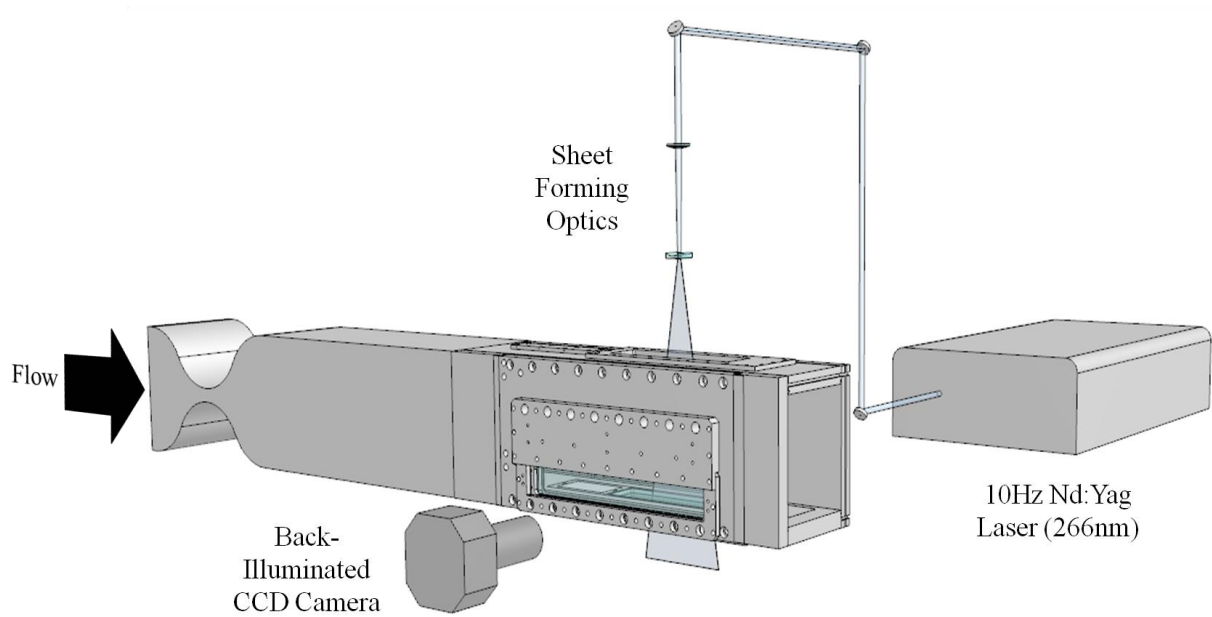
Laser induced fluorescence (LIF) is species specific and allows for the measurement of minor species, such as naphthalene vapor from sublimation, in flows. In this technique the absorption of a photon of light from a laser is used to excite the atom or molecule from a lower energy state into a higher energy state. The excited state is in non-equilibrium and thus will return to equilibrium, which for naphthalene the process is outlined in section 2.4. In returning to ground state a photon of light may be emitted. This can be imaged and can lead to quantitative information of the flowfield.

In general, LIF signals are a function of several flow variables, including pressure and temperature. However, predicting the effect of pressure and temperature on the signal can be challenging because this usually necessitates that a model be developed describing the physics of the excitation/de-excitation processes. Therefore, developing an understanding of the naphthalene LIF physics, and thus how the signal depends on thermodynamic variables is one of the main objectives of complementary investigations.

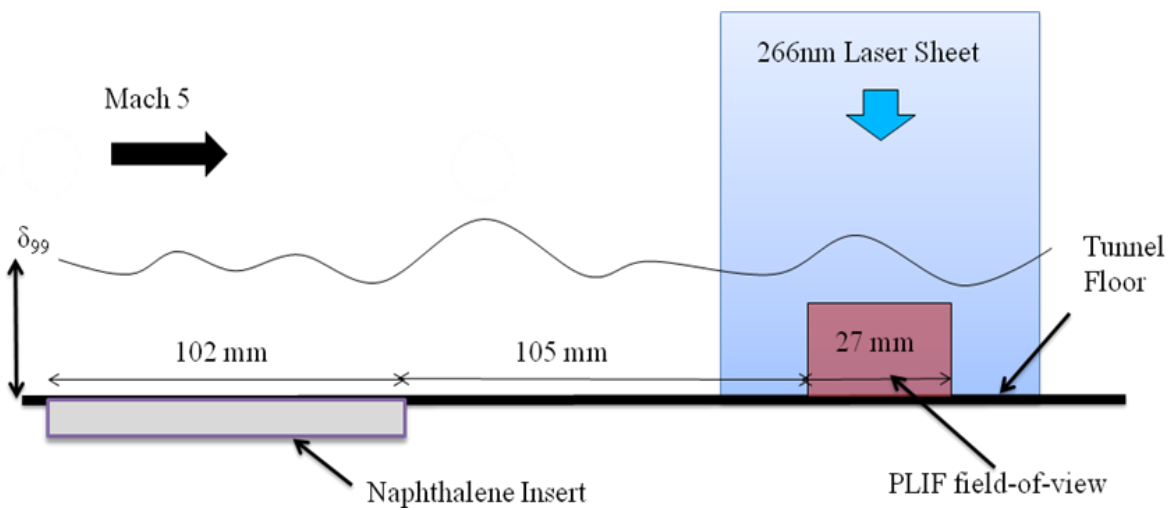
3.4.2 PLIF System Setup

A schematic of the PLIF system setup in the Mach 5 wind tunnel is shown in Figure 3.13. The naphthalene fluorescence was excited with a laser sheet from a quadrupled Nd:YAG laser operating at 266 nm. Fused silica windows were downstream of the naphthalene insert to enable the laser sheet to pass through the test section and reduce reflections. An intensified CCD camera (Princeton Instruments PI-Max) imaged the fluorescence through a fused silica window in the tunnel side wall during the use of the first campaign floor model. A back-illuminated CCD camera (PixelVision SpectraVideo Model SV512V1) imaged the fluorescence during the use of the second campaign floor model. The image resolution was 512 x 267 pixels and the exposure time was 80 ms, capturing one laser pulse per frame. The cameras were fitted with a 100 mm focal length, f/2.8 UV lens (Eads Sodern Circo) operated at full aperture. Three Schott WG-295 filters and one Schott UG-5 filter were used to pass the fluorescence (in the range 295nm to 400nm), while rejecting most of the elastically scattered light. The imaging field of view was 27 mm (1.06 in.) wide by 14 mm (.55 in.) tall. Figure 3.14 shows an image of the camera and naphthalene plug in the test section.

The sublimation rate at standard conditions is quite slow and no noticeable mass is lost even if the insert sits for hours without flow. Only a small amount of ablation (less than a fraction of a millimeter) is observed over the course of a 1 minute wind tunnel run. Therefore the naphthalene plug does not need to be recast after each run. The plug was recast after approximately every 7 to 10 runs



(a)



(b)

Figure 3.13 Schematic diagram of the naphthalene PLIF setup in the Mach 5 wind tunnel.
(a) Overall assembly and (b) inside the test section

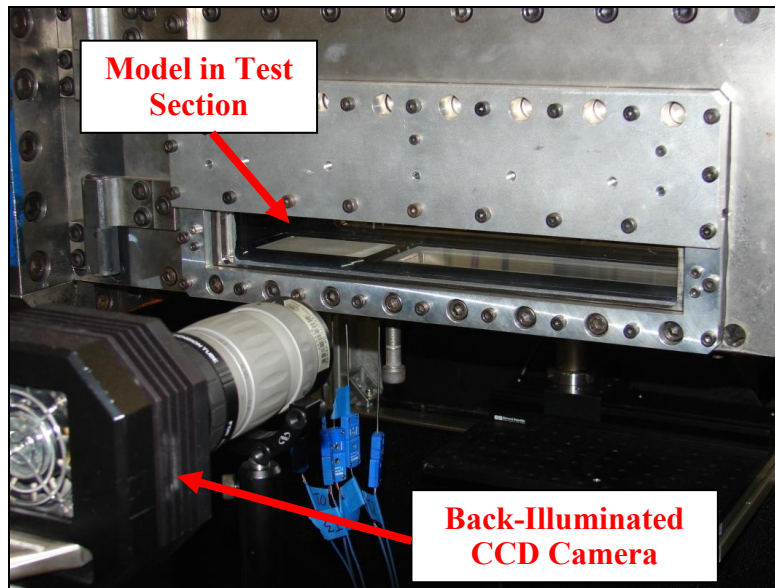


Figure 3.14 Back-illuminated CCD camera focusing on a field of view downstream of the naphthalene plug in the Mach 5 test section

Temperature measurements were obtained using type-T thermocouples imbedded into the naphthalene. The stagnation temperature was also monitored using a type-J thermocouple. These were recording using a National Instruments Compact RIO system cRIO-9014 (controller), seen in Figure 3.15.



Figure 3.15 Compact RIO System with thermocouples

3.4.3 Image Processing

The PLIF images were acquired using the PixelVision software. The raw images were in 16-bit TIFF format. Each run acquired between 10 to 20 images depending on run length and the amount of time it took for the stagnation temperature to remain constant. The images were post-processed in MatLab. The instantaneous images were filtered using a 3 x 3 median filter to reduce noise effects. All averaging and statistical analyses were also performed using MatLab.

Chapter 4: Results

The experimental investigations of naphthalene ablation in the Mach 5 wind tunnel and the complementary investigations of naphthalene fluorescence linearity, temperature dependence and pressure dependence are presented in this chapter. First, the first-campaign Mach 5 ablation investigation will be presented that proved the viability of the technique. The complementary studies will then be presented, as the information learned is necessary to obtain quantitative information from the measured naphthalene PLIF signal. Finally, the second-campaign Mach 5 ablation investigation as well as the extraction of quantitative information will be presented.

4.1 MACH 5 NAPHTHALENE ABLATION RESULTS: FIRST CAMPAIGN

The goal of this preliminary study was to verify the viability of using naphthalene PLIF in the Mach 5 wind tunnel to visualize the transport of ablation products throughout the turbulent boundary layer. The design of the plug used is described in section 3.2.1 and the experimental setup is the same as in Figure 3.13. The stagnation temperature for these experiments was 345 K. A typical runtime lasted 45 seconds and 10 usable images were obtained during each run. The laser energy delivered to the test section was about 50 mJ per pulse and the sheet width and thickness were 150 mm (5.91 in.) and 1 mm (.04 in.), respectively. This gave a fluence of about 330 J/m². This is somewhat outside of the linear region, which will be discussed in the following section. Example PLIF images are shown in Figure 4.1. These were imaged using an intensified CCD camera (Princeton Instruments PI-Max). The field of view for this image is 22.9 mm (.90 in.) wide by 15.7 mm (.62 in.) high, and is 50 mm (1.97 in.) downstream of the naphthalene insert. This figure shows that the naphthalene ablation technique is quite promising for visualizing

the transport of ablation products, but we saw the signal-to-noise ratios are quite low (less than 5). The observed mass loss is essentially negligible during a 60 to 100 second run.

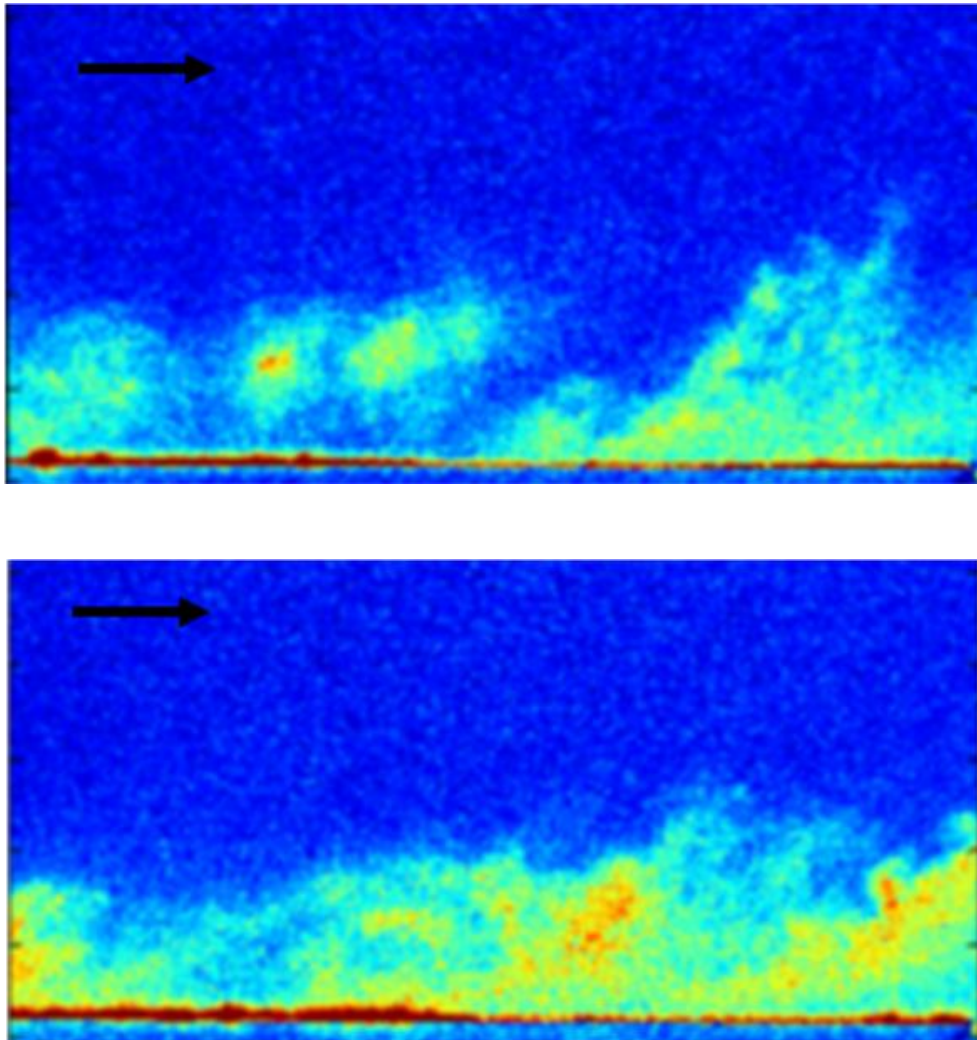


Figure 4.1 Example naphthalene instantaneous PLIF images from the first campaign in the Mach 5 wind tunnel.

In addition, a second field of view closer to the naphthalene plug was observed. The field of view for these images was 22.9 mm (.90 in.) wide by 15.7 mm (.62 in.) high, and is 25.4 mm (1 in.) downstream of the naphthalene insert. Figure 4.2 shows a composite image made from two different images captured at different locations and times to reveal the spatial evolution of the scalar. An unrelated velocity field has been added to this image to show the boundary layer thickness in comparison to the ablative product.

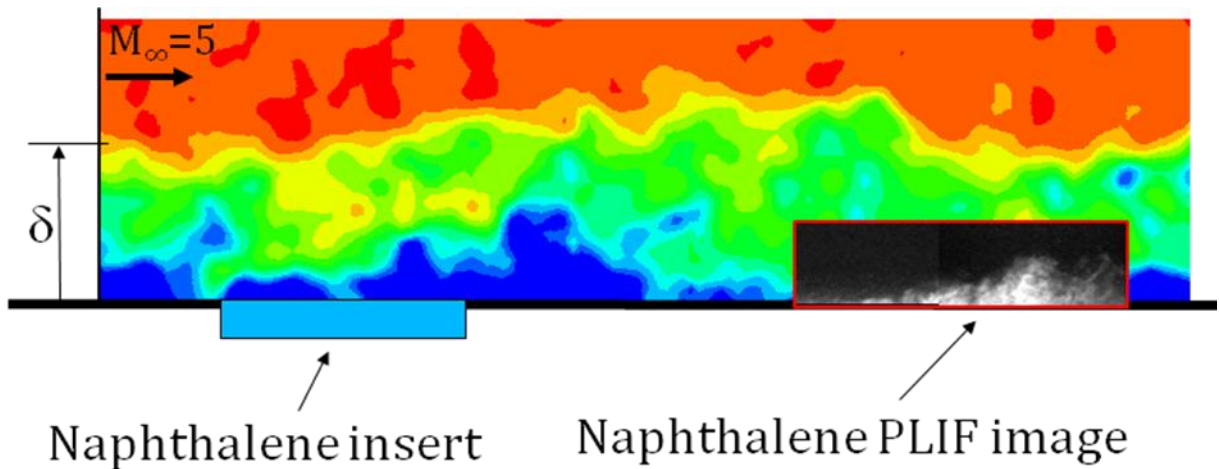


Figure 4.2 Composite of two instantaneous naphthalene PLIF images taken from two adjacent locations at different times. *Uncorrelated velocity field is displayed behind the images to show the boundary layer thickness*

The ablation products are seen to be confined quite close to the wall of the wind tunnel. It appears though, that the scalar is transported out into the boundary layer in bursts in accordance with known transport mechanisms in turbulent boundary layers. Despite the modest quality of the data presented, the figures show that the technique is quite promising.

After observing the results of the first campaign it was apparent for the second campaign experimental tests, the main object would be to improve the quality of the PLIF imaging. The PLIF signal was improved in four important ways. The first was to increase the size of the naphthalene plug (in the streamwise direction) so that more ablation products were transpired into the flow. A new floor plug for the Mach 5 wind tunnel was developed with an area of 101.6 mm (4 in.) long by 57.2 mm (2.25 in.) wide, as described in section 3.2.3. The larger surface area led to a greater integrated amount of mass in the boundary layer and hence higher fluorescence signal. The second way that the signal was improved was to increase the tunnel stagnation temperature, since this increases the naphthalene vapor pressure and hence its sublimation rate. The increase in vapor pressure is not directly related to the increase in stagnation temperature because of the coupled effects of heat and mass transfer that occurs due to the naphthalene sublimation. This effect will be explored in the next section. and will be ignored, thus sublimative cooling doesn't affect the assumption of adiabatic flow. This coupled effect was explored in section 3.2.2. The third improvement was to use a back-illuminated CCD camera (PixelVision SpectraVideo Model SV512V1) with higher quantum efficiency compared to the ICCD camera used in the first campaign. In this case the signal was shot noise limited, so an increase in quantum efficiency led to an improvement in the signal-to-noise ratio. The fourth was to increase the laser energy to increase the resultant fluorescence signal. The amount the laser energy could be increased is limited by the fluence (energy/area of the sheet) at which the LIF signal was no longer linear. After this fluence, sheet corrections are difficult to make. The linear regime of the fluence is discussed in the following section. The effect of each of these techniques will be discussed in the results of the second campaign in section 4.3.

4.2 Mass/Heat Transfer Analysis

The coupled effects of mass and heat transfer were then investigated in order to obtain an estimate of the expected depth removal rate from the naphthalene plug during a typical run in the Mach 5 wind tunnel. Ablation presents a coupled heat and mass transfer problem as the mass flux from the surface cools the surface, while the heat flux due to the recovery temperature heats the surface.

The sublimation process is very similar to evaporative cooling and an outline of the coupled mass and heat transfer effects can be found in Incropera and DeWitt (2002). The heat flux (in W/m^2) is given by,

$$q'' = h_h (T_r - T_s) \quad (4.1)$$

where h_h is the heat transfer coefficient, T_s is the surface temperature, and T_r is the recovery temperature defined from White (2001) as,

$$T_r = T_\infty \left(1 + r \frac{\gamma - 1}{2} M^2 \right) \quad (4.2)$$

where T_∞ is the free stream temperature, γ is the specific heat ratio, M is the mach number, and r is the recovery factor defined as a function of the Prandtl number as: $r = \text{Pr}^{1/3}$. The Prandtl number is the ratio of the kinematic viscosity, ν , to the thermal diffusivity, α . The mass flux is given by,

$$\dot{m}'' = h_m (\rho_{sv} - \rho_\infty), \quad (4.3)$$

the heat and mass fluxes are related by,

$$q'' = \dot{m}'' h_{sg} = h_{sg} h_m (\rho_{sv} - \rho_\infty), \quad (4.4)$$

where h_m is the mass transfer coefficient, ρ_{sv} is the surface vapor density, ρ_∞ is the freestream vapor density, and h_{sg} is the latent heat of vaporization. The surface vapor density is obtained using the ideal gas law and an equation for the vapor pressure from Ambrose et al. (1975). This vapor pressure is dependent on the surface temperature, T_s , thus the heat and mass flux equations are both dependent on the surface temperature. For flow over a flat plate, Von Karmen (1939) derives the heat and mass transfer Stanton numbers which can be related to the heat transfer and mass transfer coefficients, respectively. The heat and mass transfer coefficients are given by,

$$h_h = \frac{u_\infty \rho C_p (C_f / 2)}{1 + \sqrt{C_f / 2} (5 \text{Pr} + 5 \ln(5 \text{Pr} + 1) - 14)} \quad (4.5)$$

$$h_m = \frac{u_\infty (C_f / 2)}{1 + \sqrt{C_f / 2} (5 \text{Sc} + 5 \ln(5 \text{Sc} + 1) - 14)} \quad (4.6)$$

where u_∞ is the freestream velocity, C_p is the specific heat capacity, C_f is the skin friction coefficient taken to be 7.7×10^{-4} in the Mach 5 wind tunnel, and Sc is the Schmidt number. The Schmidt number is the ratio of the kinematic viscosity, ν , and mass diffusivity, D . Goldstein (1995) reports the relationship for the Schmidt number for naphthalene in air as,

$$\text{Sc} = 2.28 \left(\frac{T}{298.16} \right)^{-0.1526} \quad (4.7)$$

The surface temperature and heat flux may be solved for by equating the heat transfer equation, Equation 4.1, and mass transfer equation, Equation 4.4. The naphthalene plug surface temperature versus the stagnation temperature is shown in Figure 4.3. The heat flux versus stagnation temperature is shown in Figure 4.4. In addition these results allow for the calculation of the mass flux and thus the expected depth removal rate from the surface of the plug, Figure 4.5. The expected mass loss during a 60 second run at a stagnation temperature of 375 K was predicted to be 67 μ m. The expected depth removal rate is consistent with the observed mass loss per run in the first-campaign. Since the mass transfer is essentially negligible, the coupled effects of heat and mass transfer that occurs due to the naphthalene sublimation can be ignored and the assumption of adiabatic flow could be made.

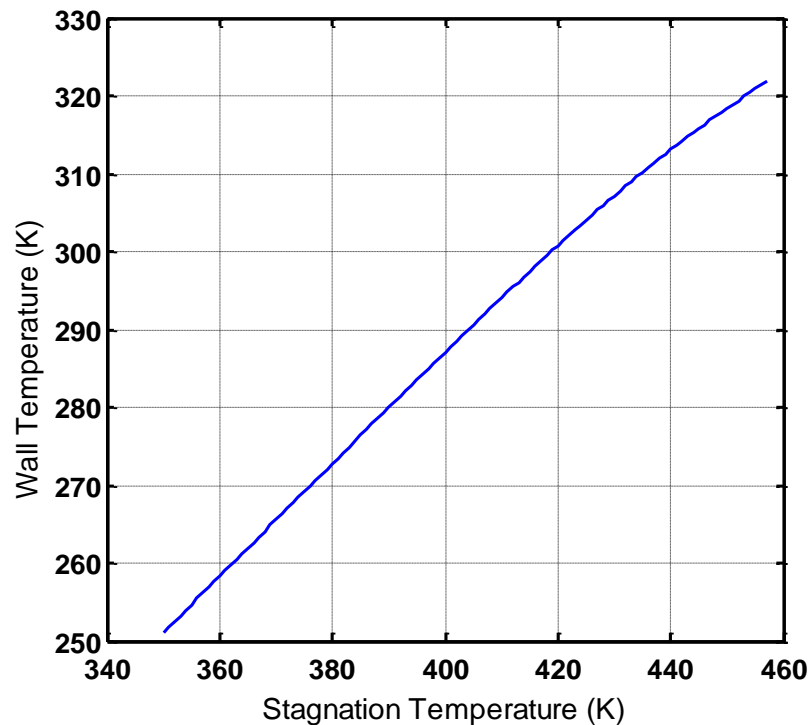


Figure 4.3 Calculated temperature of the wall of the naphthalene plug as a function of the stagnation temperature

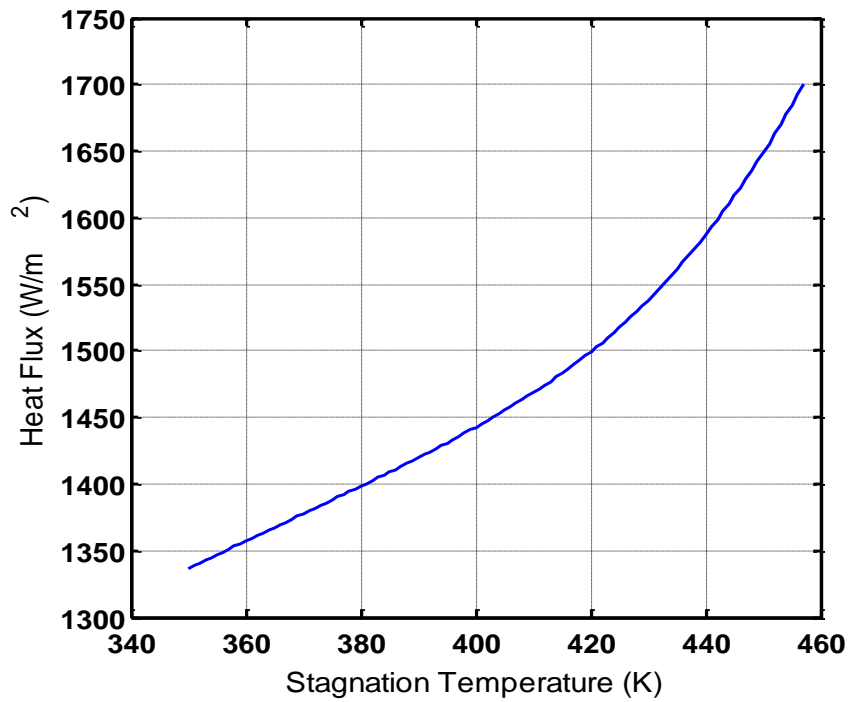


Figure 4.4 Calculated heat flux through the naphthalene plug as a function of the stagnation temperature

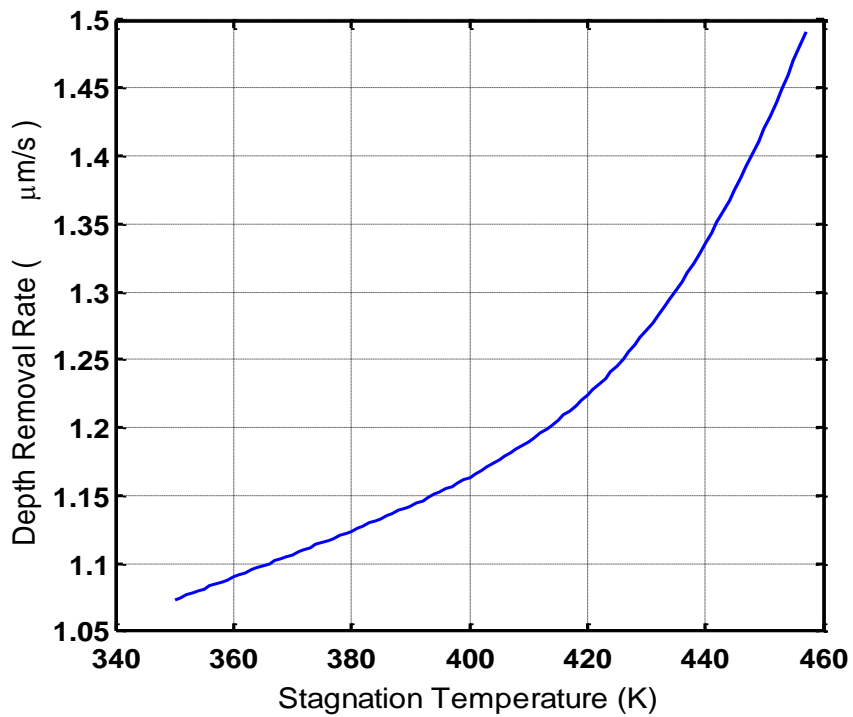


Figure 4.5 Calculated naphthalene plug depth removal rate as function of temperature

4.3 COMPLEMENTARY INVESTIGATIONS OF NAPHTHALENE LIF

The major objective of this study was to obtain quantitative information from the PLIF images. In order to meet this objective, an understanding of the effect temperature and pressure variations on fluorescence signal must be developed.

In addition, the linear regime of the LIF signal versus the fluence must also be understood so that a valid sheet correction can be made.

4.3.1 Naphthalene LIF Linearity

To determine the effect of laser fluence on the fluorescence signal, the fluorescence signal from the naphthalene jet was imaged on a back-illuminated CCD camera at varying laser energy. The description of this setup is explained in section 3.3.1 and a schematic is shown in Figure 3.10. The frequency quadrupled Nd:YAG laser had a pulse duration of about 20 ns. Here, we are ignoring the effect of pulse duration since it is constant for this study. The laser energy was varied by passing the beam through a variable number of fused silica flats to reflect different fractions of the energy. For the lowest energy cases the fused silica flats were combined with a 90% beam splitter. The laser energy was measured with a Joule meter (Coherent FieldmaxII-Top). The laser beam was passed through the potential core of the air naphthalene jet and the resulting fluorescence was imaged.

To obtain the area of the laser beam, intensity profiles were then extracted from the images. Examples of the beam profiles extracted are displayed in Figure 4.3. The fluence was then computed as the energy per pulse divided by the area of the laser beam. The use of fused silica flats and a beam splitter kept the beam profile consistent during each experiment. The area of the beam was assumed to correspond to that of a disk with diameter equal to the full-width-at-quarter maximum of the fluorescence signal profiles. Full width at quarter maximum was used instead of full width at half maximum due to a

plateau region in the beam profile near the half maximum point, which made the width very sensitive to the exact value of maximum intensity used. This is visible in the beam profiles in Figure 4.6. Typically, the areas derived from the full-width-at-quarter-max points are about 1.56 times larger than those computed from the half-maximum points.

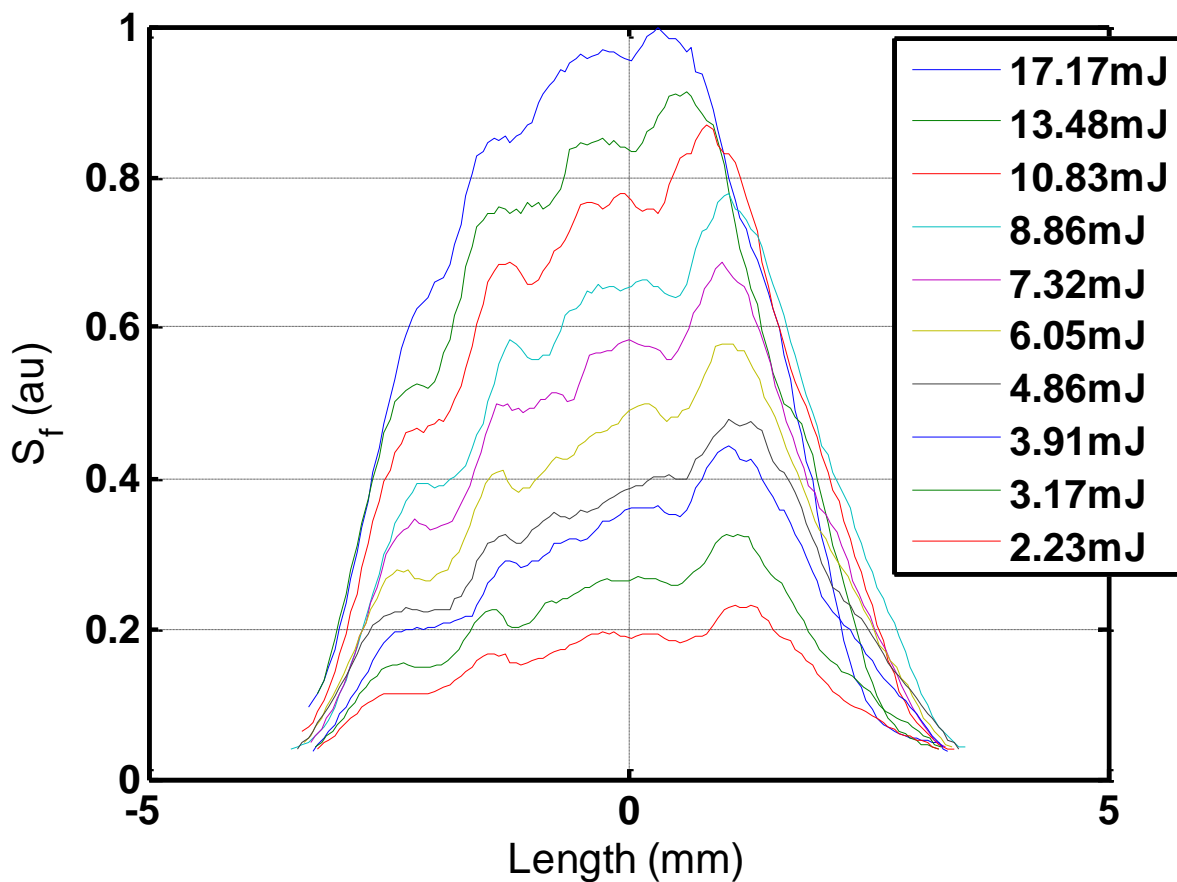


Figure 4.6 Beam profiles of naphthalene and air jet with varying input energy from the laser.

The results are shown in Figure 4.7. The error bars represent a 95 percent confidence interval determined from the standard error computed from six different sets of experimental results, and the pre-factor obtained from the student's t distribution. Each data point of each set represents an average of 100 images over which the fluorescence signal was spatially-averaged over the jet potential core.

Figure 4.7 shows that there is a region where the fluorescence signal is linear with laser fluence but it levels off with increasing fluence. From the figure, the LIF signal diverges from linear for fluences that are greater than about 200 J/m^2 . This value of fluence that maintains linear behavior is relatively low as compared to other popular tracers, such as acetone.

In PLIF imaging, we typically want to maintain linear behavior because this improves our ability to make accurate sheet corrections. So say we use a 5 cm wide and $500 \text{ }\mu\text{m}$ thick laser sheet with 10 ns pulse duration, then the maximum laser energy that can be used is only 5 mJ. Now, approximately linear behavior is achieved for fluence that is nearly twice this value, and the resultant bias error may be acceptable if achieving higher signals is critically important. The data in Figure 4.7 were acquired at atmospheric pressure, but the fluorescence linear regime may not be the same at the conditions of interest in the Mach 5 wind tunnel (30 Torr), and so these measurements were checked at lower pressures.

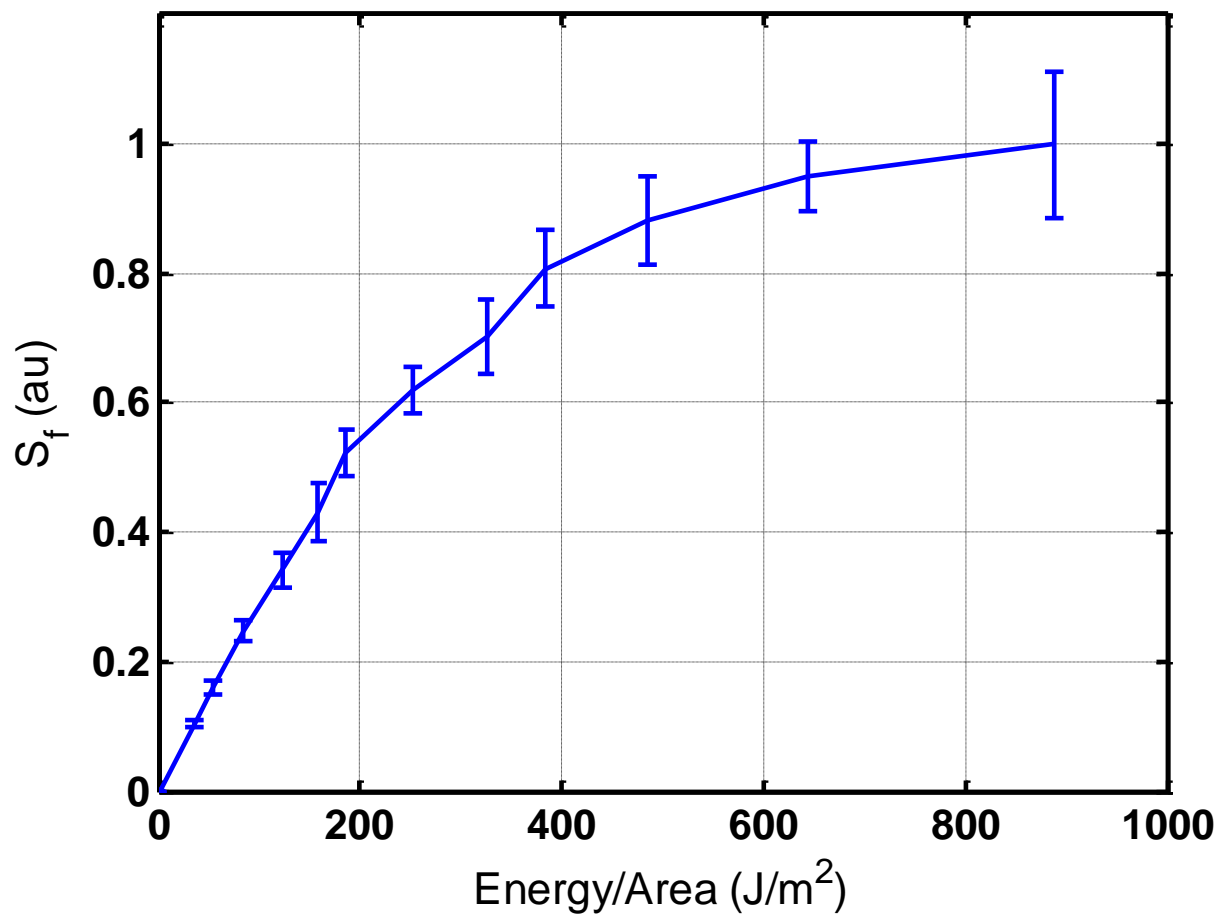


Figure 4.7 Dependence of naphthalene LIF signal on laser fluence at 297 K and 1 atm. *The naphthalene is carried in air and the laser wavelength is 266 nm.*

4.3.2 Naphthalene LIF Temperature Dependence

The temperature dependence of naphthalene was determined by imaging the fluorescence of a heated naphthalene-air jet. The description of this setup is explained in section 3.3.2 and a schematic is shown in Figure 3.10. Here we normalize the fluorescence signal by the room temperature value ($T_{ref}=300$ K), i.e.

$$\frac{S_f(T)}{S_f(T_{ref})} = \frac{T_{ref} \sigma(T) \phi(T)}{T \sigma(T_{ref}) \phi_{ref}(T)} \quad (4.8)$$

In the quenching dominated limit where we assume the quenching cross-section is constant over our temperature range then we have,

$$\frac{\sigma(T)}{\sigma(T_{ref})} = \frac{S_f(T)}{S_f(T_{ref})} \left(\frac{T}{T_{ref}} \right)^{1/2} \quad (4.9)$$

The temperature dependence of the fluorescence signal per unit-mole-fraction of naphthalene is shown in Figure 4.5. These measurements represent the time- and spectrally-integrated fluorescence signal. Four sets of data were collected to determine the 95 percent confidence intervals. The pre-factor is obtained from the student's t distribution. The large uncertainty results from day-to-day variations in the naphthalene vapor pressure. The data sets were collected by both increasing the temperature throughout the run and decreasing it. Each point in the data sets consisted of an average of 100 fluorescence images over which the fluorescence signal was spatially-averaged over the jet potential core. The energy per pulse was in the linear regime of naphthalene fluorescence at room temperature and verified at 525 K. The monitored energy per pulse

was used to correct the fluorescence signal. The temperature of the naphthalene saturation cell was closely monitored, which was used to correct the fluorescence signal for changing naphthalene vapor pressure (De Kruif et al., 1981), but there still seems to be some lack of precision in this process. Figure 4.8 shows that the fluorescence increases sharply at lower temperatures and levels off with higher temperatures, but this trend is not entirely trustworthy considering the uncertainty. Future work will be directed at reducing the uncertainty of these measurements.

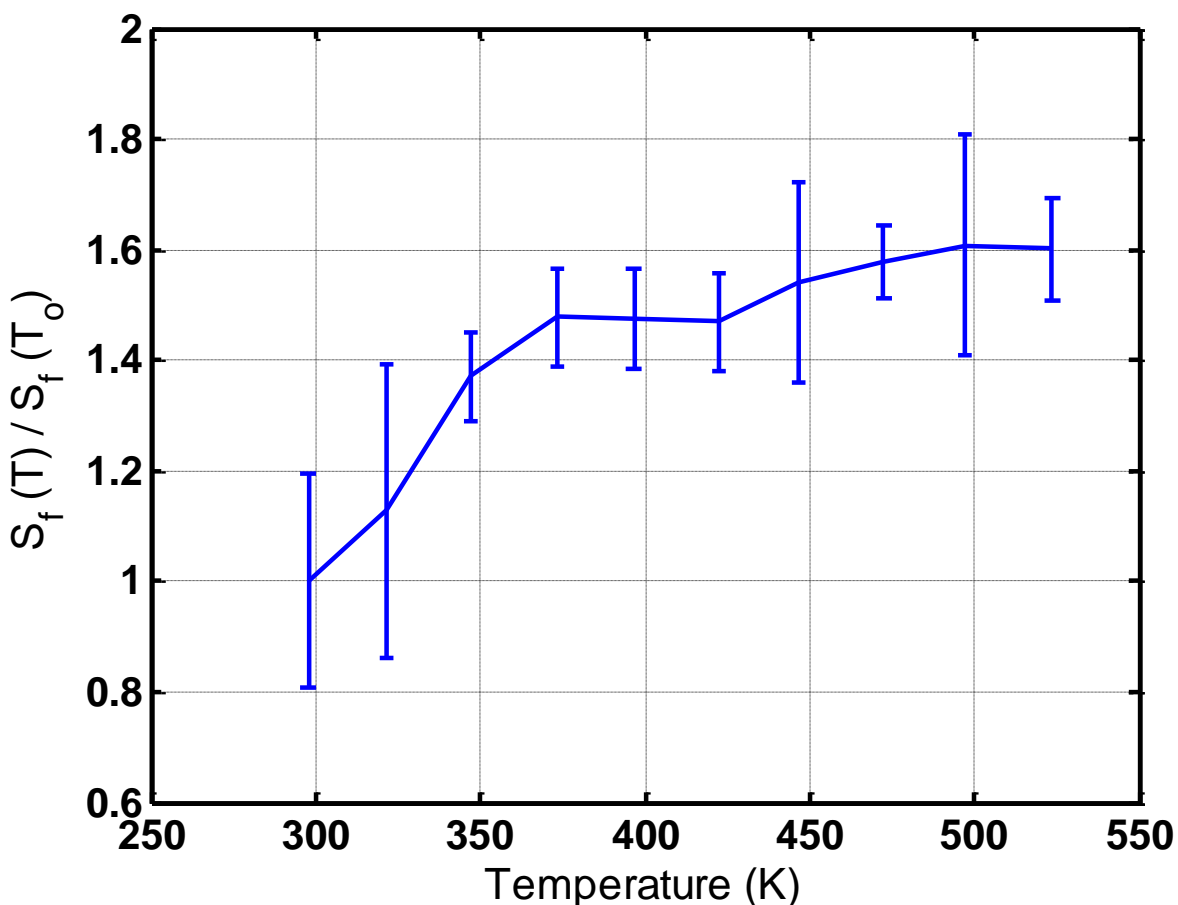


Figure 4.8 Temperature dependence of the naphthalene LIF signal at atmospheric pressure ($T_0=300$ K)

The normalized absorption cross-section is presented in Figure 4.6. The cross-sections were obtained by multiplying the fluorescence signals by the temperature factor as shown in Equation 4.9. Figure 4.9 shows that the cross-sections exhibit a monotonic increase with temperature.

Similar measurements of other complex organic molecules, such as acetone, show that the dependence of the signal on temperature will depend strongly on the excitation wavelength (Thurber et al., 1998), and so these results are likely to be strongly dependent on the wavelength of the laser used.

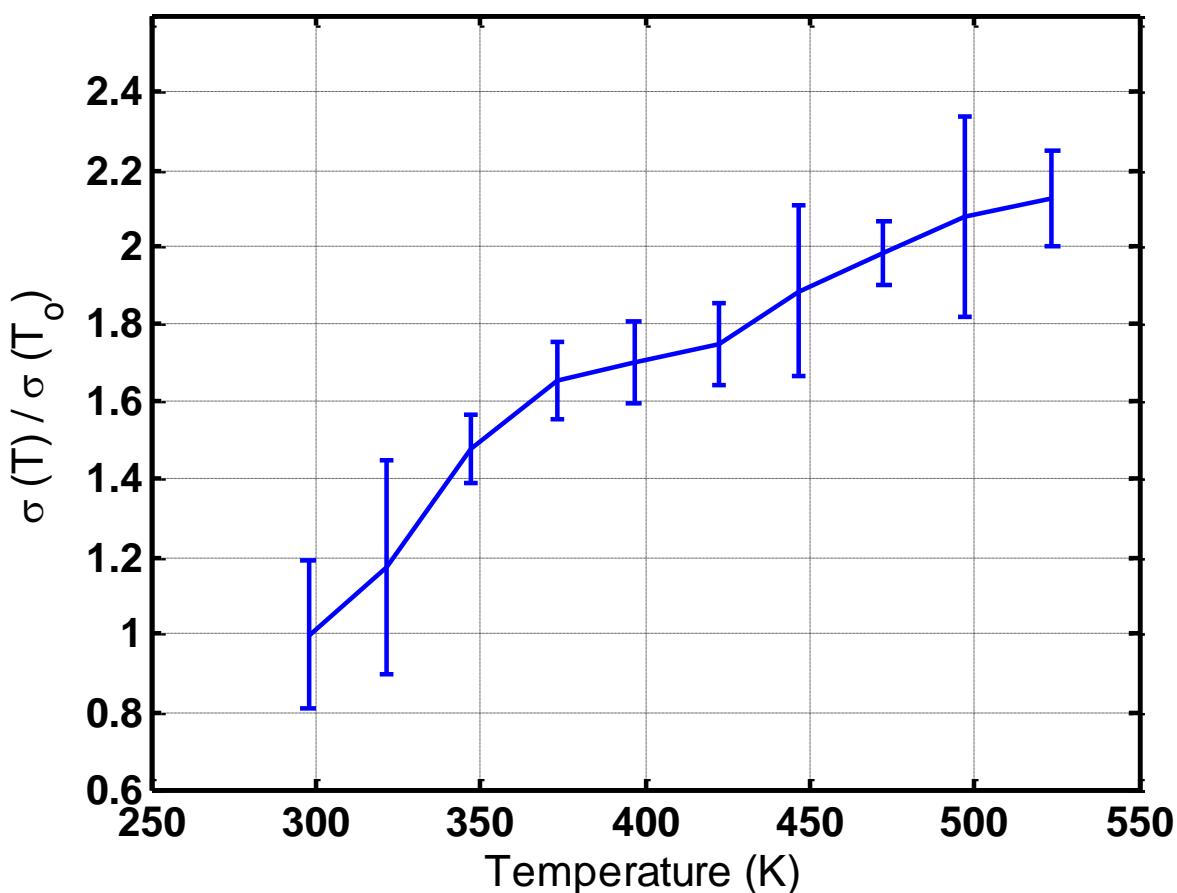


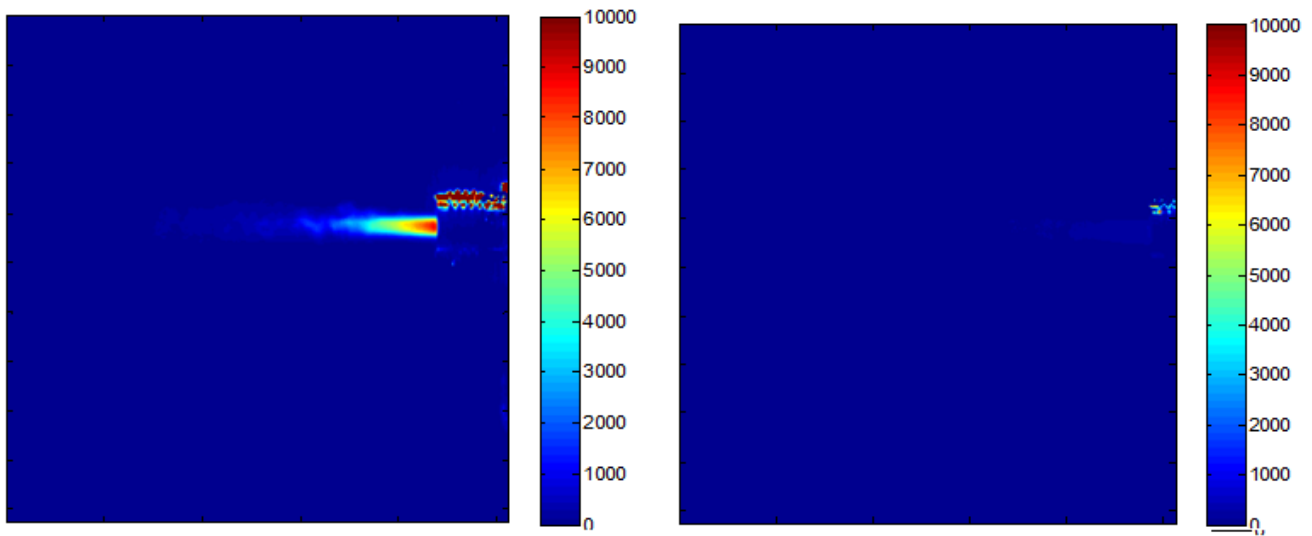
Figure 4.9 Temperature dependence of the naphthalene absorption cross-section at atmospheric pressure ($T_0=300$ K)

4.3.3 Naphthalene LIF Pressure Dependence

4.3.3.1 Preliminary Fluorescence Study

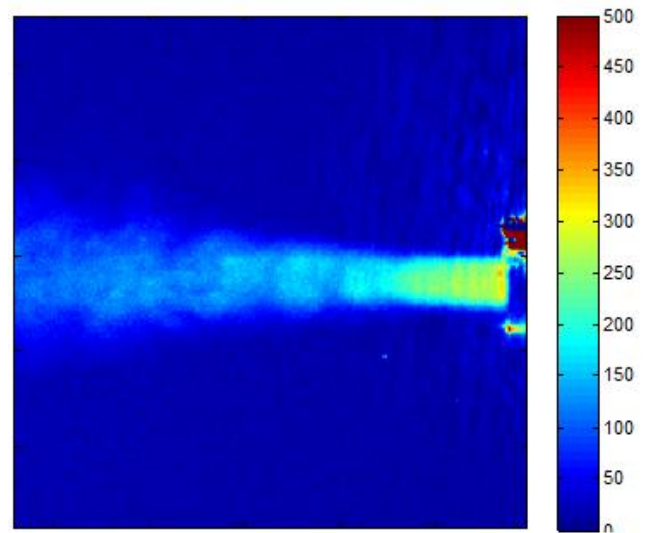
A preliminary study of the fluorescence of naphthalene vapor was first investigated through imaging a jet seeded with naphthalene vapor exhausting into atmospheric conditions with an experimental setup similar to that in Figure 3.10. The jet of naphthalene was formed using both air and nitrogen exhausting into air. The jet outlet was 6.35 mm (.25 in.). Instead of a 266 nm laser beam as in Figure 3.10, a 266 nm laser sheet was used at the exit to excite the entire jet. A back-illuminated CCD camera (Micro Lumimetrics, Inc. Cryocam Model S5AB1660) with a resolution of 512 x 512 pixels was used to image the fluorescence. Figure 4.10 shows a comparison of the fluorescence signal at constant laser energy when the naphthalene is seeded into air versus nitrogen. All images represent an average of 50 instantaneous images that have been background subtracted. For this preliminary case the fluence of the sheet was above the linear regime, so a sheet correction was not performed. Since these were for qualitative purposes rather than quantitative purposes this did not present a problem.

It was observed that the nitrogen case resulted in a signal that was approximately 20 times that of the air jet. This difference in fluorescence signal from the air/naphthalene jet and the nitrogen/naphthalene jet is consistent with previous quenching rate measurements by Martinez et al. (2004). The nitrogen jet also shows a representation of the potential core of the naphthalene jet because as soon as the naphthalene/nitrogen jet mixes with the air around it, the naphthalene fluorescence is quenched by oxygen and thus the signal is dramatically reduced as compared to the unmixed region.



(a)

(b)



(c)

Figure 4.10 Naphthalene jet exhausting into air with (a) nitrogen driving the flow, (b) air driving the flow and (c) same image as in (b) except with a rescaled color map that highlights the lower signal range

4.3.3.2 Fluorescence Lifetime Pressure Dependence

To obtain more quantitative information regarding the pressure dependence of naphthalene LIF, the fluorescence lifetime of naphthalene vapor was measured at different pressures in a nitrogen environment and in a pure-air environment (ultra zero-air). The experimental setup for this investigation is described in section 3.3.3. The output of the PMT was monitored on a Tektronix oscilloscope with a sampling rate of 5 GS/s and a bandwidth of 500 MHz (TDS 3054). An on scope average of 128 images was saved to a 3 ½ inch floppy disk to be analyzed. The quadrupled Nd:YAG laser operated at 10 Hz and so a typical run took 12.8 seconds. Measurements were recorded over the pressure range of 1 kPa to 7 kPa in an air/naphthalene jet and from 1 kPa to 40 kPa in a nitrogen/naphthalene jet.

Since nitrogen is not an efficient quencher of naphthalene fluorescence, the fluorescence decay in a nitrogen environment is due mainly to self-quenching (naphthalene-naphthalene collisions) and natural decay (spontaneous emission and non-radiative internal transfer). In contrast, the decay in an air environment is dominated by oxygen quenching, which is very efficient as seen by the preliminary study and by Beddard et al. (1973), Kaiser et al. (2005), and Martinez et al. (2004). The fluorescence signal versus time for pressures ranging from 2 kPa to 6.7 kPa in air is displayed in Figure 4.11a. This figure shows a decrease of fluorescence lifetimes with pressure. The fluorescence lifetimes themselves were determined by taking the logarithm of the fluorescence signal versus time curves, as shown in Figure 4.11b, and fitting the linear region of the decay time. The fluorescence decay time-constant, τ_f (Equation 2.5), is equal to the negative of the slope of this linear fit. It should be emphasized that the measured fluorescence decay is the average of the radiative decay from different vibrational levels; hence, fitting an exponential to the observed signal provides the

measure of the average lifetime of the different vibrational levels that participate in the radiation.

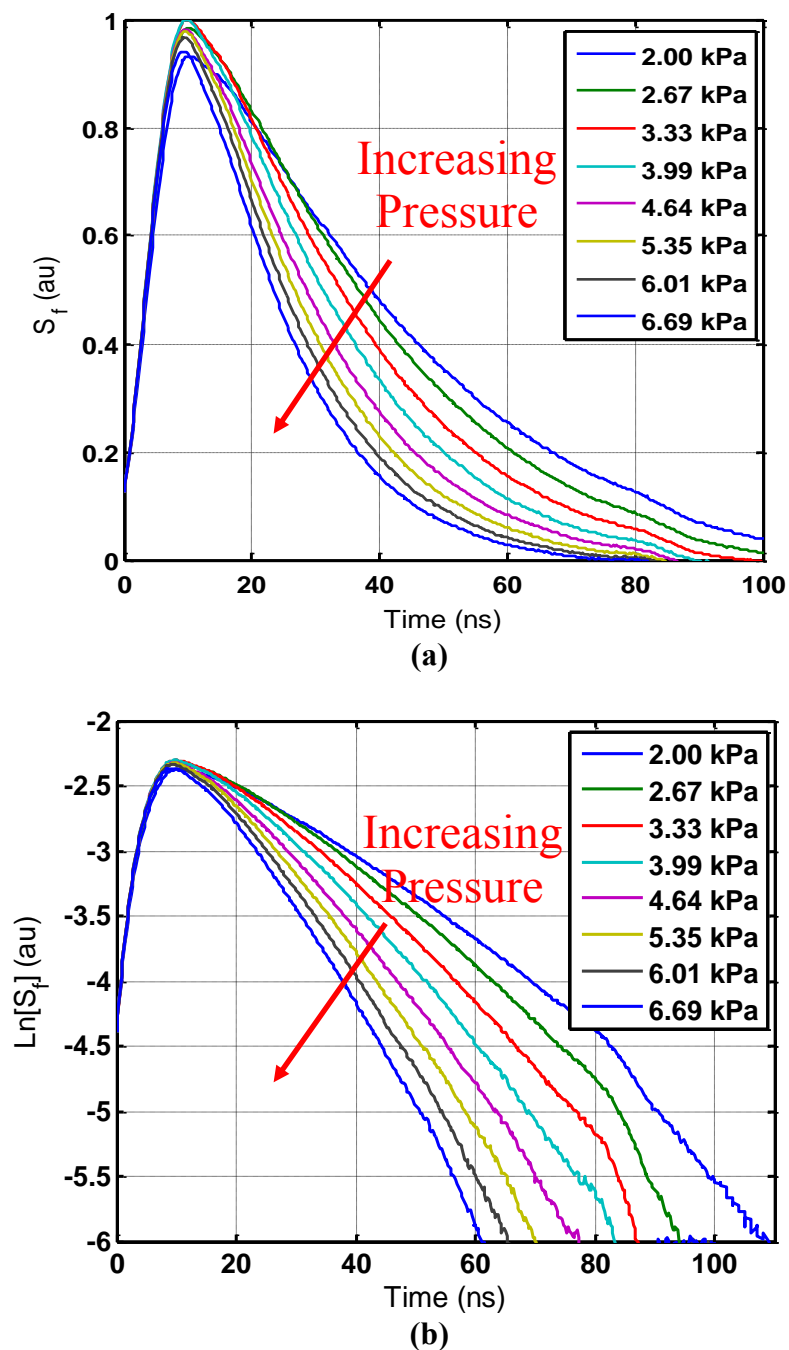


Figure 4.11 Pressure dependence of the naphthalene (a) fluorescence lifetime and (b) the natural logarithm of the fluorescence lifetime

Figure 4.11b also displays a bi-exponential behavior of the observed fluorescence decay. There are two linear regions as the time increases that can be seen at pressures greater than 3.33 kPa. These correspond to the two different fluorescence decay time-constants. Bi-exponential behavior was observed in the past by Behlen and Rice (1981) and Reyle and Brechignac (2000).

Figure 4.12 shows a Stern-Volmer plot of the quenching of the naphthalene vapor by air. This plot is the variation of the reciprocal of the fluorescence decay time-constant with pressure. It can be seen that the variation of the reciprocal time-constant is linear with pressure for pressures greater than 2 kPa (40 torr). This linear variation indicates that the fluorescence is dominated by quenching at these pressures. A straight line was fitted to this linear region in order to determine the slope and the y-intercept of the line. The quenching rate obtained from the slope of the Stern-Volmer plot was $k_Q = 0.0096 \text{ (kPa ns)}^{-1}$. For this fit the last two points at the low-pressure end were omitted. Since air is composed of 21% O_2 , this gives a quenching rate of $k_Q = 0.046 \text{ (kPa ns)}^{-1}$ for O_2 . This value is reasonably close to the value of $0.06 \text{ (kPa ns)}^{-1}$ measured by Martinez et al. (2004) using 308 nm excitation.

In the linear curve fit of Figure 4.12, the y-intercept, which gives the sum of the fluorescence decay and non-radiative non-collisional de-excitation, is estimated to give a lifetime of about 123 ns. Although, the actual lifetime at zero-pressure is lower than this as will be discussed below. The value of 123 ns can be considered an effective lifetime that is appropriate for higher pressure conditions where the trend is linear.

An interesting feature is the deviation from the linear trend at low pressures. In particular, it can be seen that the magnitude of the lifetime is less than that predicted by the Stern-Volmer variation (i.e., the reciprocal of time is larger than the linear trend would extrapolate to). This deviation indicates the role of internal de-excitation

mechanisms (k_{int}) becomes important as the collisional de-excitation rate (k_Q) approaches zero. Therefore the internal quenching rate begins to dominate and the fluorescent decay time constant behaves as:

$$\tau_f = \frac{1}{k_f + k_{\text{int}} + k_Q} \rightarrow \frac{1}{k_f + k_{\text{int}}} \quad (4.10)$$

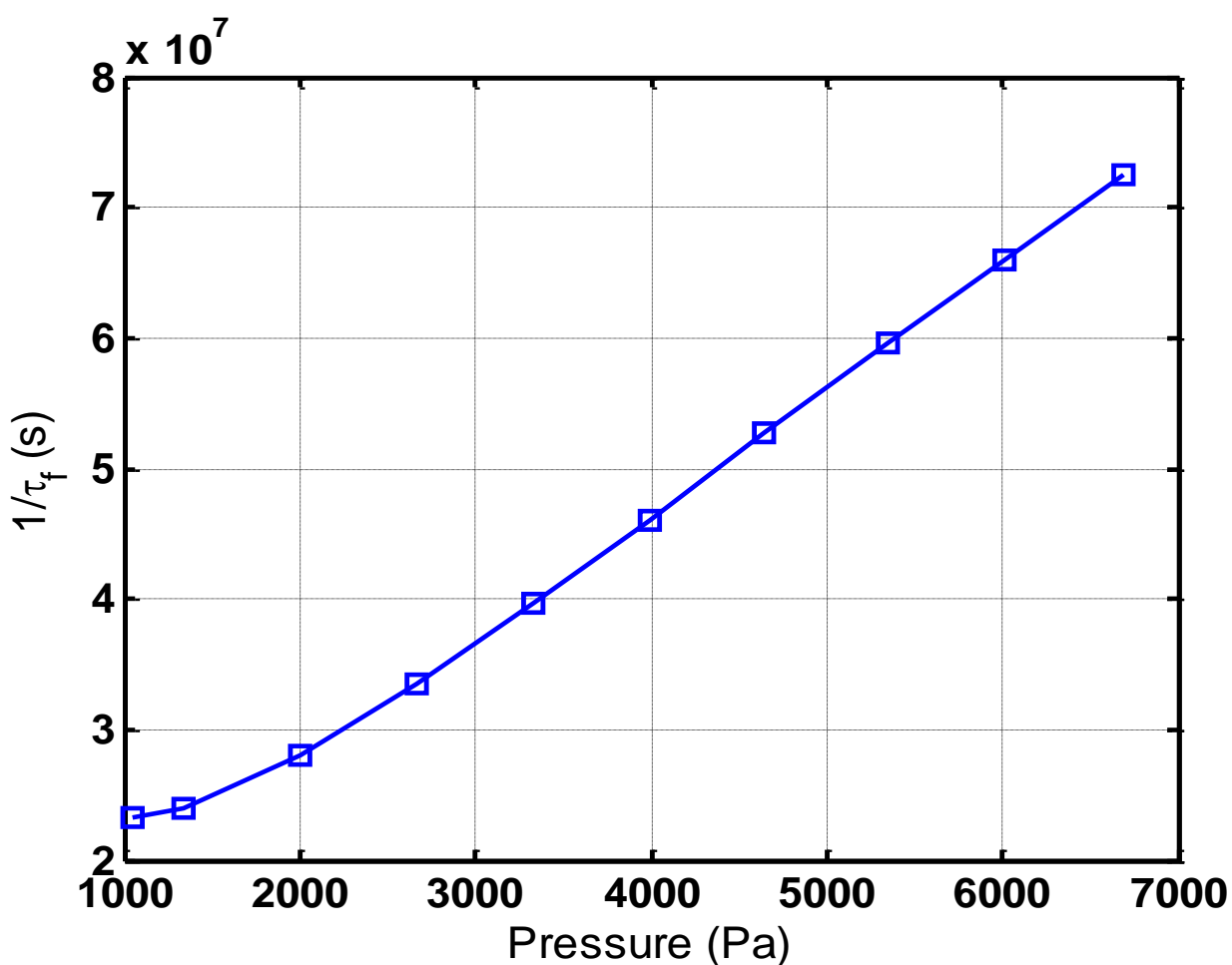


Figure 4.12 Stern-Volmer plot of naphthalene vapor in a pure-air environment. *Note that the plot is linear at high pressure (> 2 kPa), and deviation from linearity can be seen close to 1 kPa.*

A study of the effect of nitrogen dilution on the fluorescence lifetime was also conducted. Since N_2 is a relatively weak quencher, the internal transfer mechanisms on the fluorescence lifetime are exposed. Figure 4.13 shows the variation of the fluorescence lifetime with pressure in a nitrogen environment, and for reference, the air environment is also shown. The variation is markedly different from that in the pure-air environment. The fluorescence lifetime actually increases with increasing pressure in the pure-nitrogen situation. A qualitatively similar increase in lifetime with increasing pressure was also reported by Beddard et al. (1973), who excited naphthalene vapor in an argon environment using 268 nm irradiation. Figure 4.14 compares the lifetimes measured in the current nitrogen environment and those of Beddard et al. (1973) who used an argon environment. It is seen that the trends are similar but the lifetime in Beddard et al. (1973) reaches a plateau above about 8 kPa (70 torr), but such a plateau is not reached even at the highest pressures of the current study. Beddard et al. (1973) proposed that the increase in fluorescence lifetime with increasing pressure is because the vibrational levels are not in equilibrium at low pressures, but they attain equilibrium at high pressure. An estimate of the lifetime at high pressures (equilibrium distribution) using previously measured quenching constants was also made in this same study. They estimated a lifetime of 180 ns at a pressure of about 80 torr, which is very similar to the value that we obtain in our measurement. The differences observed in Figure 4.14 may be due to the weak quenching effects of the nitrogen as compared to argon, or possibly to self-quenching of naphthalene. Naphthalene is a weak quencher but is present at a mole fraction of about 1%.

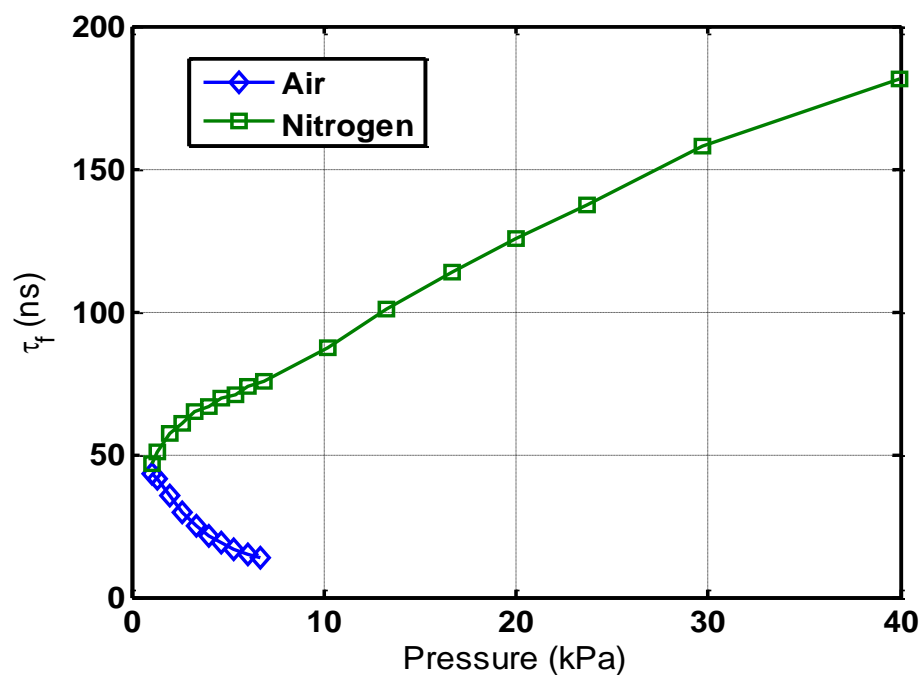


Figure 4.13 Fluorescence lifetime measurements for naphthalene diluted in nitrogen and air

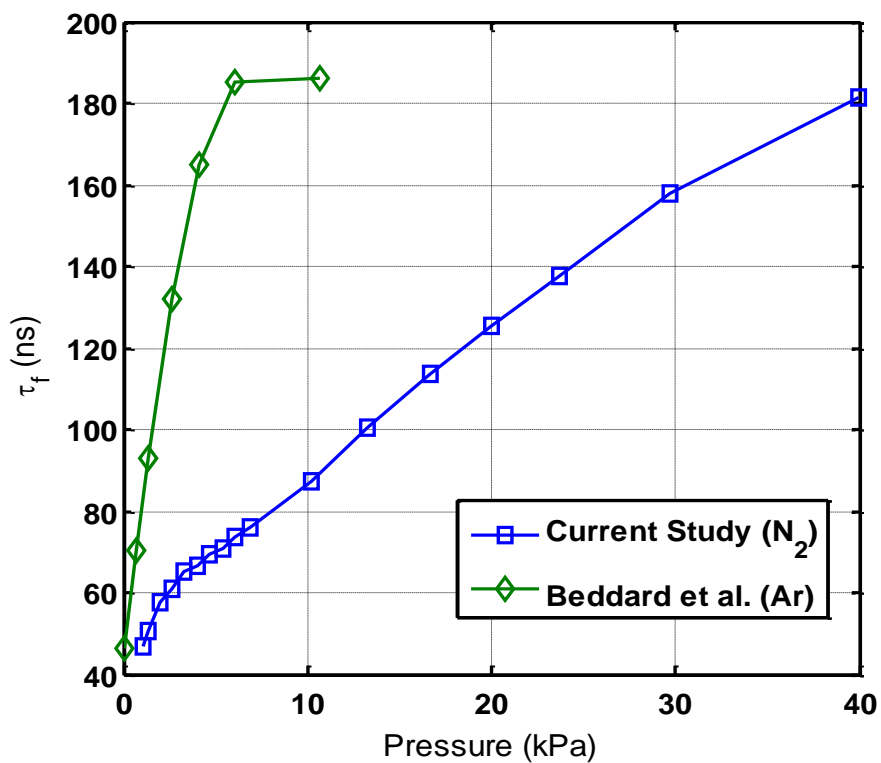


Figure 4.14 Fluorescence lifetime measurements for naphthalene diluted in nitrogen (current work) and argon (Beddard et al., 1973)

The collisional stabilization limit of Beddard et al. (1973) has apparently not been established at the pressures tested for the case of nitrogen since a plateau has not yet been reached. Other researchers have also reported non-equilibrium of the vibrational levels at low pressures (Avouris et al., 1977, Stockburger et al., 1975b). Behlen and Rice (1981) investigated the effect increasing excitation frequency (increasing photon energy) has on the fluorescence lifetime, and found that the fluorescent lifetimes decreased with increasing frequency, although the lifetimes demonstrated enormous variation from state to state. They attributed it to an increase in population in higher vibrational levels with increasing photon energy. This view was further corroborated by Schlag et al. (1971b), who showed that the fluorescent lifetime decreases with increasing vibrational levels. Avouris et al. (1977) and Schlag et al. (1971b) present a detailed discussion of the lifetimes of different vibronic states.

The trend in the fluorescence lifetime found in the present experiments can be explained with the above results. At low pressures, the laser pulse excites the molecules to the S_2 vibronic states, and the molecules undergo a rapid internal transfer to the S_1 vibronic states (at rates of 10^{10} s^{-1}) (Schlag et al., 1971b). At low pressures, lack of collisions locks the population in these upper vibrational states, whose fluorescent decay times are short (on the order of 50 ns). However, at higher pressure, the upper states are more thermalized and so the lower vibrational states are more highly populated. These lower vibrational states have a longer decay time constant compared to the higher states, which is seen as the increased fluorescence decay time-constant at higher pressures. Figure 4.13 also shows that the lifetimes measured in the nitrogen environment and in pure-air environment are very similar to one another as the pressure goes to zero. This of course is expected, and provides some validation of the experimental technique employed.

4.4 MACH 5 NAPHTHALENE ABLATION RESULTS: SECOND CAMPAIGN

4.4.1 Improvement of Naphthalene PLIF Images

The second campaign was focused on improving the PLIF signal levels. The naphthalene PLIF signals were improved by four methods as outlined in section 4.1. Since the fluorescence saturates at relatively low laser energy, it is not possible to significantly improve the SNR by increasing the laser energy in a given pulse. Instead, two laser pulses of laser light were used, separated in time by 100ns, so that more energy could be delivered to the flow, but without increasing the laser intensity. Each laser pulse had energy of 30 mJ per pulse delivered to the flow. The laser sheet was about 150 mm wide and 1 mm thick. The resulting fluence was about 200 J/m^2 , which is within the linear regime. Note that since the cameras integrate over the two pulses, the images are slightly blurred due to flow motion. However, this blurring effect is negligible because the flow convects a maximum of .08 mm, which is about one pixel width, between pulses. The double-pulsing enabled us to obtain about a factor-of-two increase in signal, but the main means of improving SNR was to increase the naphthalene concentration in the boundary layer.

Another main improvement was to increase the size of the ablating surface. The size of the insert was increased by about a factor of six and this design was described in section 3.2.2. The original design was 25.4 mm (1 in.) long by 50.8 mm (2 in.) wide and the new design was 101.6 mm (4 in.) long by 57.15 mm (2.25 in.) wide.

The largest improvement was obtained by increasing the stagnation temperature of the tunnel from about 345 K to 380 K. The saturation pressure of naphthalene increases by about a factor of 3 for each 10° C increase in temperature, and so heating is potentially very effective at increasing the signal. Note, however, that the surface of the naphthalene is not necessarily the same as the recovery temperature since the sublimation

process cools the surface, which is the purpose of an ablator. However, the amount of mass loss is still quite small and so the sublimative cooling is expected to be small. It was noted that as the stagnation temperature increased to its steady state value at the beginning of each run, the fluorescence signal was seen to increase. This simply reflected the increase in naphthalene vapor pressure with temperature. It took about 50 seconds for the temperature to reach a semi steady state, and typically images were captured for about 30 seconds during this steady state period. The stagnation temperature was monitored using a type-J thermocouple that was read by the Compact RIO and LabView and a typical run is shown in Figure 4.15.

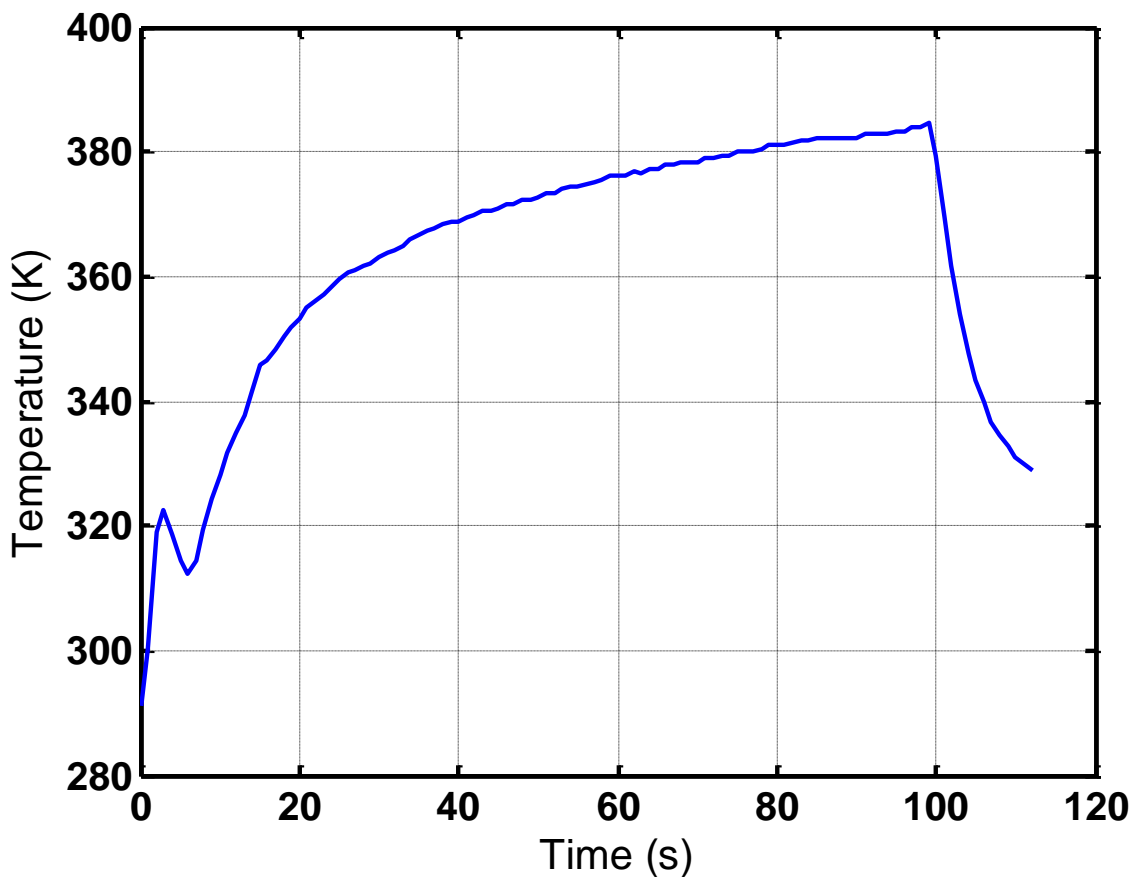
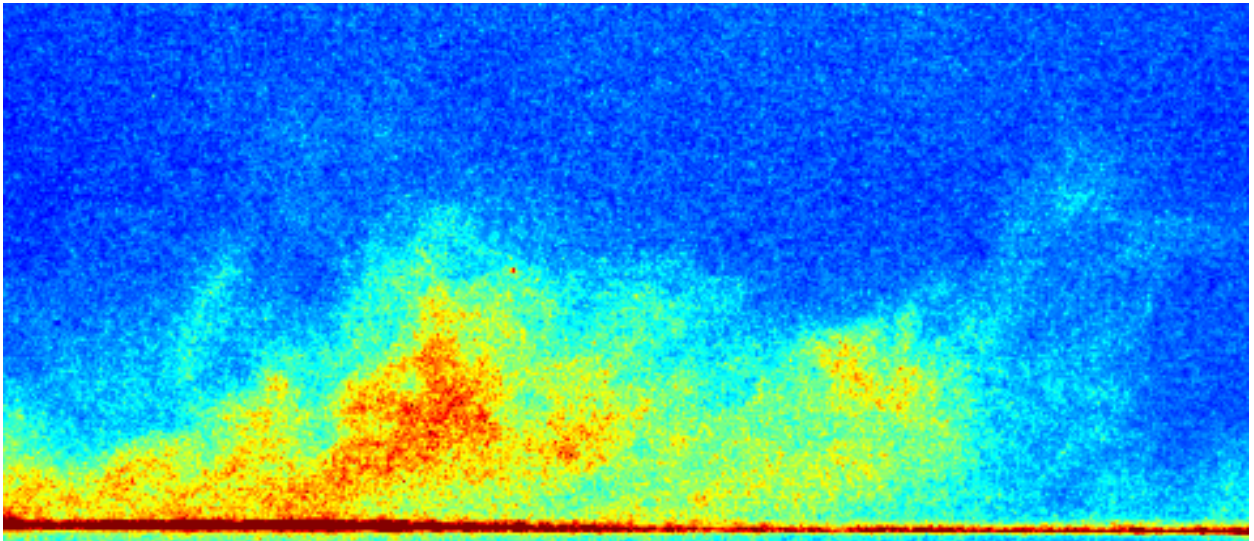


Figure 4.15 Stagnation temperature during a typical run

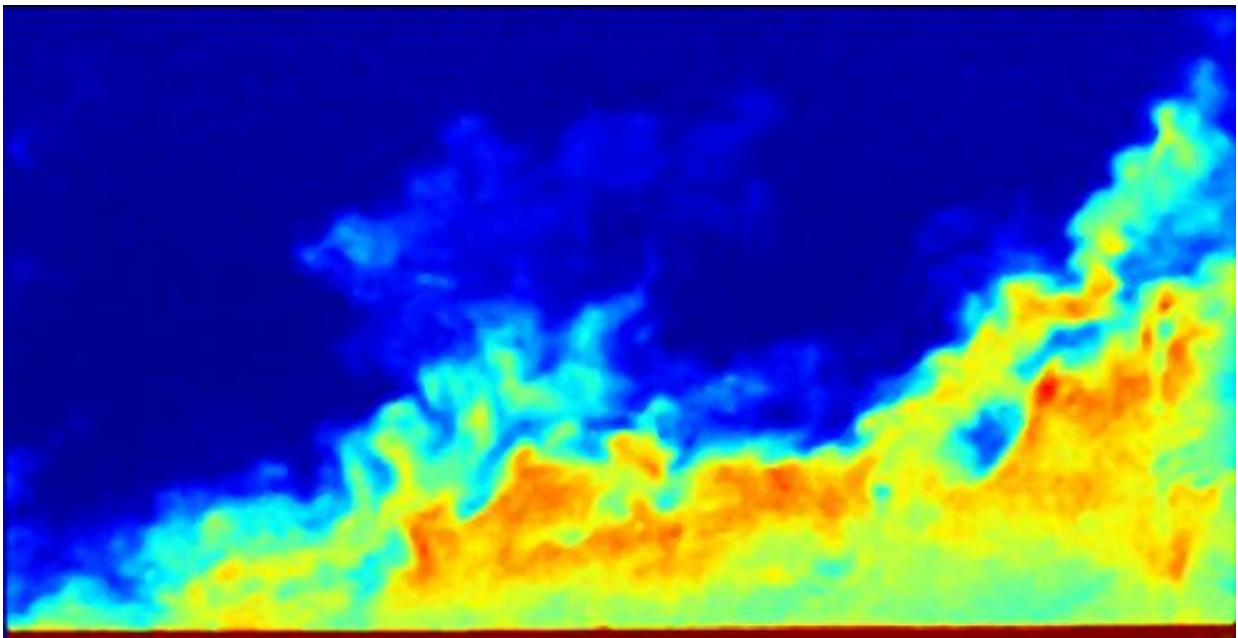
Figure 4.16 shows a comparison between instantaneous naphthalene PLIF images from the first campaign and from the second campaign. In this case the field of view started 105 mm ($x/\delta_{99}=5.4$) downstream of the downstream edge of the naphthalene insert. The size of the field of view was 27 mm (1.06 in.) wide by 14 mm (.55 in.) high as seen in Figure 3.13b. The second campaign images were post-processed using a 3 x 3 median filter that was applied in MatLab. The images show that the fluorescence signal-to-noise ratio is approximately 20, which represents a major improvement over the images obtained in the first campaign.

Figure 4.17 shows several instantaneous naphthalene PLIF images after the stagnation temperature had reached a steady state. The ablation products are seen to be confined quite close to the wall of the wind tunnel, although the transport of the ablation product through the boundary layer is evident.

To show the development of the scalar transport over a wider field of view, Figure 4.18 shows a composite of two instantaneous (but uncorrelated) naphthalene PLIF images. The total field of view spans $2.8 \delta_{99}$ in the streamwise direction. The first image starts 78 mm ($x/\delta_{99}=3.98$) downstream of the downstream edge of the naphthalene insert. The capabilities of the plug allow for the field of view to span from 23.5 mm ($x/\delta_{99}=1.24$) to 264.8 mm ($x/\delta_{99}=13.94$) downstream of the downstream edge of the naphthalene plug (Figure 3.8).



(a)



(b)

Figure 4.16 Instantaneous naphthalene PLIF images during (a) the first campaign and (b) the second campaign

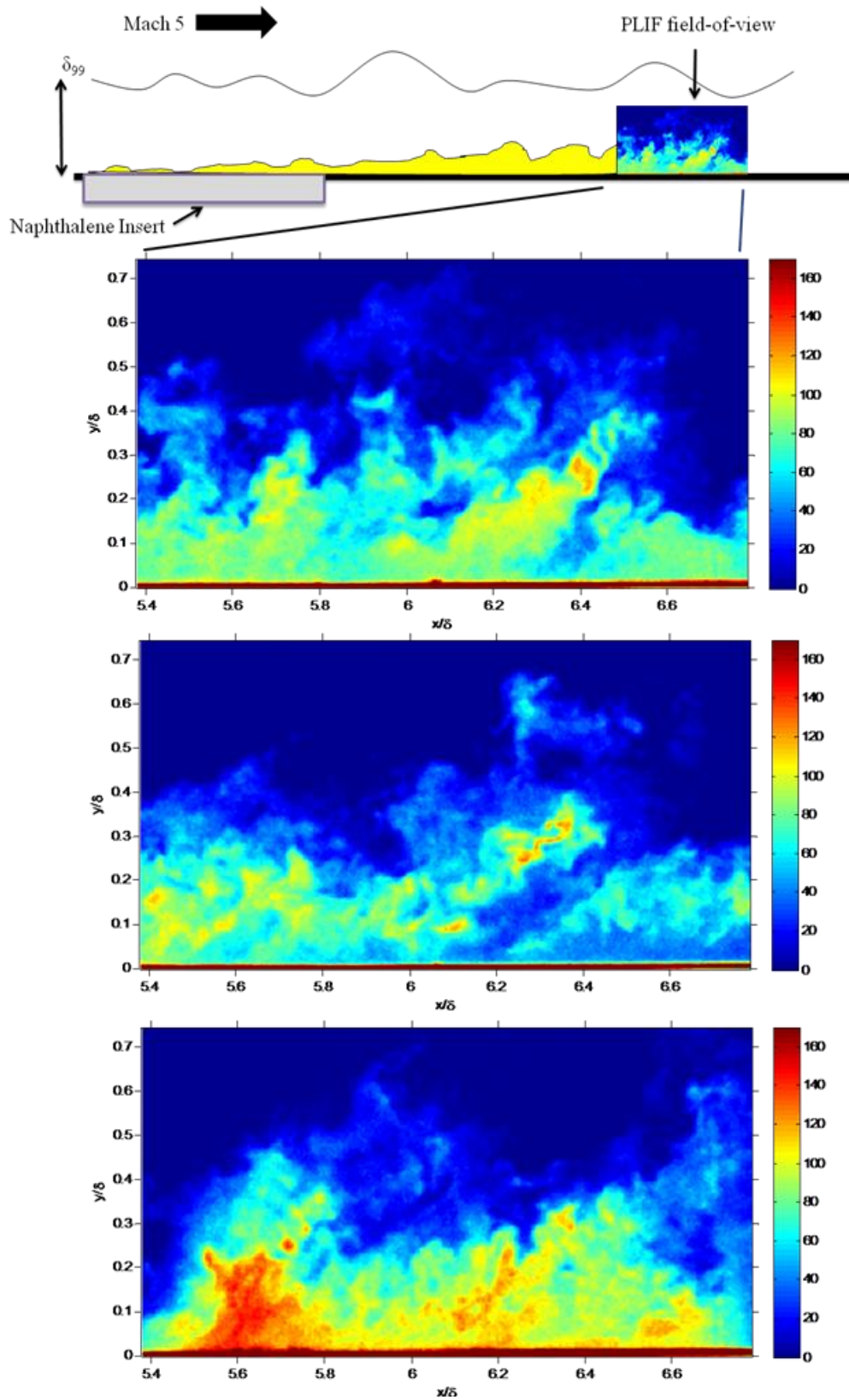


Figure 4.17 Instantaneous naphthalene PLIF images in a Mach 5 turbulent boundary layer.

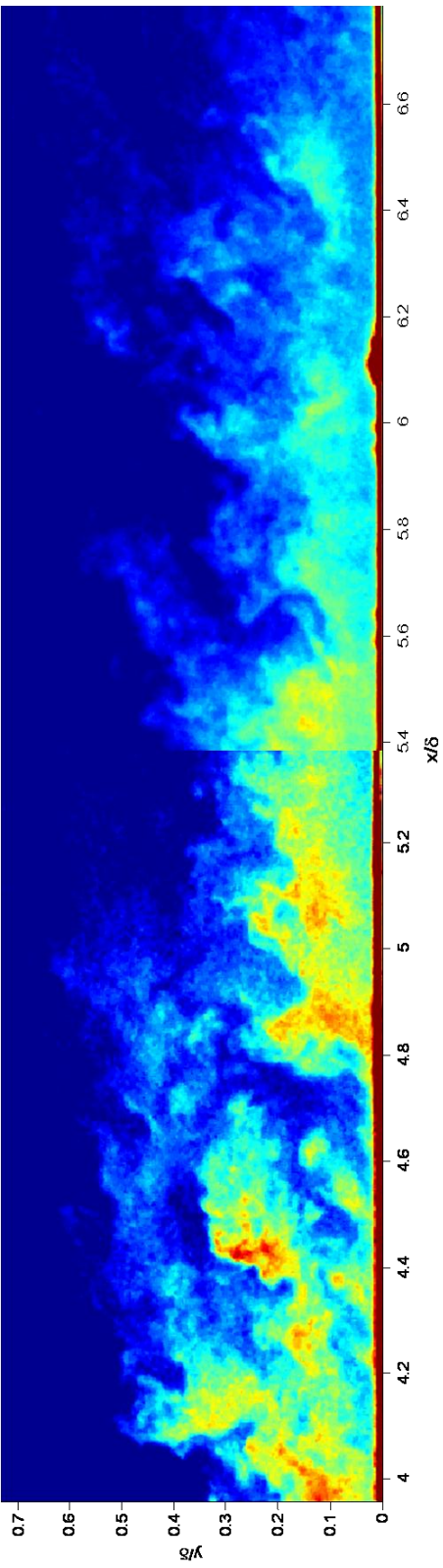


Figure 4.18 Composite of two instantaneous naphthalene PLIF images taken at two adjacent locations at different times

4.4.2 Thermocouple Measurements

The temperatures 1mm, 5.1mm, and 8.9mm below the surface of the naphthalene plug were measured during each of these initial runs run at the center of the naphthalene plug with type-T thermocouples. Figure 4.19 shows the schematic of the thermocouple positions, while Figure 4.20 displays the readouts. These temperatures were found to be steadily increasing. At 1mm below the surface, the sharp increase at the beginning and ending of each run represent the normal shock passing over the naphthalene plug. The heat flux through the surface from the combined effects of the recovery temperature near the wind tunnel wall and mass transfer from the naphthalene plug is visible in the steady increase of the thermocouples.

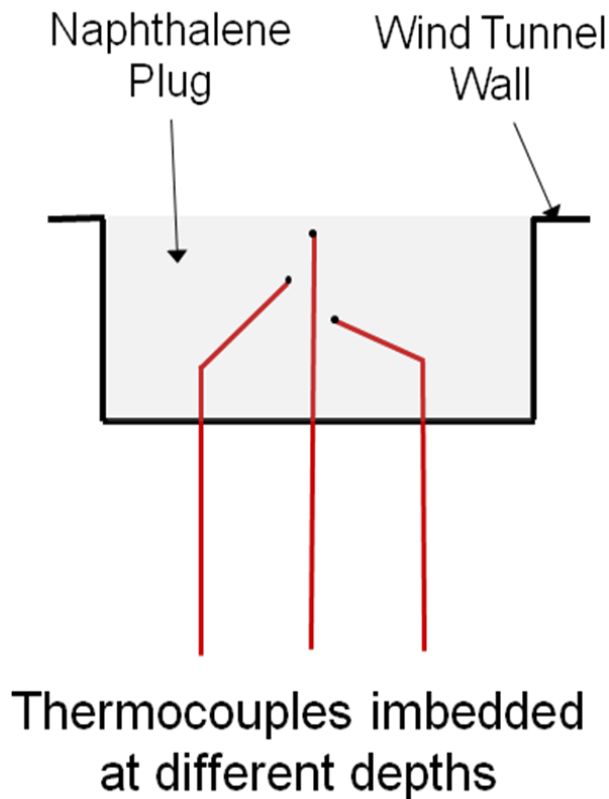


Figure 4.19 Naphthalene plug with thermocouples imbedded at varying depths

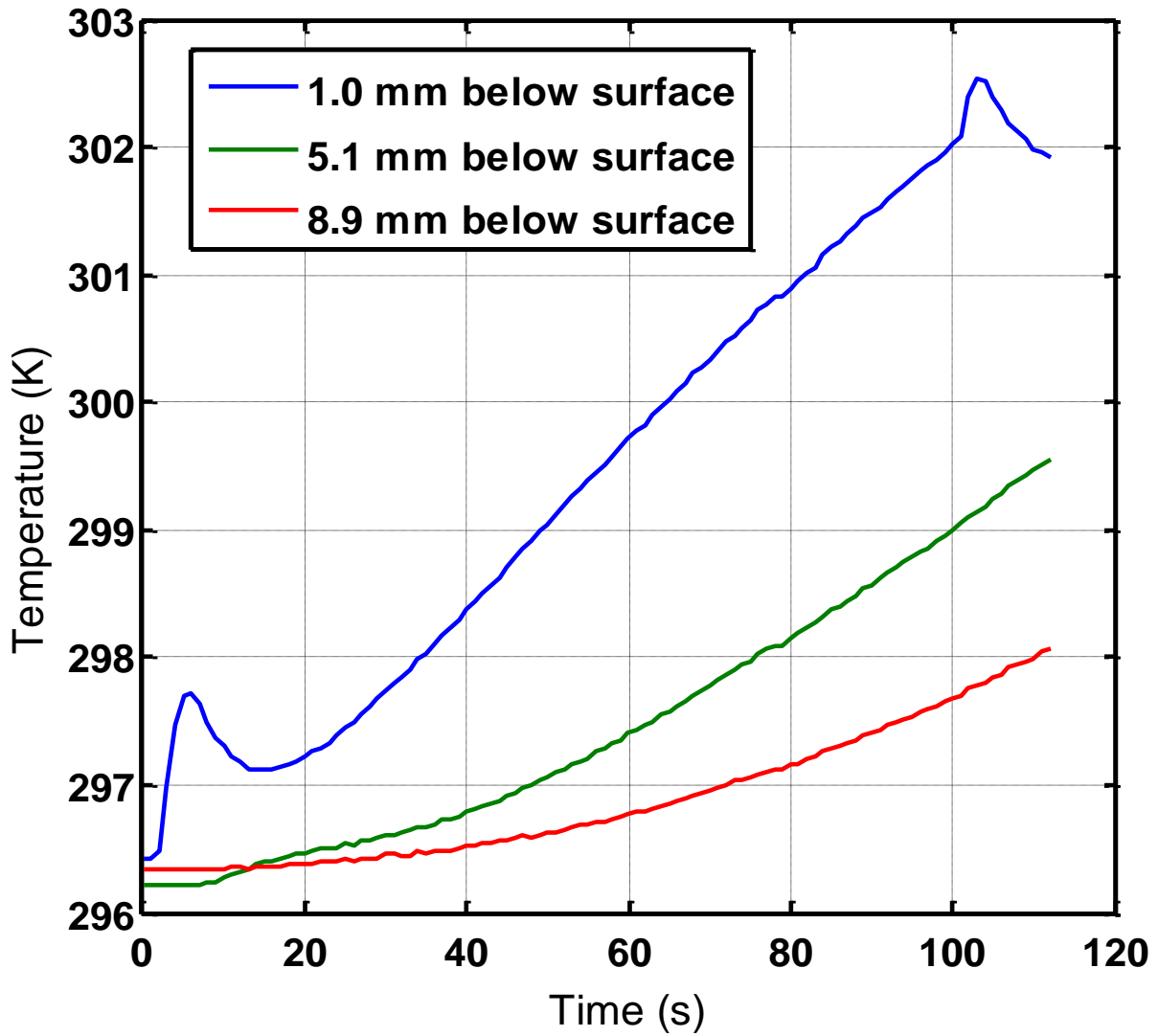


Figure 4.20 Thermocouple measurements at different depths during a typical Mach 5 wind tunnel run

4.4.3 Average of Instantaneous PLIF Images

The mean fluorescence profile was computed from a set of 18 PLIF images similar to that shown in Figure 4.17. Only 18 images were averaged due to a compressor failure that ended this round of experiments. To improve the statistics, the pixel-columns were averaged; i.e., the images were averaged in the streamwise direction as well as time. Figure 4.21 shows the average image, while Figure 4.22 shows a plot of the normalized mean LIF signal through the boundary layer and the standard deviation. Both the mean LIF signal and standard deviation are normalized by the maximum mean LIF signal. The naphthalene PLIF signal is seen to reach a peak at the wall and exhibit a gradual decrease in magnitude with increasing distance from the wall.

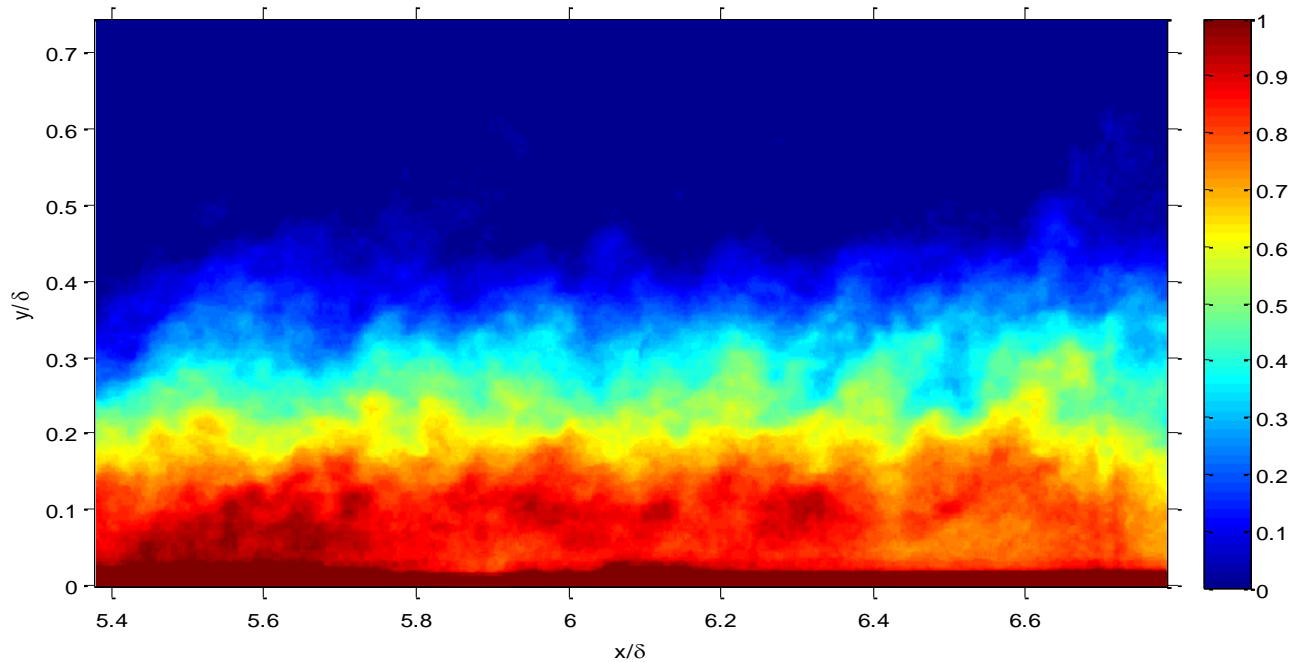


Figure 4.21 Average of 18 instantaneous naphthalene PLIF images

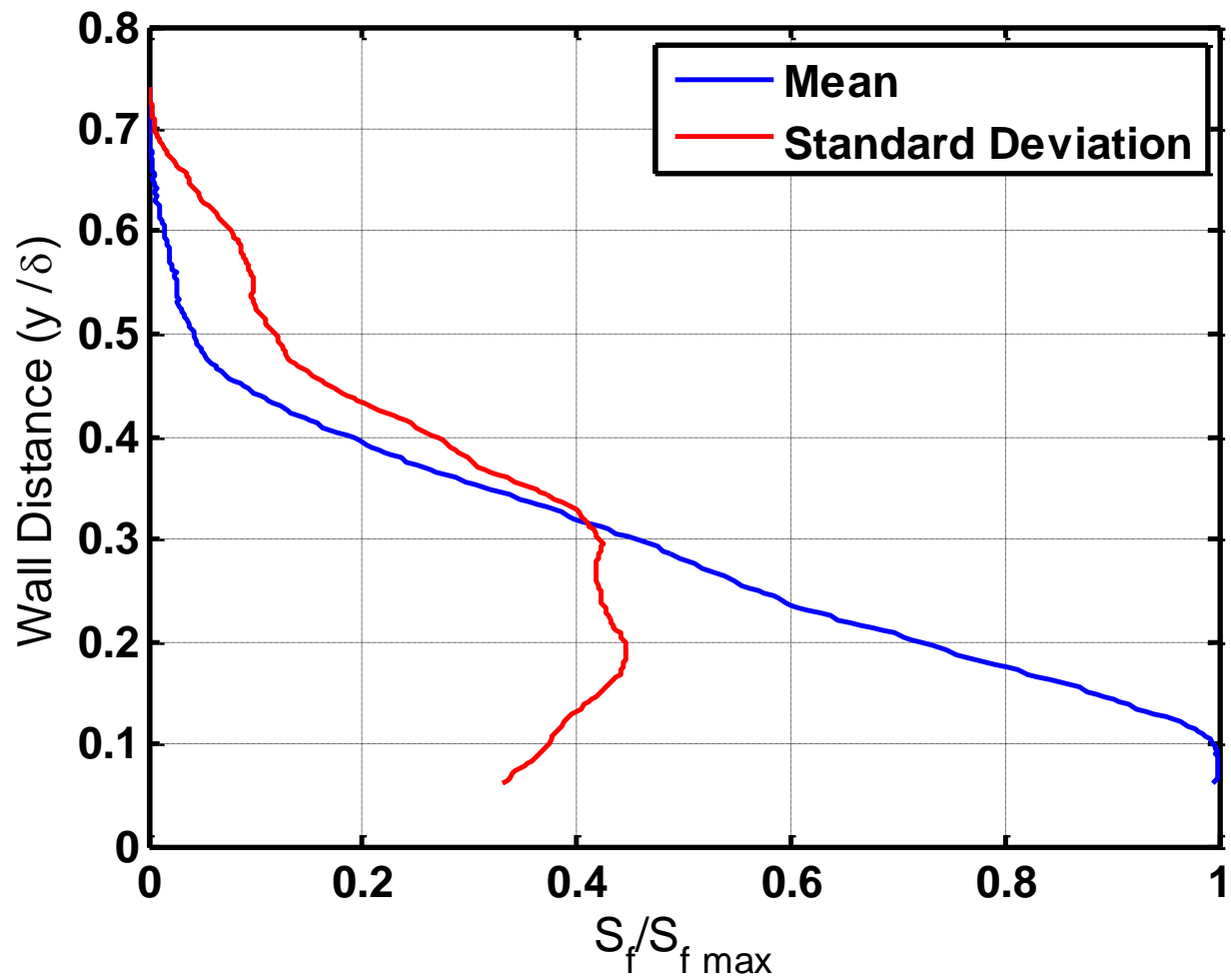


Figure 4.22 Normalized average fluorescence signal through the Mach 5 boundary layer with standard deviation

4.4.4 Obtaining Quantitative Measurements

The objective of the previously described spectroscopic studies was to enable us to correct the measured naphthalene LIF signals to obtain quantitative measurements of the naphthalene mole fraction. The dominant effect on the fluorescence signals will be the temperature effect, since the mean pressure across the boundary layer is approximately constant. For example, as the naphthalene is transported from the wall to say the midpoint of the boundary layer it may cool from approximately the recovery temperature of 370 K at the wall to 100 K. Although there currently is not spectroscopic data at temperatures below 300 K, below we will develop a correction process that will be used once the data are available. For example, currently there is data on the temperature dependence of the fluorescence signal and absorption cross-section at atmospheric pressure, for which the fluorescence is quenching dominated. In this case we have,

$$\frac{S_f(T)}{S_f(T_{ref})} = \frac{T_{ref} \sigma(T) k_f(T) k_Q(T_{ref})}{T \sigma(T_{ref}) k_f(T_{ref}) k_Q(T)} \quad (4.11)$$

If we assume that the spontaneous emission rate and quenching cross-section for oxygen are temperature independent, then we have,

$$\frac{S_f(T)}{S_f(T_{ref})} = \frac{\sigma(T)}{\sigma(T_{ref})} \left(\frac{T_{ref}}{T} \right)^{1/2} \quad (4.12)$$

which we can use to obtain the temperature dependence of the cross-sections. Now, at the conditions of the Mach 5 boundary layer, the pressure is 36 Torr (.7 psi) and the

fluorescence is not quenching dominated. In this case, for the same assumptions as above, we can write,

$$\frac{S_f(P, T)}{S_{f \max}} = \frac{\chi_{naph}}{(\chi_{naph})_{\max}} \frac{(T/T_{ref})_{\max}}{(T/T_{ref})} \frac{\sigma(T)/\sigma(T_{ref})}{(\sigma(T)/\sigma(T_{ref}))_{\max}} \frac{(k_f + k_{\text{int}} + k_Q(P, T_{\max}))}{(k_f + k_{\text{int}} + k_Q(P, T))} \quad (4.13)$$

This equation can be used to obtain the normalized mole-fraction of naphthalene vapor from the normalized fluorescence signal. Here we obtain the temperature profile in the boundary layer from the Crocco-Busemann formula and the known mean velocity profile. As outlined in White (1991), the energy equation can simplify to the Crocco-Busemann formula after several approximations are made: (a) steady flow, (b) $Pr = 1$, (c) adiabatic flow, (d) zero pressure gradient, and (e) boundary layer approximation hold ($V \ll U$ and $\partial/\partial x \ll \partial/\partial y$). The energy equation will then reduce to the familiar form of the Crocco-Busemann relation:

$$T = T_0 - \frac{(U^2 + V^2)}{2C_p} \quad (4.14)$$

The assumption of adiabatic flow could be made due to negligible mass loss during a typical run as explained in section 4.2. In this preliminary investigation the mean velocity field is obtained from Pitot probe measurements in the Mach 5 boundary layer Beresh (1999).

Since we do not have absorption cross-section data at lower temperatures, we simply extrapolate the data in Figure 4.9 to lower temperatures. Obviously, this is a very coarse assumption that will be checked in the future studies.

Finally, we take the quenching rate from the quenching measurements and the assumed form as given in Equation 4.13. The corrected mean is shown in Figure 4.23. This is only a proof-of-concept exercise to show how the fluorescence data can be corrected to obtain quantitative results, provided the absorption data can be measured at low-temperatures. In future work, the intention is to make the required LIF temperature-dependence measurements.

It is clear that if this technique is to be made quantitative, it will be necessary to have some idea of the local conditions, because the fluorescence signal is strongly dependent on them. It is clear that having a simultaneous measurement of temperature is critical. In the case of a boundary layer, the mean temperature can be achieved with a separate velocity measurement (and Crocco-Busemann), but in cases where measuring velocity is not possible then it may be possible to use a dual-line excitation method to infer the temperature, as has been done with acetone (Thurber et al., 1998). In cases where the freestream pressure varies widely, such as over the shoulder of a blunt re-entry vehicle, it may be necessary to use simultaneously-acquired data from pressure taps, or perhaps a numerical simulation, to obtain a first-order estimate for the local pressure.

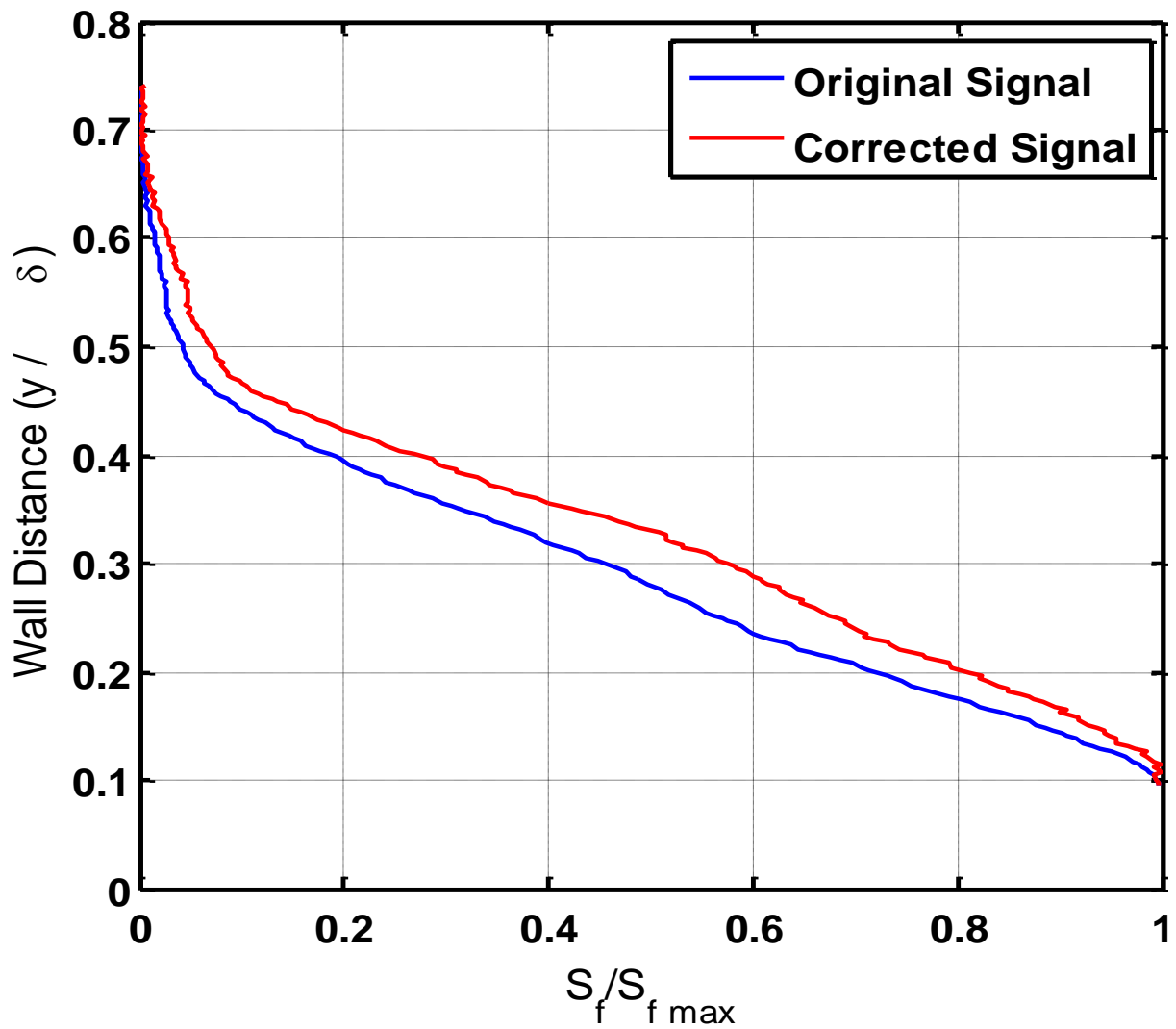


Figure 4.23 Normalized average fluorescence signal profiles through the Mach 5 boundary layer. *Uncorrected signal and signal corrected for temperature effects.*

Chapter 5: Conclusions and Future Work

5.1 CONCLUSIONS

Planar laser-induced fluorescence has been used to image the ablation products given off by a sublimating ablator in the presence of a Mach 5 boundary layer. Naphthalene is used as the ablator because its vapor is readily detected by the laser-induced fluorescence technique with 266 nm excitation. The results show that excellent signal-to-noise-ratio PLIF images can be obtained with this technique. Furthermore, it is an objective of this work to conduct targeted spectroscopic studies to enable the quantitative interpretation of the PLIF signal in terms of naphthalene mole fraction. Test-cell measurements were made to determine the fluorescence signal and absorption cross-section dependence on temperature, over the temperature range of 297 K to 525 K. On a per-mole basis, the temperature dependence of naphthalene fluorescence increases sharply at lower temperatures and levels off with higher temperatures, whereas the absorption cross-section exhibits a more gradual increase with temperature. Stern-Volmer plots show a linear variation of the inverse lifetime with pressure, which indicates the fluorescence follows a conventional quenching model at pressures greater than 2 kPa (40 torr). It was further found that for the fluorescence remained linear with laser fluence provided the laser fluence was less than about 200 J/m².

To obtain quantitative concentration information in the Mach 5 turbulent boundary layer, the naphthalene PLIF images will need to be corrected for temperature effects since the boundary layer temperature can vary considerably with distance from the wall. A correction procedure was demonstrated that used mean velocity data and the Crocco-Busemann relation to obtain the needed temperature information. However, a

limitation of this process was the lack of absorption cross-section data at the lowest temperatures encountered in the boundary layer.

5.2 SUGGESTED FUTURE WORK

Future work should be directed at finishing the spectroscopic study of naphthalene LIF, expanding the database of images of naphthalene PLIF in the Mach 5 blow down wind tunnel, and obtaining simultaneous PIV and PLIF data in the Mach 5 wind tunnel. The temperature dependence of the absorption cross-section data will need to be further investigated. The experimental setup to obtain the pressure dependence and lifetime information of the naphthalene LIF will be used to obtain the absorption cross-section data at low pressure. In addition, the absorption cross-section will need to be investigated to the lowest temperature encountered in the boundary layer. One way to do these low temperature measurements is to expand the naphthalene-laden gas through a supersonic nozzle. The temperature effects on the quenching cross-section will also need to be investigated. In this preliminary investigation the quenching cross-section was assumed to be constant, but the validity of this assumption will need to be checked.

Expanding the database of naphthalene PLIF images is necessary in order to obtain statistically converged data sets. A thousand images per position may be necessary to compute the gradient of the mean scalar field. The gradient of the mean scalar field will be used in validation of LES sub-filter models.

Simultaneous quantitative PLIF and PIV measurements in the Mach 5 turbulent boundary layer is the overall goal of this entire investigation. The development of a PIV system for the Mach 5 wind tunnel is currently in testing stages, which would allow for these simultaneous diagnostics to begin. In the future, these data will be taken in multiple side-view locations downstream of the naphthalene plug, as well as in multiple

plan-view locations. These results will give scalar/velocity correlations will also be used in validation of LES sub-filter models.

Bibliography

- Ambrose, D., Lawrenson, I. J., and Sparke, C. H. S., "The vapor pressure of naphthalene," *J. Chem. Thermodynam.*, 7: 1173-1176, 1975.
- Ashpole, C. W., Formosinho, S. J., and Porter, G., "Pressure dependence of intersystem crossing in aromatic vapours," *Proc. Roy. Soc. Lond. A*, 323: 11-28, 1971.
- Avouris, P., Gelbart, W. M., and El-Sayed, M. A., "Nonradiative electronic relaxation under collision-free conditions", *Chemical reviews*, 77 (6): 793–833, 1977.
- Beddard, G. S., Fleming, G. R., Gijzeman, O. L. J., and Porter, G., "Vibrational energy dependence of radiationless conversion in aromatic vapours," *Proc. R. Soc. Lond. A*, 340: 519-533, 1974.
- Beddard, G. S., Formosinho, S. J., and Porter, G., "Pressure effects on the fluorescence from naphthalene vapour", *Chem. Phys. Letters*, 22 (2): 235–238, 1973.
- Behlen, M. F. and Rice, S. A., "Intersystem crossing in cold isolated molecules of naphthalene", *J. Chem. Phys.* 75 (12): 5672–5684, 1981.
- Bryant, R. A., Donbar, J. M., Driscoll, J. F., "Acetone laser induced fluorescence for low pressure/low temperature flow visualization," *Experiments in Fluids*, 28: 471-478, 2000.
- Callaway, D. W., Reeder, M. F., and Greendyke, R. B., "Experimental Studies of Low Temperature Ablation using Dry Ice," AIAA 2008-2554, 15th AIAA International Space Planes and Hypersonic Systems and Technologies Conference, Dayton, Ohio, 2008.
- Callaway, D. W., Reeder, M. F., Greendyke, R. B., and Gosse, R., "Photogrammetric Measurement of Recession Rates of Low Temperature Ablators in Supersonic Flow," AIAA 2010-1216, 48th AIAA Aerospace Sciences Meeting, Orlando, Florida, 2010.
- Charwat, A. F., "Exploratory studies on the sublimation of slender camphor and naphthalene models in a supersonic wind-tunnel," 1968.
- Clemens, N. T., "Flow Imaging," *Encyclopedia of Imaging Science and Technology*, John Wiley and Sons, New York, 2002.

- Covington, M. A., Heinemann, J. M., Goldstein, H. E., Chen, Y.-K., Terrazas-Salinas, I., Balboni, J. A., Olejniczak, J., and Martinez, E. R., "Performance of a Low Density Ablative Heat Shield Material," *Journal of Spacecraft and Rockets*, 45 (4): 854-864, 2008.
- De Kruif, C. G., Kuipers, T., Van Miltenburg, J. C., Schaake, R. C. F., and Stevens, G., "The vapor pressure of solid and liquid naphthalene," *J. Chem. Thermodynam*, 13: 1081-1086, 1981.
- Du, H., Fuh, R. A., Li, J., Corkan, A., and Lindsey, J. S., "PhotochemCAD: A computer-aided design and research tool in photochemistry," *Photochemistry and Photobiology*, 68: 141-142, 1998.
- Eckbreth, A. C., *Laser Diagnostics for Combustion Temperature and Species*, Abacus Press, Cambridge, 1988.
- Gatski, T. B., Hussaini, M. Y., and Lumley, J. L., *Simulation and Modeling of Turbulent Flows*, Oxford University Press, New York, 1996.
- Gattermann, H. and Stockburger, M., "Spectroscopic studies on naphthalene in the vapor phase III, phosphorescence and intersystem crossing yields of single vibronic levels", *J. Chem. Phys.*, 63 (10): 4541-4545, 1975.
- Ghandhi, J. B. and Felton, P. G., "On the fluorescent behavior of ketones at high temperatures," *Experiments in Fluids*, 21: 143-144, 1996.
- Gnoffo, P. A., Weilmuenster, K. J., and Hamilton II, H. H., "Computational aerothermodynamics design issues for hypersonic vehicles," *Journal of Spacecraft and Rockets*, 36 (1): 21-43, 1999.
- Goldstein, R. J. and Cho, H. H., "A review of mass transfer measurements using naphthalene sublimation," *Experimental Thermal and Fluid Science*, 10: 416-434, 1995.
- Greathouse, J. S., Kirk, B. S., Lillard, R. P., Truong, T. H., Robinson, P., and Cerimele, C. J., "Crew exploration vehicle (cev) crew module shape selection analysis and cev aerospace project overview," AIAA 2007-603, 45th AIAA Aerospace Sciences Meeting and Exhibit, Reno, Nevada, 2007.
- Griffith, B. J., Edenfield, E. E., and Strike, W. T., "Wind-Tunnel Simulation of Ablation," *Journal of Spacecraft and Rockets*, 14 (10): 593-599, 1977.
- Grossman, F., Monkhouse, P. B., Ridder, M., Sick, V., and Wolfrum, J., "Temperature and pressure dependences of the laser-induced fluorescence of gas-phase acetone and 3-pentanone," *Applied Physics B*, 62: 249-253, 1996.

- Ho, D. W. K., Koo, J. H., Bruns, M. C., and Ezekoye, O. A., "A Review of Numerical and Experimental Characterization of Thermal Protection Materials – Part III. Experimental Testing," AIAA 2007-5773, 43rd AIAA/ASME/SAE/ASEE Joint Propulsion Conference & Exhibit, Cincinnati, Ohio, 2007.
- Hsieh, J. C., Huang, C., and Lim, E. C., "Radiationless singlet deactivation in isolated large molecules. I. Naphthalene, naphthol, and naphthylamine," *J. Chem. Phys.*, 60 (11): 4345-4353, 1974.
- Incropera, F. P. and DeWitt, D. P., *Fundamentals of Heat and Mass Transfer*, John Wiley & Sons, 2002.
- Inman, J. A. (Wilkes), Danehy, P. M., Alderfer, D. W., and Buck, G. M., "Plif imaging of capsule rcs jets and simulated forebody ablation," AIAA 2008-248, 46th AIAA Aerospace Sciences Meeting and Exhibit, Reno, Nevada, 2008.
- Kaiser, S., Kyritsis, D. C., Dobrowolski, P., Long, M. B., and Gomez, A., "The electrospray and combustion at the mesoscale," *J. Mass Spectrom. Soc Jpn.*, 51: 42-49, 2003.
- Kaiser, S. A. and Long, M. B., "Quantitative planar laser-induced fluorescence of naphthalene as fuel tracers," *Proceedings of the Combustion Institute*, 30: 1555-1563, 2005.
- Kohlman, D. L. and Richardson, R. W., "Experiments on the use of dry ice ablating wind-tunnel models," *Journal of Spacecraft and Rockets*, 6 (9): 1061-1063, 1969.
- Laor, U. and Ludwig, P. K., "Fluorescence lifetimes of vibronic states of naphthalene vapor in the region of excitation from 3080 – 2150 Å," *J. Chem. Phys.*, 54 (3): 1054–1057, 1971.
- Lim E. C. and Huang C., "Radiationless transition in large isolated molecules: Variation of excess energy dependence of its decay rate with initially prepared electronic state," *J. Chem. Phys.*, 58 (3): 1247-1248, 1973.
- Lipfert, F. and Genovese, J., "An experimental study of the boundary layers on low-temperature subliming ablators," *AIAA Journal*, 9 (7): 1330-1337, 1971.
- Martinez, M., Harder, H., Ren, X., Leshner, R. L., and Brune, W. H., "Measuring atmospheric naphthalene with laser-induced fluorescence," *Atmos. Chem. Phys. Discuss*, 4: 343-363, 2004.
- Milos, F. S. and Chen, Y.-K., "Ablation and Thermal Response Property Model Validation for Phenolic Impregnated Carbon Ablator," AIAA 2009-262, 47th AIAA Aerospace Sciences Meeting, Orlando, Florida, 2009.

- Ni, T. and Melton, L. A., "Two-dimensional gas-phase temperature measurements using fluorescence lifetime imaging," *Applied Spectroscopy*, 50 (9): 1112-1116, 1996.
- Ossler, F., Metz, T., and Aldén, M., "Picosecond laser-induced fluorescence from gas-phase polycyclic aromatic hydrocarbons at elevated temperatures. I. Cell measurements," *Appl. Phys. B*, 72: 465-478, 2001.
- Reyle, C. and Brechignac, P., "Fluorescence of jet-cooled naphthalene: emission spectra, lifetimes and quantum yields," *Eur. Phys. J. D*, 8: 205–210, 2000.
- Schlag, E. W., Schneider, S., and Chandler, D. W., "Fluorescence lifetimes of vibronic levels of naphthalene vapour," *Chem. Phys. Letters*, 11 (4): 474–477, 1971a.
- Schlag, E. W., Schneider, S., and Fischer, S. F., "Lifetimes in excited states," *Annual Review of Physical Chemistry*, 22, 465-526, 1971b.
- Silton, S. I. and Goldstein, D. B., "Ablation Onset in Unsteady Hypersonic Flow About Nose Tip with Cavity," *Journal of Thermophysics and Heat Transfer*, 14 (3): 421-434, 2000.
- Smits, A. J., Martin, M. P., and Girimaji, S., "Current status of basic research in hypersonic turbulence," AIAA 2009-151, 47th AIAA Aerospace Sciences Meeting and Exhibit, Orlando, Florida, 2009.
- Soep, B., Michel, C., Tramer, A., and Lindqvist, L., "Study of intersystem crossing in naphthalene and 1-methylnaphthalene in collision free conditions and pressure effects," *Chem. Phys.*, 2: 293-303, 1973.
- Stock, H. W., "Surface Patterns on Subliming and Liquefying Ablation Materials," *AIAA Journal*, 13 (9): 1217-1223, 1975.
- Stock, H. W. and Ginoux, J. J., "Experimental Results on Crosshatched Ablation Patterns," *AIAA Journal*, 9 (5): 971-973, 1971.
- Stockburger, M., Gattermann, H., and Klusmann, W., "Spectroscopic studies of naphthalene in the vapor phase I," *J. Chem. Phys.*, 63 (10): 4519 – 4529, 1975a.
- Stockburger, M., Gattermann, H., and Klusmann, W., "Spectroscopic studies of naphthalene in the vapor phase II. Fluorescence quantum yields from single vibronic levels in the first excited singlet state – behavior of higher excited singlet states," *J. Chem. Phys.*, 63 (10): 4529–4540, 1975b.
- Suto, M., Wang, X., Shan, J., and Lee, L. C., "Quantitative photoabsorption and fluorescence spectroscopy of benzene, naphthalene and some derivatives at 106 – 295 nm," *J. Quant. Spec. Radiat. Transfer*, 48 (1): 79–89, 1992.

- Thurber, M. C., Grisch, F., Kirby, B. J., Votsmeier, M., and Hanson, R. K., "Measurements and modeling of acetone laser-induced fluorescence with implications for temperature-imaging diagnostics," *Applied Optics*, 37 (21): 4963-4978, 1998.
- Vojvodich, N. S. and Winkler, E. L., "The Influence of Heat Rating and Test Stream Oxygen Content of the Insulation Efficiency of Charring Materials," NASA TN D-1889, July 1963.
- Von Karman, T. H., "The Analogy Between Fluid Friction and Heat Transfer," *Trans. ASME*, 61: 705-510, 1939.
- Watts, R. J. and Strickler, S. J., "Fluorescence and Internal Conversion in Naphthalene Vapor," *J. Chem. Phys.*, 44 (6): 2423-2426, 1966.
- White, F. M., *Viscous Fluid Flow*, McGraw-Hill, Boston, 1991.

Vita

Bryan Lochman is the son of Mrs. Linda Lochman and Dr. John Lochman, and is married to Natalie Busby. After graduating from Northridge High School in Tuscaloosa, Alabama in 2004, he attended Northwestern University in Evanston, Illinois and received his Bachelor of Science in Mechanical Engineering in June of 2008. In August of 2008 he enrolled into the Graduate School of the University of Texas at Austin in the department of Aerospace Engineering and Engineering Mechanics pursuing a Master of Science degree.

Permanent email address: bryan.lochman@gmail.com

This thesis was typed by the author.